Chemistry Dissertations   Department of Chemistry

Electrokinetic Modeling of Free Solution Electrophoresis

Yao Xin

Follow this and additional works at: https://scholarworks.gsu.edu/chemistry_diss

Part of the Chemistry Commons

Recommended Citation

ELECTROKINETIC MODELING OF FREE SOLUTION

ELECTROPHORESIS

by

YAO XIN

Under the Direction of Stuart Allison

ABSTRACT

Modeling electrophoresis of peptides, proteins, DNA, blood cells and colloids is based on classical electrokinetic theory. The coupled field equations-Poisson, Navier-Stokes or Brinkman, and ion transport equations are solved numerically to calculate the electrophoretic mobilities.

First, free solution electrophoretic mobility expressions are derived for weakly charged rigid bead arrays. Variables include the number of beads (N), their size (radius), charge, distribution (configuration), salt type, and salt concentration. We apply these mobility expressions to rings, rigid rods, and wormlike chain models and then apply the approach to the electrophoretic mobilities and translational diffusion constants of weakly charged peptides. It is shown that our bead model can predict the electrophoretic mobilities accurately. In order to make the method applicable at higher salt concentrations and/or to models consisting of larger sized subunits, account is taken of the finite size of the beads

making up the model structure. For highly charged particles, it is also necessary to account for ion relaxation. This ion relaxation effect is accounted for by correcting "unrelaxed" mobilities on the basis of model size and average electrostatic surface, or "zeta" potential. With these corrections our model can be applied to the system with absolute electrophoretic mobilities exceeding approximately 0.20 cm^2/kV sec and also models involving larger subunits. This includes bead models of duplex DNA.

Along somewhat different lines, we have investigated the electrophoresis of colloidal particles with an inner hard core and an outer diffusive layer ("hairy" particles). An electrokinetic gel layer model of a spherical, highly charged colloid particle developed previously, is extended in several ways. The charge of the particle is assumed to arise from the deprotonation of acidic groups that are uniformly distributed over a portion (or all) of the gel layer. Free energy considerations coupled with Poisson-Boltzmann theory is used to calculate the change of the local pKa of the acidic groups depending on the local electrostatic environment. Based on the modeling of electrophoresis and viscosity, we predict that the thickness of the gel layer decreases as the salt concentration increases. And only the outermost portion of the gel layer is charged.

INDEX WORDS: Free solution electrophoresis, Peptides, Bead model, Gel layer,

Electrokinetic modeling

ELECTROKINETIC MODELING OF FREE SOLUTION

ELECTROPHORESIS

by

YAO XIN

A Dissertation Submitted in Partial Fulfillment of the Requirements for the Degree of

Doctor of Philosophy

in the College of Arts and Sciences

Georgia State University

2007

ELECTROKINETIC MODELING OF FREE SOLUTION

ELECTROPHORESIS

by

YAO XIN

Committee Chair: Stuart Allison

Committee: Jerry Smith
Jenny Yang

To my parents, my sister and my husband

ACKNOWLEDGMENTS

This dissertation has been accomplished with the assistance and support of many people.

First and foremost, I would like to express my sincere appreciation and gratitude to my advisor, Dr. Stuart Allison. He taught me how to start academic pursuits step by step. From him I learned a lot and have improved in the area of critical thinking and algorithm development. Without his encouragement and help I could not have completed this work. My time in his group was really happy and will sit in my mind forever. Also I want to thank my committee members: Dr. Jenny Yang and Dr. Jerry Smith for their great advice on my dissertation.

I would like to thank the Department of Chemistry for offering me the great opportunity to pursue my Ph.D. degree, for offering great classes and for offering me the opportunity to teach undergraduate tutorials. All of these provided me good training. Thanks Dr. Stuart Allison, Dr. Dabney White Dixon, Dr. Kathryn Betty Grant, Dr. Thomas L. Netzel, Dr. Jenny Yang for their interesting and impressive classes.

I would also like to thank Hongxia Pei, Margaret Haynes and other group members for discussions and help. I would like thank all my friends for their support. Sharing happiness with them has made my study enjoyable.

Last but not least, I would like to express my gratitude to my family. I would like to thank my grandmother and my parents for their love and support. Having them feel proud of me has been a big incentive for me to work hard. I would like to thank my sister Miao Xin for her encouragement. Special thanks go to my husband, Chunming Zhao, for his love and companionship. He has taken care of me since I met him.

TABLE OF CONTENTS

viii

LIST OF TABLES

LIST OF FIGURES

Chapter 1

Introduction

1.1   Brief Description of Electrophoresis

Charged particles placed in an applied electric field move at different velocities depending on their size and charge. This phenomenon is called electrophoresis.   Theoretical studies focus on the ratio of the velocity of the charged particle, u, over the strength of the electric field, E, which is defined as the electrophoretic mobilities, μ . For the simplest case, a spherical particle of charge Q, radius a immersed in a neutral solvent with viscosity η in the presence of electric field E, is shown in Figure 1-1.

E   U

$F_{hyd} = - 6\pi\eta aU$ $F_{ele} = QE$
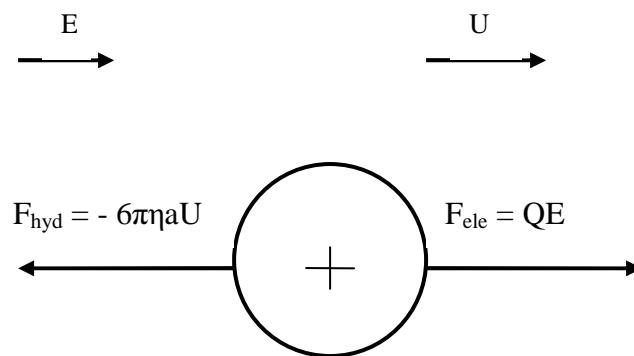
Figure 1-1) A Charged Spherical Particle Moving in an Electric Field in Neutral Solvent.

Under steady state conditions, the determination of the mobility of the particle is straightforward. From force balance on the particle,

$$6\pi\eta aU = QE \qquad (1\text{-}1)$$

so

$$\mu = \frac{U}{E} = \frac{Q}{6\pi\eta a} \qquad (1\text{-}2)$$

However, in real applications, the solvent contains charged mobile ions, which are influenced by the electric field and affect the mobility of the particle. In addition, the particle may be irregular in shape. Hence, the hydrodynamic force is not simply $-6\pi\eta aU$. These factors make the modeling of electrophoresis complicated. Wiersema[1] has described the electrophoresis of spheres in detail in his dissertation.
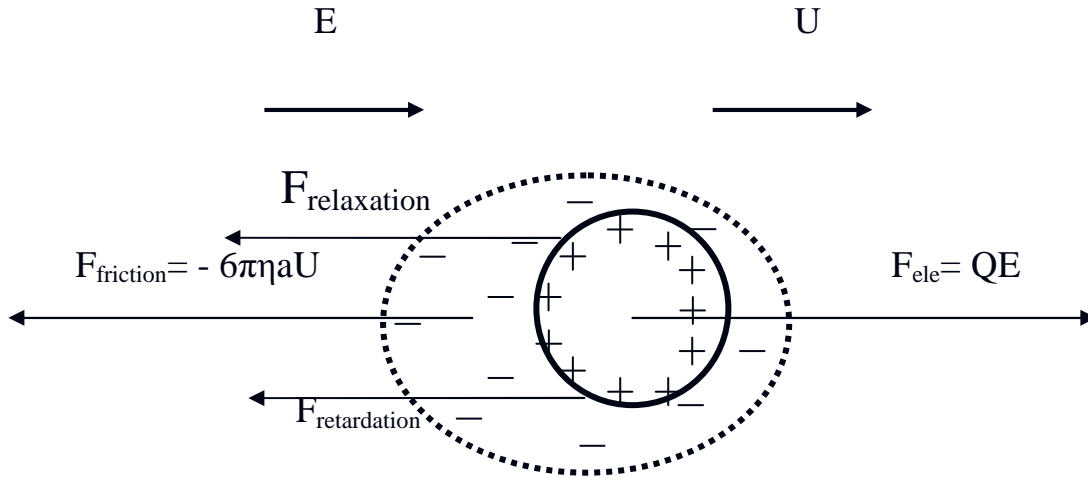
Figure 1-2) A Charged Spherical Particle Moving in an Electric Eield in Salt Containing Mobile Ions.

As shown in Figure 1-2, a spherical charged particle is moving in a salt solution in the presence of E. Assuming the particle is positively charged, there will be a counter-ion cloud consisting of negative charged ions from the salt around the particle. This counter-ion cloud, together with the positive charge on the particle is called double layer (total charge = 0). There are four forces acting on the particle. First, the electrical force exerted by the electric field, F_{ele}, equals to the product of the total charge of the particle, Q, and the electric field, E. Next, the Stokes friction force exerted by the fluid, $F_{friction} = - 6\pi\eta aU$.

The remaining two forces arise from the ion atmosphere surrounding the particle. When the particle is moving toward the cathode, the ion atmosphere will move in the opposite direction, exerting a drag on the nearby fluid. This resulting back flow will cause a hydrodynamic drag on the particle, which will decrease the speed of the particle. This effect is called electrophoretic retardation. The other effect on elecrtrophoretic mobility is caused by distortion of the ion atmosphere and is called the ion relaxation effect. Under the presence of an electric field, the counter-ion cloud surrounding the particle becomes asymmetric under steady state conditions and this causes an additional electrostatic drag on the particle. This effect will also decrease the speed of the particle. The relaxation effect is not significant for weakly charged particles, but becomes important for highly charged ones.

1.2 Application of Electrophoresis

Capillary electrophoresis (CE) has proven to be powerful in the separation and characterization of charged particles, such as peptides, proteins, nucleic acids and colloidal particles. There are a very large number of CE options, for example, capillary micellar

electrochromatography (CMCE), capillary gel electrophoresis (CGE), free solution capillary electrophoresis (FSCE) and capillary isotacophoretic (CITP).[2] Among these, free solution capillary electrophoresis, without a support medium, provides the simplest way of examining the relation between mobility and chemico-physical properties, such as size and charge. Within the past few years, substantial progress has been made in both the measurement and interpretation of free solution electrophoretic mobilities. A number of investigations have studied electrophoresis of peptides and proteins. These topic include: effect of different secondary structures of peptides,[3, 8, 13] such as α-helix and β-sheet,[3] on electrophoretic mobilities; charge dependence of mobiblities;[4-6, 9] peptides electrophoresis maps with potential use as fingerprints of proteins;[7, 12, 14] mobilities studies of peptides with post-translational modifications, such as phosphorylation, methylation, and citrullination;[10] determination of dissociation constants and limiting mobilities of amino acids by free solution electrophoresis;[11] exploring information on hydrodynamic size and shape of peptides and proteins from electrophoresis.[16, 17]

Besides peptides and proteins, nucleic acids are another charged system studied extensively by electrophoresis. DNA condensation by multivalent cations,[18] protein-DNA binding affinities in free solution,[19] abnormalities of bent DNA mobilites,[38, 39] length dependence of free solution electrophoretic mobilities of duplex DNA[20]have been examined. Over the past few years, interests in the field of nanoparticles and colloidal particles have been increasing. The structural properties, such as charge distribution and thickness of the gel layer, of polystyrene sulfonate, a typical model for particles with a uncharged hard core inside and a charged "hairy" gel layer outside, have been studied.[21, 22] Gold nanoparticles, with different sizes and surface charge properties are synthesized to be drug carriers. Electrophoresis proves a good tool to characterize and control their size and charge, and hence their transport properties.[36, 37]

Additionally, several researchers have investigated the electrophoresis behavior of biological cells.[23-25]

1.3 Existing Method of Modeling Electrophoresis

There have been two different approaches followed in modeling free solution electrophoresis of peptides and other charged particles. Modeling firmly grounded in continuum electro-hydrodynamic theory and semi-empirical method bases on extensive experimental data under specific operating conditions. Development of electrophoresis theory of finite rigid particles started in the 1920s, when Huckel[26] derived an expression for the electrophoretic mobility of a small, weakly charged sphere

$$\mu_{Huckel} = \frac{2}{3}\frac{\varepsilon_r \zeta}{C\eta} \qquad (1-3)$$

where ε_r is the relative dielectric constant of the solution, ζ is the surface or "zeta" potential ($\zeta = \frac{Q}{4\pi\varepsilon_r a(1+\kappa a)}$), η is the solvent viscosity, and $C = 4\pi$ (in CGS units) or $1/\varepsilon_0$ where ε_0 is the permittivity of free space (in MKSA units). Previously, Smoluchowski[27] obtained a slightly different expression for the mobility of a large sphere. In essence, the factor of 2/3 in Eq. (1) had to be replaced by 1. Subsequently, Henry investigated the electrophoresis of a conducting sphere. For a very large sphere, Henry's results reduced to those of Smoluchowski. For small particles, however, Henry obtained[28]

$$\mu_{Henry} = \frac{2}{3}\frac{\varepsilon_r \zeta}{C\eta}\left(1 + \frac{1}{16}\kappa^2 a^2 - \frac{5}{48}\kappa^3 a^3 + ...\right) \qquad (1-4)$$

where κ is the Debye-Huckel screening parameter. The fluid contains ions modeled as a

continuum and the ionic strength, I,

$$I = \frac{1}{2}\sum_{\alpha} c_{\alpha 0} z_{\alpha}^2 \qquad (1-5)$$

where the sum extends over the different ionic species present, $c_{\alpha 0}$ is the ambient concentration of species α, and z_{α} is its valence. The Debye-Huckel screening parameter is[29]

$$\kappa = \sqrt{\frac{2q^2 C I}{\varepsilon_r k_B T}} \qquad (1-6)$$

where q is the protonic charge, k_B is Boltzmann's constant, and T is absolute temperature. Thus, Henry's mobility expression reduced to that of Debye for small particles and to that of Smoluchowski for large particles. Henry[28] also gave mobility expressions of a cylinder with a symmetric charge distribution:

$$\mu_{\perp} = \frac{f_{\perp}\varepsilon_r \varsigma}{8\pi\eta} \qquad (1\text{ - }7)$$

$$\mu_{//} = \frac{\varepsilon_r \varsigma}{4\pi\eta} \qquad (1\text{ - }8)$$

where $\mu_{\perp}/\mu_{//}$ is the mobilities perpendicular/parallel to the electric field, $f_{\perp}=1$ if $\kappa a \to 0$, and $f_{\perp}=2$ if $\kappa a \to \infty$.

Starting in the 1960's, numerical strategies requiring computers have been successful in modeling the electrophoresis of charged particles. In late 20th century, Wiersema,[1, 30] O'Brien and White[31] determined the mobility of highly charged spheres numerically. Later on, Yoon and Kim[32] investigated the electrophoresis of weakly charged ellipsoids and Stigter[33] studied the highly charged long rod. Allison[34,35] applied the boundary element method to solve the more general case of electrophoresis of irregularly shaped, highly charged particles with an arbitrary charge distribution.

Independent of the fundamental strategies described above, considerable work has been carried out in developing semi-empirical models to predict the mobility of a peptide using peptide molecular weight, hydrodynamic radius, charge and the number of amino acids in the peptide. Amongst the simplest models, the Offord model ($\mu = Z/M^{2/3}$)[40] has been shown to give good correlation for a lot of experimental data,[12] where μ is the free solution electrophoretic mobility, Z is the net charge, and M is the molecular weight. In the last few years, more sophisticated semi-empirical computer models have been developed that take more detailed account of peptide charge, composition, and number of amino acids.[7,12,43,44] Under specific experimental conditions (pH, temperature, solvent, and buffer composition), these models can be very accurate.

1.4 Outline of this Dissertation

In this dissertation, modeling the free solution electrophoresis of peptides, proteins, DNA and colloidal particles that are based on classic electrokinetic theory is carried out. How factors such as composition, size, charge distribution and salts influence the mobility are examined. Chapter 2 describes the development of the electrophoresis of a bead array model of weakly charged macroions. In Chapter 3, this bead model is applied to the electrophoretic mobility and diffusion of a large number of weakly charged peptides where experimental data is available. Chapter 4 is an extension of Chapter 3, which focuses on the improvements in the bead model to include the ion relaxation and finite size effects. Chapter 5 investigates the electrokinetic transport of rigid macroions in the thin double layer limit. Chapter 6 studies the electrokinetic transport of a spherical gel-layer model particle (polystyrene sulfonate), developing an approach

of charge regulation. Chapter 7 summarizes this dissertation.

Chapter 2

Bead Array Model for Electrophoresis of Weakly Charged Macroions

2.1 Theory of Bead Array Model

A bead array model is developed to determine the electrophoretic mobility of charged macroions numerically.[43] The advantage of the present bead model over the full boundary element calculation of electrophoretic mobility is a tremendous reduction in computation time. This advantage makes the bead model more suitable to model the electrophoresis of a flexible molecule, when numerous conformations need to be sampled.

Before deriving a simple expression for determining electrophoretic mobilities of a bead array, several assumptions will have to be made. The first assumption we shall make is the neglect of ion relaxation. According to a number of investigations,[6,30,31,33,34,44] neglect of ion relaxation is a fairly accurate approximation when the absolute surface or "zeta" potential is less than approximately 25 mV, that is equivalent to a mobility of 0.20 cm^2/kV sec.[7] Under this approximation the bead array model is appropriate for weakly charged macroions. In Chapter 4, the ion relaxation effect will be included in order to model more highly charged macroions.

A second assumption is that when modeling electrophoresis in solution, the reaction field or in the other words, the internal field effect, is ignored. For a sphere with internal dielectric constant ε_I and radius, a, placed in a constant external electric field, **E**, the actual field at position **x** in the fluid where the origin is chosen at the center of the sphere is given by[46]

$$E_{actual}(\underline{x}) \;=\; \underline{E} + \lambda \left(\frac{a}{x}\right)^3 [\underline{\underline{I}} - 3\underline{\underline{X}}]\cdot\underline{E} \qquad (2-1)$$

where $\lambda = (\varepsilon_r - \varepsilon_I)/(2\varepsilon_r + \varepsilon_I)$, $x = |\mathbf{x}|$, and $\mathbf{X} = \mathbf{xx}/x^2$ is the unit position dyadic. From Eq. (2-1) is

clear that the actual field of some point in the fluid is affected by the charged particle placed in it.

However, in the present work this affect has been ignored, corresponding to set $\lambda = 0$ in Eq. (2-1).

Additional assumptions include: first, the solution is dilute so that the interaction between

different bead arrays can be neglected. Second, external fields are weak so that the bead array

does not orient in the direction of the external field. Third, it is possible that the bead array would

rotate as it translates.[47-49] In the modeling of electrophoresis,[49] this "translation-rotation"

coupling has been demonstrated to be small and will be neglected in this work.
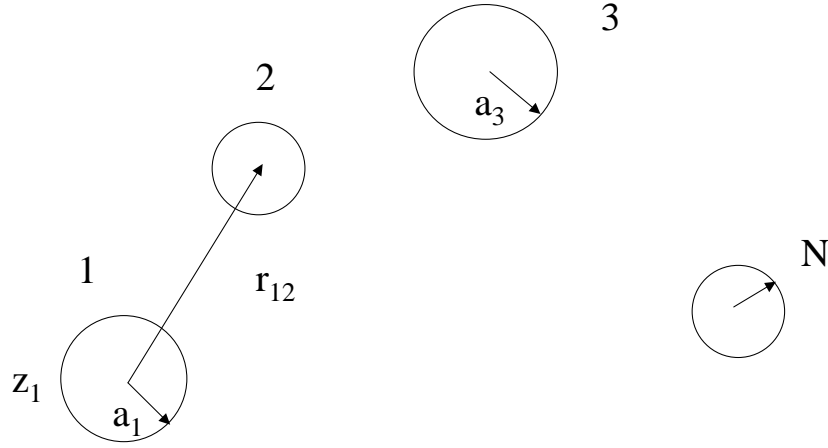
Figure 2-1) Schematic of the Bead Array Model.   The rigid macroion array consists of N beads of radii (a_1, a_2, …. a_N) that are not necessarily equal, and carry net charges, (z_1, z_2, …. z_N). In the figure, r_{12} is the distance between the beads 1 and 2.

A macroion array consisting of N beads of variable radii (a_1, a_2,…a_N) and net charge (z_1, z_2, …z_N) in the units of protonic charge, q, is depicted in Figure 1. In the figure, $r_{jk} = |\mathbf{x}_j - \mathbf{x}_k|$ denotes the center-to-center distance between beads j and k. The array is placed in a Newtonian fluid in the presence of an electric field E. The fluid is assumed to obey the linear Navier-Stokes and solvent incompressibility equations

$$\eta \nabla^2 \underline{v}(\underline{x}) - \underline{\nabla} p(\underline{x}) \;\; = \;\; -\underline{s}(\underline{x}) \qquad (2-2)$$

$$\underline{\nabla} \cdot \underline{v}(\underline{x}) \;\; = \;\; 0 \qquad (2-3)$$

where $\mathbf{v}(\mathbf{x})$, $p(\mathbf{x})$, and $\mathbf{s}(\mathbf{x})$ are the local fluid velocity, pressure, and external force/volume on the

fluid. Also, $\nabla\cdot$ in Eq. (2-2) represents divergence. In the present work, $\mathbf{s(x)}$ arises from the interaction of local ion densities with the external electric field

$$\underline{s}(\underline{x}) = -\rho(\underline{x})\underline{\nabla}\Lambda(\underline{x}) = \rho_0(\underline{x})\underline{E} \qquad (2-4)$$

where $\rho(\mathbf{x})$ is the local charge density, $\rho_0(\mathbf{x})$ is the local equilibrium charge density, $\Lambda(\mathbf{x})$ is the local electric potential, and $\mathbf{E}$ is the external electric field (assumed uniform). Neglecting ion relaxation allows us to replace $\rho(\mathbf{x})$ by $\rho_0(\mathbf{x})$.

It is convenient to rewrite Eq. (2-2) and (2-4) in tensor form.

$$\underline{\nabla}\cdot\underline{\underline{\sigma}}_{Total} = \underline{\nabla}\cdot(\underline{\underline{\sigma}}_H + \underline{\underline{\sigma}}_E) = \underline{0} \qquad (2-5)$$

where

$$\underline{\underline{\sigma}}_H = -p\underline{\underline{I}} + \eta(\underline{\nabla}\underline{v} + \underline{\nabla}\underline{v}^T) \qquad (2-6)$$

$$\underline{\nabla}\cdot\underline{\underline{\sigma}}_E = \underline{s} = \rho_0\underline{E} \qquad (2-7)$$

The "T" superscript in Eq. (2-6) reprensents transpose of a second rank dyadic tensor.

Begin with the differential form of the Lorentz Reciprocal Theorem,[47-49]

$$\underline{s}'\underline{v} + \underline{\nabla}\cdot(\underline{v}\cdot\underline{\underline{\sigma}}_H') = \underline{s}\cdot\underline{v}' + \underline{\nabla}\cdot(\underline{v}'\underline{\underline{\sigma}}_H) \qquad (2-8)$$

where $\underline{v}$, $\underline{s}$ and $\underline{\underline{\sigma}}_H$ represent the velocity field, external force, and hydrodynamic stress of the bead array and the primed fields represent some other solution we are free to choose. In most Boundary Element applications, a singular solution based on the Oseen tensor is chosen.[20,34,45,48] In the present work, the singular (Green's Function) solution of a small, weakly charged particle is chosen.[50] This velocity/pressure field satisfies

$$\eta\nabla^2\underline{v}'(\underline{r}) - \underline{\nabla}p'(\underline{r}) = -q\underline{E}\delta(\underline{r}) + q\kappa^2 F(\kappa,r)\underline{E} \qquad (2-9)$$

$$\underline{\nabla}\cdot\underline{v}'(\underline{r}) = 0 \qquad (2-10)$$

where $\mathbf{r} = \mathbf{x} - \mathbf{y}$, $r = |\mathbf{r}|$, the differential operators act on variable x, δ is the delta function, and

$$F(\kappa, r) \;=\; \frac{e^{-\kappa r}}{4\pi r} \qquad (2-11)$$

The solutions are[50]

$$\underline{v}'(\underline{r}) \;=\; q\underline{\underline{U}}(\underline{r}) \cdot \underline{E} \qquad (2-12)$$

$$p'(\underline{r}) \;=\; q\underline{P}(\underline{r}) \cdot \underline{E} \qquad (2-13)$$

where

$$\underline{\underline{U}}(\underline{r}) \;=\; \frac{1}{4\pi\eta}\left\{ [w_1(r)+\frac{1}{\kappa}w_2(r)-\frac{1}{\kappa^2}(v_3(r)-w_3(r))]\underline{\underline{I}} \right.$$

$$\left. +[\frac{3}{\kappa^2}(v_3(r)-w_3(r))-(w_1(r)+\frac{3}{\kappa}w_2(r))]\underline{\underline{R}} \right\} \qquad (2-14)$$

$$\underline{P}(\underline{r}) \;=\; \frac{e^{-\kappa r}}{4\pi r^3}(1+\kappa r)\underline{r} \qquad (2-15)$$

I is the 3 by 3 identity tensor, **R** = **rr**/r2 is the position dyadic, and

$$v_n(r) \;=\; \frac{1}{r^n} \qquad (2-16)$$

$$w_n(r) \;=\; \frac{e^{-\kappa r}}{r^n} \qquad (2-17)$$

In the limit of $\kappa \to 0$, Eq. (2-14) reduces to the Oseen tensor.

Next, focus on the problem at hand, electrophoresis of a bead array. Integrate Eq. (2-5) over S_b, where b is the radius of a large spherical volume enclosing the bead array and surrounding fluid.

$$\underline{0} \;=\; \sum_{j=1}^{N} S_j \underline{F}_j + \int_{S_b}\underline{\underline{\sigma}}_H \cdot \underline{n}\, dS_x + \underline{E}\int_V \rho_0\, dV_x \qquad (2-17)$$

where

$$\underline{F}_j \;=\; -\int_{S_j}\underline{\underline{\sigma}}_H \cdot \underline{n}\, dS_x / S_j \qquad (2-18)$$

Because there is no net force exerted by the bead array on fluid at the surface S_b,

$$\sum_{j=1}^{N} q\, z_j\, \underline{E} \;=\; \sum_{j=1}^{N} S_j \underline{F}_j \qquad (2-19)$$

Before using Eq. (2-8) and the singular solution, consider an uncharged bead (call it bead j) moving with the fluid at the same velocity. Under these conditions, s = 0, and $\underline{\underline{\sigma}}_H = 0$. Integrate Eq. (2-8) over a large sphere inclosing the bead, apply the divergence therem to the σ'_H term, and assume $\kappa b \gg 1$ to obtain

$$\int_{S_j} \underline{\underline{\sigma}}_H ' \cdot \underline{n}\, dS_x \;=\; q\underline{E}\left[\Phi(\underline{y},V_{ej}) - \kappa^2 \int_{V_{ej}} F(\kappa,r)\, dV_x \right] \qquad (2-20)$$

where S_j represents the surface of bead j, $\underline{n}$ is the local outward normal from S_j, V_{ej} is the volume exterior to bead j, $\Phi(\underline{y},V_{ej})$ equals 1 if $\underline{y}$ lies within V_{ej}, 0 if $\underline{y}$ lies outside of V_{ej} , 1/2 if $\underline{y}$ lies on the boundary surface, S_j.

Now, going back to the problem of the bead array, integrate Eq. (2-8) over the entire fluid inside the sphere of radius b, making use of the singular solution of a small, weakly charged sphere, and apply the divergence theorem. It is straightforward to show

$$\underline{v}(\underline{y})\Phi(\underline{y},V) \;=\; \int_V [\underline{\underline{U}}(\underline{r}) \cdot \underline{s}(\underline{x}) + \kappa^2 F(\kappa,r)\underline{v}(\underline{x})]\, dV_x + \sum_{j=1}^{N} \int_{S_j} \underline{\underline{U}}(\underline{r}) \cdot \underline{f}(\underline{x})\, dS_x$$

$$+ \sum_{j=1}^{N} \underline{v}_{j0}\Phi(\underline{y},V_{ej}) - \kappa^2 \sum_{j=1}^{N} \underline{v}_{j0} \int_{V_{ej}} F(\kappa,r)\, dV_x \qquad (2-21)$$

where

$$\underline{f}(\underline{x}) \;=\; -\underline{\underline{\sigma}}_H(\underline{x}) \cdot \underline{n}(\underline{x}) \qquad (2-22)$$

The last two terms on the right hand side, rhs, of Eq. (2-21) can be written

$$\sum_{j=1}^{N} \underline{v}_{j0}[\Phi(\underline{y},V_{ej}) - \kappa^2 \int_{V_{ej}} F(\kappa,r)\, dV_x] \;\cong\; \sum_{j=1}^{N} \underline{v}_{j0}[\Phi(\underline{y},V_{ej}) - 1] \qquad (2-23)$$

f($\underline{x}$) in the second term of Eq. (2-21) can be replaced with F_j (Eq. (2-18)), assuming f($\underline{x}$) is

uniform over individual bead. Ignoring ion relaxation and the internal field effect, $s(\underline{x})$ can be approximated with Eq. (2-4). For the local equilibrium charge density in the vicinity of the macroion array,

$$\rho_0(\underline{x}) \;=\; q\sum_{\alpha} z_{\alpha} c_{\alpha 0} e^{-q z_{\alpha} \Lambda_0(\underline{x})/k_B T} \;\cong\; \frac{\varepsilon_r \kappa^2}{C} \Lambda_0(\underline{x}) \qquad (2-24)$$

only linear terms of the equilibrium potential, $\Lambda_0(\underline{x})$, are retained. The equilibrium potential of a bead array of radius $\{a_j\}$ and charge $\{z_j\}$ is approximated by the solution of the linear Possion-Boltzman equation.

$$\Lambda_0(\underline{x}) \;=\; \frac{qC}{\varepsilon_r} \sum_{j=1}^{N} z_j F(\kappa, r_j) \qquad (2-25)$$

where $r_j = |x - x_j|$ and x_j is the center of bead j.

From Eq. (2-4), (2-24), and (2-25),

$$\underline{s}(\underline{x}) \;\cong\; -q \kappa^2 \underline{E} \sum_{j=1}^{N} z_j F(\kappa, r_j) \qquad (2-26)$$

The most difficult term to deal with in Eq. (2-21) concerns the volume intergral over $v(\underline{x})$ since we do not know what $v(\underline{x})$ is. However, an approximate solution of $v(x)$ can be obtained compared with the solution of $s(\underline{x})$. For the singular solution we choose, it is clearly shown in Eq. (2-9) that

$$\underline{s}'(\underline{x}) = -q \underline{E} \delta(\underline{r}) + q \kappa^2 F(\kappa, r) \underline{E} \qquad (2-27)$$

Ignoring the delta function, which only contributes at the single source point in any event, and comparing with Eq. (2-26), we see that our singular solution corresponds to a point charge of charge +1 in external field, E, translating under steady state conditions. Thus an approximate velocity field to use in the first term on the rhs of Eq. (2-21) is

$$\underline{v}(\underline{x}) \quad \cong \quad qA \sum_{j=1}^{N} z_j \underline{\underline{U}}(\underline{r}_j) \cdot \underline{E} \qquad (2-28)$$

where A is a constant to be discussed. Choose a local origin to be at the center of any particular bead, call it bead k, and average Eq. (2-28) over a_k, where a_k is a point on the surface of bead k. Retaining terms to first terms to first order in κa_κ, Eq. (2-28) becomes

$$<\underline{v}(\underline{x})>_{S_k} \quad = \quad qA \left[\frac{z_k e^{-\kappa a_k}}{\varsigma_k} + \sum_{j \neq k} z_j c(\underline{r}_{jk}) \right] \cdot \underline{E} \qquad (2-29)$$

where $<>_{Sk}$ indicates averaging over the surface of bead k and $\varsigma_k = 6\pi\eta a_k$ is the friction coefficient of bead k. For a bead array undergoing steady state translation in a constant electric field, we should have

$$<\underline{v}(\underline{x})>_{S_k} \quad = \quad \underline{\underline{\mu}} \cdot \underline{E} \qquad (2-30)$$

where $\underline{\underline{\mu}}$ denotes the electrophoretic mobility tensor of our bead array. If stick boundary conditions are assumed, the particle velocity and fluid velocity should match on S_k. In practice, Eq. (2-29) and (2-30) cannot be satisfied on all beads simultaneously and further approximations have to be made. A common approximation in polymer transport theories that originated with Kirkwood[51] involves orientational preaveraging of the hydrodynamic interaction tensor. In past work, this has been applied to the Oseen tensor and in the present case, orientational preaveraging is applied to $\underline{\underline{U}}$. This is accomplished by replacing $\underline{\underline{U}}$ given by Eq. (2-14) with 1/3 of its trace

$$<\underline{\underline{U}}(\underline{r})>_{opa} \quad = \quad \frac{2F(\kappa,r)}{3\eta} \underline{\underline{I}} \qquad (2-31)$$

Also, the mobility tensor, $\underline{\underline{\mu}}$ in Eq. (2-30) is replaced with a scalar mobility μ. Although Eq. (2-29) and (2-30) cannot be satisfied simultaneously for all beads, A can be chosen so that, on

average, they are satisfied. Mutiply Eq. (2-29) by

$$m_k = \frac{S_k}{S_{Tot}} \qquad (2-32)$$

where S_{Tot} is the total surface area of all the beads. Next, sum this over all beads and set it equal

to μE. Solving for A then yields

$$A = \frac{6\pi\eta\mu}{q\kappa P_1} \qquad (2-33)$$

$$P_1 = \sum_{k=1}^{N} m_k \left[\frac{z_k}{\kappa a_k} e^{-\kappa a_k} + \sum_{j \neq k} \frac{z_j e^{-\kappa r_{jk}}}{\kappa r_{jk}} \right] \qquad (2-34)$$

where $r_{jk} = |\mathbf{x}_j - \mathbf{x}_k|$. Choose $\mathbf{y} = \mathbf{x}_k$, the center of bead k. The first term on the right hand side of

Eq. (2-26) can then be approximated

$$\int_V [\underline{U}(r_k) \cdot \underline{s}(\underline{x}) + \kappa^2 F(\kappa, r)\underline{v}(\underline{x})] dV_x$$

$$\cong \frac{2q\kappa^2}{3\eta}(A-1)\underline{E}\sum_{j=1}^{N} z_j \int_V F(\kappa, r_k)F(\kappa, r_j) dV_x$$

$$\cong \frac{q\kappa(A-1)}{12\pi\eta} P_2^{(k)} \underline{E} \qquad (2-35)$$

where

$$P_2^{(k)} = z_k e^{-2\kappa a_k} + \sum_{j \neq k} e^{-\kappa r_{jk}} \qquad (2-36)$$

After straightforward substitution, Eq. (2-26) can be written

$$\mu(1 - \frac{P_2^{(k)}}{2P_1}) = \frac{\kappa q}{6\pi\eta} \left[\sum_{j=1}^{N} x_{kj} g_j - \frac{1}{2} P_2^{(k)} \right] \qquad (2-37)$$

where $x_{kj} = \exp(-\kappa a_k)/(\kappa a_k)$ if $k = j$ and $\exp(-\kappa r_{jk})/(\kappa r_{jk})$ if $k \neq j$. Also, g_j is defined by the identity

$$S_j \underline{F}_j = q g_j \underline{E} \qquad (2-38)$$

Also introduce the identities

$$P_2 = \sum_{k=1}^{N} m_k P_2^{(k)} \qquad (2-39)$$

$$P_1^{'(k)} = \sum_{j=1}^{N} m_j z_T x_{jk} \qquad (2-40)$$

$$z_T = \sum_{j=1}^{N} z_j \qquad (2-41)$$

$$P_1^{'} = \sum_{k=1}^{N} m_k P_1^{'(k)} \qquad (2-42)$$

Multiply Eq. (2-37) by m_k, sum over k, use the above identities, and solve for μ

$$\mu = \frac{\kappa q}{6\pi\eta}\left(1 - \frac{P_2}{2P_1}\right)^{-1}\left(\sum_{j,k} m_k x_{kj} g_j\right) - \frac{\kappa q P_2}{12\pi\eta}\left(1 - \frac{P_2}{2P_1}\right)^{-1} \qquad (2-43)$$

What is unknown in Eq. (2-43) is g_j's. Eq. (2-37) and (2-43) gives a series of N equations in N

unknowns

$$\sum_{j=1}^{N} D_{kj}^{'} g_j = \xi_k^{'} \qquad (2-44)$$

$$D_{kj}^{'} = \frac{P_1^{'(j)}}{z_T}\left(1 - \frac{P_2^{(k)}}{2P_1}\right) - \left(1 - \frac{P_2}{2P_1}\right)x_{kj} \qquad (2-45)$$

$$\xi_k^{'} = \frac{1}{2}(P_2 - P_2^{(k)}) \qquad (2-46)$$

g_j's cannot be obtained by simply constructing a N by N **D**'s matrix, inverting it, and then solving

for the component, g_j. Because the N equations represented by Eq. (2-44) are not independent. If

$D_{kj}^{'}$ is multiplied by m_k and summed over k, the net sum is zero. Thus it is impossible to invert **D**.

However, From Eq. (2-19), (2-38) and (2-41),

$$\sum_{j=1}^{N} g_j = z_T \qquad (2-47)$$

If we simply replace Eq. (2-44) with Eq. (2-47) for k = 1 (or any k for that matter), then the system of equations becomes invertible. In other words, define

$$\underline{\underline{D}} \cdot \underline{g} \;=\; \underline{\xi} \qquad (2-48)$$

where $D_{kj} = D_{kj}{}'$, and $\xi_k = \xi_k{}'$ for k > 1, and $D_{kj} = 1$ and $\xi_k = z_T$ for k=1. Also, **D** in Eq. (2-48) is an N by N matrix and **g** and ξ are N by 1 column vectors. It is now possible to invert **D** and obtain the N components of **g** from

$$\underline{g} \;=\; \underline{\underline{D}}^{-1} \cdot \underline{\xi} \qquad (2-49)$$

Once the g_j are known, they can be substituted into Eq. (2-43) to determine μ.

2.2   Average Force Approximation

The mobility expression summarized by Eq. (2-43) and the solution of the components, g_j, given by Eq. (2-49) represent one of the principal results of the present work. However, numerical inversion of a potentially large matrix is still required. It is possible to simplify the results further by making one additional approximation. For an array of N beads of equal radius, a, the Kirkwood Approximation leads to the following expression (see, for example, p. 25 of reference 51) for the translational diffusion constant, D_{TK}

$$D_{TK} \;=\; \frac{k_B T}{6\pi\eta a N}\left(1 + \frac{1}{N}\sum_{k=1}^{N}\sum_{j\neq k}^{N}\frac{a}{r_{jk}}\right) \qquad (2-50)$$

Although Kirkwood himself[51] as well as a number of early investigators[52] initially believed this approximation was exact, it is now recognized that this is not true.[53-56] The origins of Kirkwood's error were first described by Ikeda[53], but a subsequent study[55] is useful in the present context since it identifies a constraint on the hydrodynamic forces, $\mathbf{F}_j$, that must be satisfied in

order for the Kirkwood Approximation to be exact. For the special case of an array of beads of equal size, the Kirkwood Approximation is exact if $\mathbf{F}_j = \mathbf{F}_{Tot}/N$ where $\mathbf{F}_{Tot}$ is the total hydrodynamic force exerted by the bead array on the fluid. In the present work, we shall also consider an "average force approximation" where the hydrodynamic force/area exerted by bead j on the fluid, $\mathbf{F}_j$, is replaced with an average force/unit area, $\mathbf{F}_{Ave.}$ From Eqs. (2-19), (2-32), (2-38), (2-47) and the above "average force approximation,"

$$g_j \;=\; m_j\, z_T \qquad (2-51)$$

Substituting Eq. (2-51) into Eq. (2-43) and making use of Eq. (2-40),

$$\mu_{AFA} \;=\; \frac{\kappa q P_1'}{6\pi\eta}\left(1-\frac{P_2}{2P_1'}\right)\left(1-\frac{P_2}{2P_1}\right)^{-1} \qquad (2-52)$$

where the "AFA" subscript emphasizes that the "average force approximation" has been made. In the special case that all beads are of equal size and charge, then $P_1 = P_1'$ and Eq. (2-52) simplifies to

$$\mu_{AFA} \;=\; \frac{qz}{6\pi\eta a}\left[e^{-\kappa a} + \frac{1}{N}\sum_{k=1}^{N}\sum_{j\neq k}^{N}\frac{a\,e^{-\kappa r_{jk}}}{r_{jk}}\right] \qquad (2-53)$$

where a and z are subunit radius and charge, respectively. Eq. (2-53) is similar to the Kirkwood Approximation for the translational diffusion constant of a bead array of identical subunits given by Eq. (2-50). Note, however, that inter-subunit "screening" falls off as exp(-κr)/r in the case of electrophoresis, but as 1/r in the case of diffusion.

2.3   Testing the Accuracy of Bead Array Model

Because of the approximations discussed in the beginning of this chapter, the mobility

expressions derived are limited to subunits that are weakly charged ($|\zeta| \leq 25$ mV or $|\mu| \leq 0.20$ cm^2/kV sec) and small ($\kappa a_j \leq 1.0$). For $\kappa a = 1.0$, for example, neglecting the internal field (distortion of the external electric field by a conducting or low dielectric sphere) causes $|\mu|$ to be underestimated by 6 %. Next, assess the effect of "preaveraging" the hydrodynamic interaction, or **U** tensor. In modeling the transport of (uncharged) freely rotating chains, Garcia de la Torre and coworkers found that orientational preaveraging introduces an error in the translational diffusion constant of between 0 % and 3 % depending on the number of subunits present and the ratio of bead radius to virtual bond length.[57] In all of the cases investigated, error caused by orientational preaveraging was 1/3 or less than the error caused by the Kirkwood Approximation.[57] In the case of electrophoresis, where hydrodynamic interactions are "cutoff" over shorter distances than in diffusion, we would expect the preaveraging approximation to be even less important. On this basis, we conclude that the orientational preaveraging approximation can introduce an error of several percent, but that it introduces less error than the AFA we shall turn our attention to next. Consider rods or rings made up of a discrete number, N, of beads of equal radius, a, near neighbor bead separation, b, and subunit charge, z. For the results summarized in Table 2-1, we set a = 1 nm, T = 20 °C, η = 1.0 cp, and z = +1.0. For this subunit radius, κa = .01 and .10 correspond to ionic strengths of 9 x 10^{-4} and 9 x 10^{-2} moles/liter, respectively. For the rings, all subunits are indistinguishable and the AFA introduces no additional error. For the rods, however, this is not the case and indeed the g_j's for the end subunits are quite different from the remaining values. (The g_j's are computed using Eq. (2-49).) In the table, we have included averages of the two end subunits, $\langle g \rangle_{end}$, and the average over the remaining subunits, $\langle g \rangle_{int}$, for the case of rods. Mobilities are given in cm^2/kV sec and are computed using Eq. (2-43) for μ, or Eq. (2-52) for μ_{AFA}. The "error" is μ_{AFA}/μ - 1.

Table 2-1

Mobility of Rings and Rods

Geometry	N	b(nm)	κa	$<g>_{int}$	$<g>_{end}$	μ	$μ_{AFA}$	Error
ring	3	2.0	.01	1.000	---	.1464	---	---
rod	"	"	"	.612	1.194	.1298	.1327	.022
ring	"	"	.10	1.000	---	.0427	---	---
rod	"	"	"	.851	1.075	.0387	.0392	.013
ring	"	4.0	"	1.000	---	.0320	---	---
rod	"	"	"	.992	1.004	.0318	.0318	.000
ring	10	2.0	.01	1.000	---	.2179	---	---
rod	"	"	"	.862	1.552	.1791	.1851	.034
ring	"	"	.10	1.000	---	.0440	---	---
rod	"	"	"	.960	1.158	.0419	.0422	.007
ring	"	4.0	"	1.000	---	.0320	---	---
rod	"	"	"	.997	1.010	.0319	.0319	.000
ring	50	2.0	.01	1.000	---	.2266	---	---
rod	"	"	"	.958	1.819	.2114	.2142	.013
ring	"	"	.10	1.000	---	.0436	---	---
rod	"	"	"	.994	1.192	.0432	.0433	.002
ring	"	4.0	"	1.000	---	.0320	---	---
rod	"	"	"	.999	1.012	.0320	.0320	.000

From the results of Table 2-1, it is clear that although actual subunit forces vary along the rod, particularly at the rod ends, the AFA leads to an overestimation of μ by several percent, at most. This error is greatest for small κa, intermediate rod lengths, and small b. It should be emphasized that for b = 2 nm, which are the cases where the error is greatest, near neighbor beads are actually touching. Increasing b to 4 nm substantially reduces error associated with the AFA.

Next, we consider discrete wormlike chain models where the number of identical subunits is N, the subunit radius is a, the virtual bond length (distance between nearest neighbors) is b, the persistence length is P, and the charge per subunit is z. A particular chain conformation is selected, at random, from an equilibrium distribution.[58] For each chain, both μ and μ_{AFA} are computed. For a particular set of model parameters, this procedure is repeated for 1000 chains and averages are determined for both μ and μ_{AFA}. Standard deviations for single chain mobilities are also computed. Since a likely application of this modeling is polypeptides, we shall choose model parameters that are anticipated to be appropriate.[10,13,59-62] Summarized in Table 2-2 are results for a = 0.3 nm, b = 0.6 nm, P = 2.0 nm, z = 0.15, I = 10^{-3} M, T = 20 °C, and η = 1.0 cp. Standard deviations are in parentheses and the "error" is μ_{AFA}/μ - 1. Consistent with earlier results on rigid rods, the AFA overestimates the mobility by several percent. Although some variation is seen in mobilities between different wormlike chain conformations, it amounts to from 2 to 2.5 % in this particular example.

Table 2-2

Mobility Results for Discrete Wormlike Chain Models

$(a = 0.3 \text{ nm}, b = 0.6 \text{ nm}, P = 2.0 \text{ nm}, z = 0.15, I = 10^{-3} \text{ M})$

N	$\mu_{AFA}^{(1)}$(sd)	μ(sd)	Error
5	.093(.002)	.091(.002)	.025
10	.121(.005)	.118(.005)	.029
15	.139(.008)	.135(.008)	.030
20	.153(.012)	.148(.010)	.031
25	.164(.014)	.159(.012)	.033
30	.175(.018)	.169(.015)	.036
35	.184(.019)	.177(.016)	.039
40	.192(.022)	.185(.018)	.038
45	.199(.022)	.190(.018)	.047
50	.206(.025)	.197(.020)	.046

(1) mobilities are in cm^2/kV sec at 20 °C with $\eta = 1cp$

In experimental studies on proteins and polypeptides,[10,13,59-62] μ is typically fit to an empirical equation of the form

$$\mu = \frac{Az_T}{M^{\alpha}} \qquad (2-54)$$

where A is a constant, z_T is the total charge (in protonic units), and M is the molecular weight. The value of α that best fits experiment depends to some extent on the peptides being

investigated and other experimental conditions, but an optimal α is typically around 0.66.[13] To see if the results in Table 2-2 are consistent with the general form of Eq. (2-54) and, if so, give physically reasonable α's, linear least squares fits to equations of the following form are considered,

$$-\ln\left(\frac{\mu}{z_T}\right) \;=\; c + \alpha\ln(N) \qquad (2-55)$$

The results of Table 2-2 are plotted in Figure 2-2 to illustrate the fit to Eq. (2-55). Diamonds and squares correspond to mobility results with and without the AFA, respectively. It is clear that the model results are entirely consistent with the functional dependence of Eq. (2-55) and consequently Eq. (2-54). Furthermore, linear fits to the curves in Fig. 2-2 give $\alpha = .657$ (AFA), .667 (no AFA) both of which are entirely consistent with independent experiment. However, the parameters c and α do depend on the wormlike chain model parameters as summarized by Table 2-3. These come from studies analogous to Table 2-2 and Figure 2-2. Other parameters being equal, α increases as P or I increases. In addition to the wormlike chain models considered above, we also examined a few cases where the charge distribution was not uniform. This, however, was found to have little influence on the results.
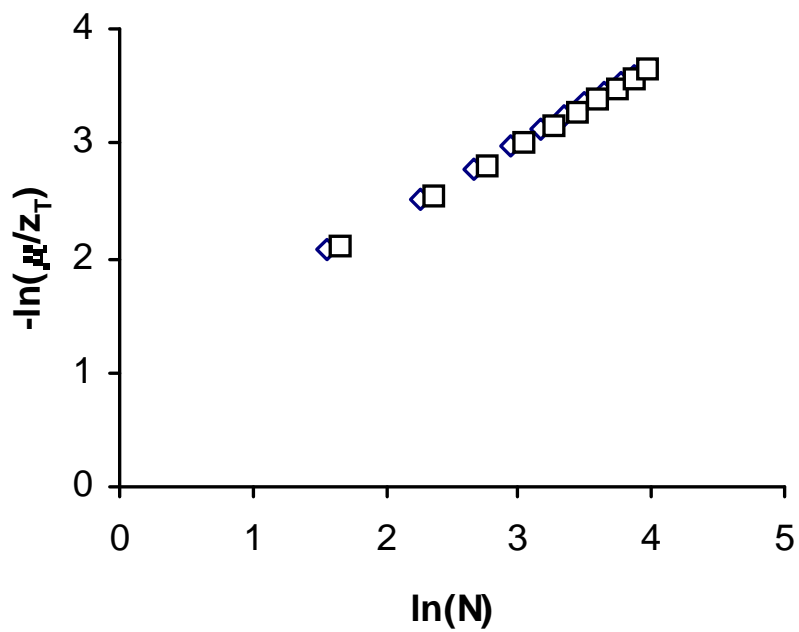
Figure 2-2) Dependence of μ on N for a Discrete Wormlike Chain Model. Model parameters are: a = 0.3 nm, b = 0.6 nm, P = 2.0 nm, z = 0.15, I = 10^{-3} M, T = 20 °C, and η = 1.0 cp. Diamonds and squares correspond to mobility results with and without the AFA, respectively

Table 2-3

Parameters α and c for Wormlike Chain Models

b(nm)	P(nm)	z	I(M)	AFA	c	α
0.6	1.0	.15	.001	yes	1.127	.569
"	"	"	"	no	1.107	.596
"	2.0	"	"	yes	1.015	.657
"	"	"	"	no	1.018	.667
"	"	.25	.010	yes	.976	.758
"	"	"	"	no	.987	.767
1.2	"	.30	.001	yes	1.290	.705
"	"	"	"	no	1.259	.724
0.6	10.0	.15	"	yes	.824	.771
"	"	"	"	no	.861	.767

2.4 Summary

In this chapter, two expressions for the free solution electrophoretic mobility, Eqs. (2-43) and (2-52), are derived that are applicable to macroions that are modeled as rigid bead arrays. It is assumed that internal field effects are small (valid for $\kappa a_j \leq 1$), ion relaxation is negligible (valid for weakly charged macroions),

interparticle interactions are negligible (valid for dilute solutions), and no orientation of the macroion occurs in the presence of external electric field, $\mathbf{E}$ (valid if $|\mathbf{E}|$ is small). In order to

obtain tractable mobility expressions, it is also necessary to "orientationally preaverage" the

hydrodynamic interaction tensor, **U**. What results is Eq. (2-43) and its supplement, Eq. (2-49).

In is concluded that this preaveraging approximation leads to an <u>overestimate</u> of μ by several

percent. To simplify the mobility expression further and avoid the necessity of matrix inversion,

an additional "average force approximation," or AFA, is made. What results is Eq. (2-52). It is

concluded that the AFA also leads to an additional overestimation of mobility by a few percent.

Specific values for rods and discrete wormlike chains are given in the Results section. It should

be emphasized that the AFA and "orientational preaveraging" approximations are deeply rooted

in polymer transport theory.[51] These approximations are applied to the problem of

electrophoretic transport in the present work. An additional point that needs to be made is that

that assumption of ignoring the internal field leads to an <u>underestimation</u> of mobililty, whereas

the AFA and "orientational preaveraging" approximations lead to an <u>overestimation</u> of mobility.

Hence, the approximations tend to be self canceling.

Chapter 3

Modeling the Electrophoretic Mobility and Diffusion of Weakly Charged Peptides

3.1 Introduction

In Chapter 2, a bead array model for determining the electrophoretic mobility is developed and tested. In this chapter this model is built on the structural and charge properties of weakly charged peptides. Shown in Figure 3-1 is a scheme of polypeptide secondary structure determined by two torsion angles: ϕ (rotation about the N- C_α bond) and φ (rotation about the C_α-C bond). It has long been recognized that free solution electrophoretic mobilities of peptides depend on size and charge, and it is physical differences between peptides such as these that is responsible for their ease of separation in the first place. In order to better understand why peptides separate the way they do, considerable work has been done using simiempirical models which usually are written [10,13,59-62] as Eq. (2-54) defined in the previous chapter. Empirically, α is found to vary from 1/3 to 2/3 although a value closer to the latter appears more appropriate under most conditions (see, for example reference 12).
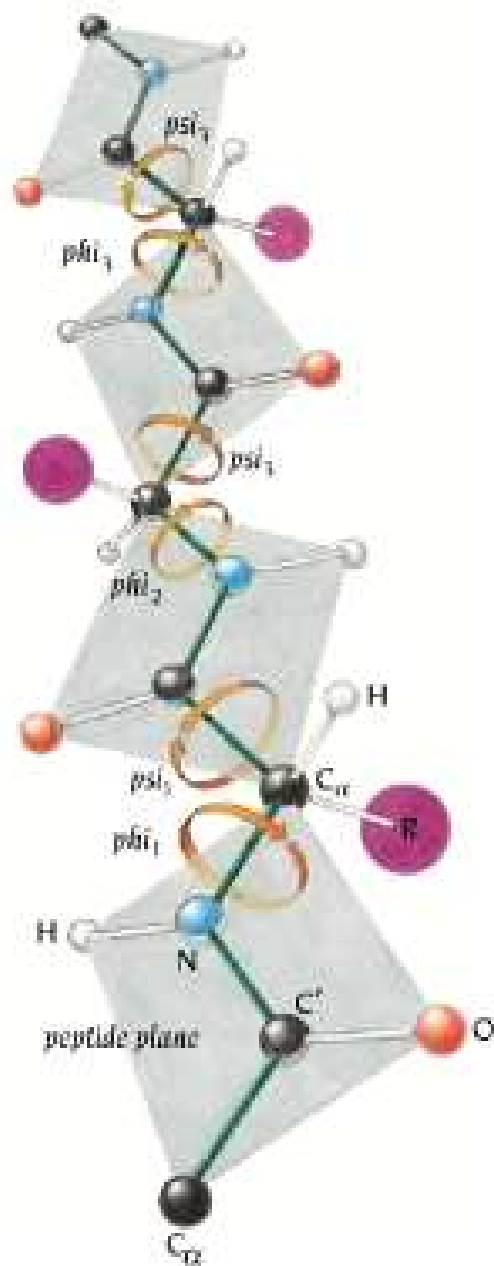
Figure 3-1) Scheme of Polypeptide Secondary Structure.[63]

The motivation of the present study is the development and evaluation of a theoretical

methodology specific to weakly charged peptides that fulfils four conditions. First, it is grounded

firmly in classical electrohydrodynamic theory. Second, it accounts in an approximate way for the irregular shape, charge distribution, and flexibility of a peptide of variable size and composition. Third, it is capable of yielding accurate mobilities. Finally, it is sufficiently simple and also computationally fast to be useful to a wide audience. Specifically, we demonstrate that classical electrokinetic theory is able to accurately predict the electrophoretic mobilities of a large number of peptides containing from 2 to over 40 amino acids. The methodology described in the present work fulfils these four conditions and because of this, should be of considerable value in predicting peptide mobilities, in understanding specific peptide mappings, and in using mobilities to extract structural information about peptides.

By "weakly charged", we mean the absolute surface or "zeta" potential does not exceed 25 mV,[29] or equivalently, the absolute electrophoretic mobility does not exceed approximately 0.20 cm^2/kV sec.[45] For more highly charged peptides, the "relaxation effect" discussed previously needs to be taken into account. This shall be discussed in the following chapter.

3.2 Modeling

A peptide made up of X amino acids is modeled as a string of N = 2X beads. This "two bead per amino acid" model allows us to account, in the simplest manner possible, for the overall composition, conformation, and transport of a linear peptide chain consisting of a particular sequence of amino acids. Odd numbered "backbone" beads (1,3,5,…) are centered on the α-carbons and represent the peptide backbone units of the chain. It is assumed that nearest neighbor backbone beads touch each other. Even numbered beads (2,4,6,…) represent the R-groups of the particular amino acids. This is shown schematically in Figure 3-2. All odd numbered beads are assigned a bead radius of 0.19 nm in order to reproduce the known near neighbor C_α to C_α distance in peptides of 0.38 nm.[64] The radii of the even numbered beads are assigned on the basis of the translational diffusion constants of the free amino acids, D_{aa}.[65-67]

The hydrodynamic radius, R_f, of a free amino acid, is given by the Stokes-Einstein relation

$$R_f = \frac{k_B T}{6\pi\eta D_{aa}} \qquad (3-1)$$

where k_B is Boltzmann's constant, T is absolute temperature, and η is the solvent viscosity.
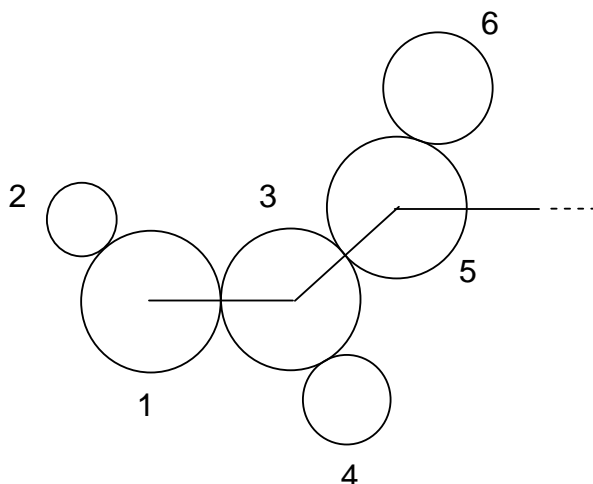
Figure 3-2) Bead model of a peptide. A peptide made up of X amino acids is modeled as N = 2X beads. Odd numbered (touching) beads represent the C_α atoms of the amino acids and even numbered beads represent the R groups. The radii of the odd numbered beads is .19 nm and the radii of the even numbered beads depends on the amino acid and is defined on the basis of the amino acid diffusion constant.

Summarized in Table 3-1 are R_f's for the amino acids. Entries that are not in parenthesis are taken directly from the literature and entries in parenthesis are estimated using the "van der Waals increment method" of Edward.[68] For small molecules with R_f in the range of 0.2 to 0.6 nm, which is the size range of the amino acids, Edward has shown that $R_f \cong (3v_w/4\pi)^{1/3}$ where v_w is the van der Waals volume of the molecule. Furthermore, v_w can be estimated from volume increments tabulated in Table 1 of reference 68. Consider two similar molecules, 1 and 2, where the diffusion constant of 1 is known but not 2. Also let $\delta v = v_w(2) - v_w(1)$ denote the difference in van der Waals volume between the two. Then R_2 can be estimated by

$$R_2 = R_1 \left(1 + \frac{3\delta v}{4\pi R_1^3} \right)^{1/3} \qquad (3-2)$$

Eq. (3-2) is used to estimate the R_f's of amino acids whose diffusion constants are unknown.

When free amino acids polymerize to form peptides, a single water molecule is lost for each amino acid that is added onto a growing peptide chain. On the basis of volume increments, $\delta v = -.0186$ nm^3. To account for the loss of water, the effective hydrodynamic radius of amino acids incorporated into a peptide chain, R_s, are estimated using Eq. (3-2) with the loss of 1 or ½ water for interior or end amino acids, respectively. These radii are also included in Table 3-1. (It should be noted that these radii have recently been modified as a result of NMR measurements of the diffusion constants of amino acids.[76] The results reported in this chapter were carried out with the older radii and consequently those are reported here. These changes do not significantly alter the model mobilities.)

Table 3-1

Hydrodynamic radii (in nm) for the amino acids

Amino acid	Reference	R_f	Interior R_s	a_s	End R_s	a_s
Ala (A)	29	.260	.236	.162	.248	.182
Arg (R)	29	.373	.362	.328	.367	.334
Asn (N)	30	.296	.278	.224	.287	.237
Asp (D)		(.296)	.278	.224	.287	.237
Cys (C)		(.285)	.276	.222	.265	.208
Gln (Q)	30	.323	.308	.264	.316	.273
Glu (E)		(.323)	.308	.264	.316	.273
Gly (G)	29	.233	.202	.0885	.218	.129
His (H)		(.310)	.302	.256	.294	.246
Ile (I)		(.339)	.326	.285	.333	.294
Leu (L)	29	.339	.326	.285	.333	.294
Lys (K)		(.343)	.337	.298	.330	.290
Met (M)		(.308)	.300	.253	.291	.243
Phe (F)	31	.347	.334	.296	.341	.303
Pro (P)	29	.268	.246	.178	.257	.196
Ser (S)	30	.279	.258	.197	.269	.212
Thr (T)	30	.307	.290	.241	.299	.252
Trp (W)	29	.350	.337	.299	.344	.306
Tyr (Y)	31	.357	.345	.308	.351	.316
Val (V)	29	.292	.274	.219	.283	.232

As is well known, polypeptides possess a combination of structural characteristics that make them unique in the realm of polymers. Because of the rigidity of the peptide bond unit, the conformation of a polypeptide chain is essentially defined by a succession of torsion angles, $\{\phi_i, \psi_i\}$.[69] In this work, the "transformation matrix" approach described in detail by Flory[70] is used to generate possible conformations of peptides. Once the ϕ - ψ angles are specified, all bead positions can be specified as well. Of the various interactions affecting chain conformation, steric encounters between nonbonded atoms are of principal importance.[71] In the present work, a particular peptide conformation is produced by using the following procedure.

A chain of 2X beads is built up sequentially. First, bead 1 (centered on the α-carbon of the first (N-terminal) amino acid) is placed at the origin. Bead 2 (along the first C_α - R bond) is placed along the +z axis of a molecule fixed reference frame at a distance equal to the sum of the first two bead radii. Next, a pair of possible ϕ - ψ angles is generated using a uniform random number generator. Using transformation matrices,[71] two new beads are placed on the growing chain at possible positions. Before being accepted, however, a check is carried out to see if either of the two new beads overlap any of the previous beads. If any overlap occurs, the positions are rejected and a new pair of possible ϕ - ψ angles is generated. This is repeated, if necessary, until no overlap occurs. The above procedure is repeated until an entire chain of N = 2X non-overlapping beads is generated. In order to sample a broad range of peptide conformations, an "ensemble" consisting of 100 or more chains are generated. This approach of analyzing transport properties of flexible macromolecules has been widely used in polymer science and biophysics for the past 25 years.[72] Mobilities and diffusion constants are computed for each conformation and the results averaged. In addition, it is possible to correlate mean square end-to-end distance and mobility as discussed in the results section of this paper.

It should be emphasized that the procedure described above to generate peptide consformations is approximate and ignores the formidable subtleties associated with protein/peptide tertiary structure.[73] On the other hand, one of the significant observations of the present study is that the electrophoretic mobility depends only weakly on peptide conformation. On that basis, it is argued that the simple procedure used in this work to generate peptide conformation is adequate for the problem under study.

A final element essential in the design of models is the assignment of charge to the ionizable residues making up the peptide. It has long been recognized that pK_a's of the charge residues in a peptide or protein can be very different from those of the free amino acids due to environmental differences.[74] A simple but effective procedure widely used by researchers has been the use of "standard" pK_a's that represent average values in a protein or peptide.[12,75,76] Although this procedure works well under many conditions, substantial error in the net peptide charge can result for certain peptides at certain pH's.[2] On the other hand, atomically detailed models based on the continuum dielectric/linear Poisson-Boltzmann equation have been developed to compute charge states of proteins.[77-81] A clear advantage of these methods is that they account, in an approximate way at least, for particular environmental effects on particular charge groups of a peptide once the conformation is specified. Although they represent a definite improvement over the use of "standard" pK_a's, their accuracy is also limited.[80,81] In the present work, we employ the approach of Lee et al.[82] and tested by Sharma et al.,[83] that effectively describes environmental influences in the state of particular charge residues. Consider charge residue site j in a solvent with dielectric constant ε_r and Debye-Huckel screening parameter, κ. Suppose we insert charge $q\Delta z_k$ ($q = 4.803 \times 10^{-10}$ esu) at site $k \neq j$. Then the change in pK_{aj}, $\Delta pK_{aj,k}$, due to this particular charge perturbation is[45]

$$\Delta pK_{aj,k} \quad = \quad -\frac{q^2 \Delta z_k}{2.303\varepsilon_r k_B T}\frac{\exp(-\kappa r_{jk})}{r_{jk}} \qquad (3-3)$$

where r_{jk} is the distance between residues j and k.

Initially, we set $pK_{aj} = pK_{aj}^0$ where pK_{aj}^0 represents the "high salt" acid dissociation constant. For these, the values of Nozaki et al.[84] and Antosiewicz et al[80] are employed: 3.8 (C-terminal), 7.5 (N-terminal), 12.0 (R), 10.4 (K), 9.6 (T), 8.3 (C), 6.3 (H), 4.4 (E), 4.0 (D). With these initial pK_{aj}^0's, an initial estimate of the charge on each residue, $z_j^{(1)}$, is made using the Henderson-Hasselbach equation at a particular pH. Charge $z_k^{(1)}$ is then used for Δz_k in Eq.(3-3) and summed over all $k \neq j$ for each charge residue to obtain revised estimates, $pK_{aj}^{(1)}$. These revised pK_{aj}'s are then used to re-estimate the charge on the residues, $z_j^{(2)}$. The new charge perturbation is then $\Delta z_k = z_k^{(2)} - z_k^{(1)}$ and the whole procedure is repeated until the charges of all residues converge. This procedure is carried out for every peptide conformation generated.

Once we have the conformations and charge state of the peptides, mobilities are computed by using equations derived in Chapter 2 for weakly charged bead arrays.

3.3 Results and Discussion

To illustrate the potential usefulness and accuracy of the bead model, we have applied it to the 58 peptides examined previously by Janini and co-workers.[12] We have chosen this particular data set because it is quite large and covers peptides in the size range of 2 to 39 amino acids, careful account is taken of the electroosmotic flow, and the experiments are carried out under conditions that minimize it. The experiments were carried out at 22 °C in a buffer system consisting of 50 mM phosphoric acid that was adjusted to pH 2.5 with triethylamine. Using a

$pK_a = 2.12$ for the first acid dissociation constant of phosphoric acid, the ionic strength, I, is estimated to be 35.3 mM which also equals the concentration of $H_2PO_4^{-1}$. The solvent dielectric constant, ε_r, and solvent viscosity, η are taken to be 80 and .955 centipoise, respectively. The Debye-Huckel screening parameter, κ, equals 0.622 nm^{-1} under the conditions of the experiment.

Table 3-2 summarizes the modeling mobilities(μ_{mod}) and experimental mobilities(μ_{exp}) of 58 peptides studied. Also summarized in this table are their sequence (Sequence), and molecular weight (M) from literature, total charge (z_T), and translation diffusion constant (D) from our modeling.

Table 3-2

Transport Properties of 58 Peptides

Peptide	Sequence	$M^{(a)}$	z_T	$\mu_{exp}^{(b)}$	$\mu_{mod}^{(b)}$	$D^{(c)}$
1	DD	248.2	.68	.103	.120(.008)	.570(.032)
2	FD	280.2	.77	.130	.120(.008)	.519(.028)
3	EE	276.3	.77	.125	.119(.009)	.518(.030)
4	GG	132.1	.82	.217	.216(.009)	.795(.028)
5	AA	160.2	.82	.193	.174(.011)	.662(.035)
6	PG	172.0	.82	.184	.188(.007)	.708(.023)
7	VV	216.3	.82	.154	.146(.010)	.577(.031)
8	FG	222.1	.82	.152	.148(.005)	.586(.017)
9	FA	236.2	.82	.149	.138(.009)	.552(.026)
10	LL	244.3	.82	.145	.118(.010)	.485(.029)
11	FV	264.2	.82	.139	.129(.010)	.523(.032)
12	FL	278.2	.82	.133	.116(.010)	.483(.009)
13	MM	280.4	.82	.139	.142(.012)	.562(.034)
14	FF	312.1	.82	.128	.114(.010)	.477(.030)
15	YY	344.4	.82	.121	.111(.010)	.465(.031)
16	WW	390.4	.82	.110	.114(.010)	.475(.030)
17	AAA	231.3	.89	.154	.154(.010)	.557(.033)
18	SSS	279.3	.89	.132	.138(.012)	.513(.033)
19	FFF	459.2	.89	.104	.099(.010)	.401(.023)

20	AAAA	302.3	.91	.139	.135(.011)	.490(.032)
21	AAAAA	373.4	.93	.123	.119(.009)	.441(.028)
22	YGGFL	555.5	.93	.097	.091(.010)	.364(.028)
23	YGGFM	573.5	.93	.095	.096(.011)	.376(.027)
24	RPPGF	572.6	1.90	.184	.194(.019)	.369(.028)
25	AAGIGILTV	813.9	.94	.065	.073(.006)	.292(.016)
26	YMDGTMSQV	1030.4	.89	.060	.061(.006)	.275(.021)
27	VLQELNVTV	1014.2	.92	.066	.064(.007)	.275(.020)
28	RPPGFSPFR	1042.1	2.93	.197	.201(.018)	.270(.022)
29	AFLPWHRLF	1186.4	2.85	.166	.183(.016)	.262(.017)
30	VISNDVCAQV	1046.5	.90	.058	.062(.007)	.273(.022)
31	KLVVVGADGV	956.2	1.90	.131	.135(.012)	.279(.022)
32	KLVVVGAAGV	912.0	1.94	.141	.139(.013)	.281(.022)
33	NSFCMGGMNRR	1272.5	2.89	.183	.176(.017)	.247(.021)
34	RPKPQQFFGLM	1348.4	2.92	.170	.171(.013)	.242(.020)
35	ACLGRDRRTEE	1305.4	3.75	.210	.217(.018)	.243(.016)
36	DAEKSDICTDEY	1387.5	1.70	.099	.097(.010)	.239(.022)
37	TTIHYNYICNSS	1414.6	1.94	.106	.109(.011)	.238(.018)
38	PHRERCSDSDGL -ace	1371.7	3.83	.195	.219(.021)	.240(.019)
39	ACPGTDRRTGGG N	1261.4	2.88	.151	.161(.020)	.234(.023)
40	ACPGKDRRTGG GN	1288.4	3.84	.191	.227(.022)	.245(.020)
41	MGGMNWRPILTI IT	1603.0	1.93	.102	.098(.012)	.219(.020)
42	SPALNKMFGELA KT	1552.7	2.86	.157	.150(.014)	.224(.018)
43	HMTEVVRHCPH HER	1768.0	6.72	.264	.333(.035)	.216(.021)
44	LAKTCPVRLWV DSTPP	1783.2	2.88	.151	.138(.015)	.211(.020)
45	VVRRCPHQRCSD SGI	1828.1	4.79	.215	.212(.039)	.202(.030)
46	LGRNSFEVCVCA CPGRD	1826.0	2.83	.137	.132(.015)	.203(.020)
47	KLVVVGAGDVG KSALTI	1626.9	2.89	.137	.139(.020)	.209(.023)
48	TPPPGTRVQQSQ HMTEV	1893.0	2.90	.142	.135(.016)	.206(.019)
49	YKLVVVGAAGV GKSALT	1632.0	2.92	.142	.136(.017)	.205(.021)
50	YGLVVVGACGV GKSALT	1665.0	2.93	.143	.135(.018)	.204(.022)

51	YNYMCNSSGMG GMNRRP	1938.5	2.84	.143	.130(.014)	.202(.019)
52	YKLVVVGAVGV GKSALT	1661.0	2.93	.151	.135(.018)	.204(.022)
53	YKLVVVGARGV GKSALT	1718.0	3.92	.178	.175(.022)	.200(.021)
54	PPPGTRVRVMAI YKQSQ	1928.3	3.90	.182	.178(.020)	.204(.019)
55	DGLAPPQHRIRV EGNLR	1928.2	4.79	.195	.196(.047)	.190(.035)
56	VPYEPPEVGSVY HHPLQLHV	2297.6	3.82	.153	.142(.019)	.176(.020)
57	FLTPKKLQCVDL HVISNDVCAQVH PQKVTK	3390.1	6.80	.187	.196(.032)	.149(.021)
58	HQIINMWQEVG KAMYAPPISGQI RRIHIGPGRAFYT TKN	4481.2	7.87	.175	.149(.046)	.117(.025)

(a) Molecular Weight in gm/mole

(b) in cm^2/kV sec, (c) in 10^{-5} cm^2/sec

For model mobilities and diffusion constants, the number in parenthesis represents the standard deviation between the different conformations of peptides. To quantify the difference between experimental and model mobilities, define the error

$$E \;=\; \frac{\mu_{exp} - \mu_{mod}}{\mu_{exp}} \qquad (3-4)$$

For the data set studied, E goes from -0.26 for peptide no. 43 to +0.19 for peptide no. 10. Peptide no. 43 (HMTEVVRHCPHHER) is one of the most highly charged peptide. Because of high charge, distortion of the ion atmosphere in the vicinity of the macroion form equilibrium (ion relaxation) has a significant influence on the mobility, hence can not be neglected.[30,31,33,34,44,45] Neglecting the ion relaxation is only valid when the mobilities is below 0.20 cm^2/kV sec. Peptide no. 43 has an experimental mobilities of 0.264 cm^2/kV sec, which

exceed this bound. Ion relaxation effect will reduce the mobilities, so it is not surprising that in

this modeling the mobility is higher than the experimental data by 26%.

The discrepancy seen for peptide # 10, LL, is more difficult to understand. The possibility that

inaccuracies in generating realistic peptide conformations is responsible for the discrepancy (E

= .19) shall be considered first. Figure 3-3 shows how the model mobility (in cm^2/kV sec) of

pentapeptide AAAAA varies with conformation.
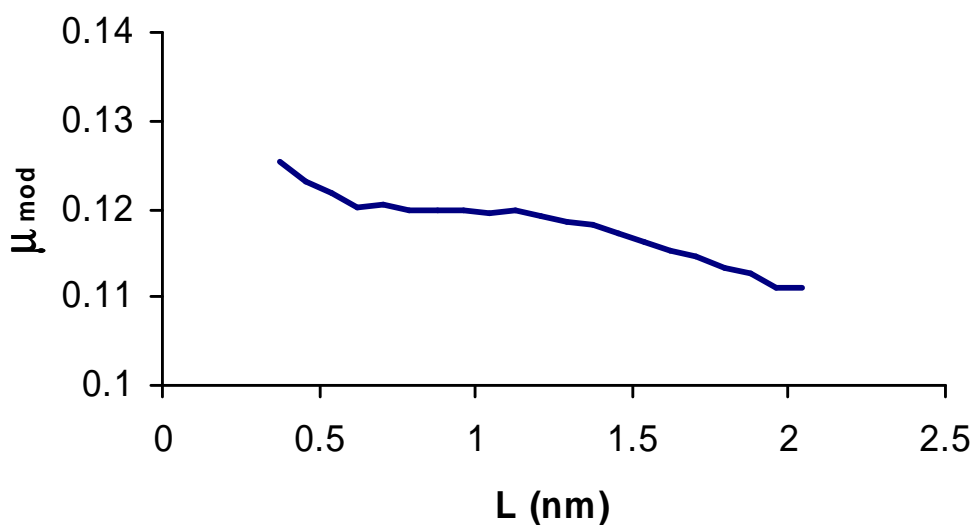
Figure 3-3) Variation of μ with Conformation for a Pentapeptide. Model mobility (in cm^2/kV sec) of the pentapeptide, AAAAA, is plotted versus the end-to-end distance, L.

A total of 5000 chain conformations were generated and averaged over narrow ranges of end-to-

end distance. (The end-to-end distance, L, is defined as the distance between the R group of the

first and last amino acids in the peptide, which corresponds to the distance between bead

positions 2 and N.). Going from the most compact (L ≈ .37 nm) to most extended (L ≈ 2.04 nm)

conformations, μ_{mod} varies from .125 to .111 cm^2/kV sec. The average overall mobility is .119 cm^2/kV sec and so the compact and extended conformations depart from the average by $\pm$ 6 percent, respectively. For the dipeptide, LL, the range in μ_{mod} is from .131 (most compact) to .109 (most extended), with an average value of .118 cm^2/kV sec. If all LL dipeptides were in the most compact form, which seems unlikely on the basis of conformational energy surfaces of small peptides (70), E would be reduced from +.19 to +.10. Although a change in the right direction, conformational considerations cannot account for the entire difference. The examples of LL and AAAAA illustrate the relatively weak dependence of mobility on conformation.

Inaccuracies in the diffusion constants of the amino acids themselves could be responsible for some of the discrepancy as well. In the case of VV (peptide # 7), E = +.05 which shows much better agreement between experimental and model mobilities than LL, despite the fact that L and V amino acids differ by a single CH$_2$ group in their side chains. If we use the volume increment method of Edward (68) with δv = .017 nm^3 (for CH$_2$) and R$_1$ = .292 nm (for V) in Eq. (3-2), then R$_2$ (for L) is estimated to be .307 nm which is lower than the experimental value listed in Table 3-1 by about 10 %. If this value is used for L, a$_s$ (for L) in Table 3-1 becomes .241 (interior), and .252 nm (end), respectively. If these bead size parameters are used for L instead of those listed in Table 3-1, μ_{mod} = .134 and E = +.076. We are not claiming that the diffusion constant of L reported in the literature is wrong, but instead are discussing possible sources of error that could account, in part at least, for discrepancies between model and experimental mobilities. Another possible source of error is the charge of the peptide which, in turn, is related to inaccuracies in the pK$_a$ of the charge groups. From the above discussion about peptides nos. 10 and 43, it is shown that modeling at the atomic or residue level that is firmly grounded in theory can be used, in conjunction with experimental mobilities, to directly address

questions related to peptide conformation, transport, and charge.

Although substantial error is seen in a few individual peptide cases as discussed in the previous paragraphs, the overall agreement between experimental and model mobilities is very good. If Eq. (3-4) is averaged over all 58 peptides, $<E> = .010$ and $(<E^2>)^{1/2} = .077$. In order to display all of the experimental and model mobility data in a reduced form, consider the empirical equation (Eq. (2-54))[10,13,59-62] written in the form

$$-\ln\left(\frac{\mu}{z_T}\right) = -\ln A + \alpha \ln M \qquad (3-5)$$

This is plotted in Figure 3-4 for both experimental (diamonds) and model (squares) mobilites. Triangles represent differences between the two. Both data sets follow Eq. (3-5) to a reasonable approximation with linear least squares fits giving $\alpha = .673$ and $.661$ for experimental and model mobilities. Also, if M is in gm/mole and μ is in cm^2/kV sec, $A = 7.135$ and 6.495 for experiment and model, respectively. From the data given in Table 3-2, $<(\mu_{exp} - \mu_{fit})^2>^{1/2} = .088$ cm^2/kV sec, and $<(\mu_{mod} - \mu_{fit})^2>^{1/2} = .097$ in cm^2/kV sec, where brackets denote averaging over all 58 peptides and μ_{fit} is computed using Eq. (2-54) with the A's and α's given above. The "scatter" seen in Fig. 3-4 for both experimental and model mobilities, as well as the rms deviations given above both demonstrate that Eqs. (2-54) give, at best, an approximate relation between mobility, peptide net charge, and molecular weight. On the other hand, $<(\mu_{exp} - \mu_{mod})^2>^{1/2} = .014$ cm^2/kV sec, which shows that the model mobilities track much better with experimental mobilities than Eq. (2-54).
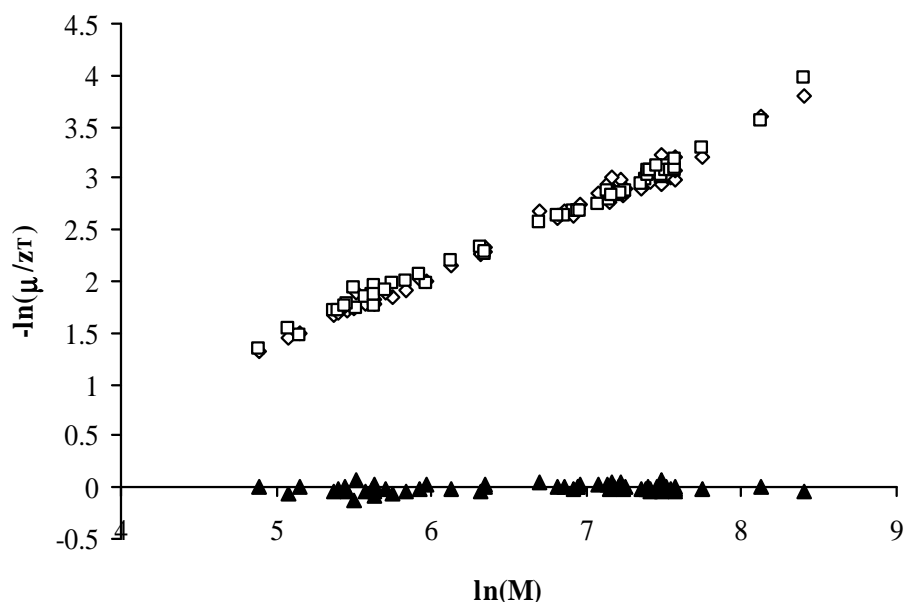
Figure 3-4) Correlation of Experimental and Model Mobilities with Charge and Molecular Weight. Experimental and model data points are denoted by diamonds and squares, respectively. All 58 peptides summarized in Table 3-2 are included in this figure. Triangles represent difference between experiment and model.

Janini and coworkers have formulated a semi-empirical multivariable model that accounts for the number of amino acids, X, average molecular weight of the amino acids side groups making up a particular peptide, W, and net peptide charge, Z.[7] Basically the mobility is written as a product of functions of X, W, and Z and the functions of W and Z are written as polynomials whose coefficients are extracted from fits to particular experimental mobility data sets. The resulting multivariable model fits are quite accurate giving $<(\mu_{exp} - \mu_{mod})^2>^{1/2} = .009$ cm^2/kV sec for the data given in Table V of reference 7. In terms of absolute accuracy, the present model is competitive with the multivariable model provided $|\mu| \leq 0.20$ cm^2/kV sec. It should also be emphasized that the input parameters of the present model are totally independent of

experimental mobilities and are based on a realistic structural model of peptides, a continuum

electrostatic model for the pK$_a$'s of charge residues, and the diffusion constants of free amino

acids. Because of that, questions related to how conformation, size of side chains, and charge

influence mobility can be addressed directly with the present model.

Next, we would like to discuss how the complimentary measurements of diffusion and

mobility could be combined to estimate the net charge of a peptide. This could be useful, for

example, in determining how the charge state and possibly the pK$_a$ of particular charge residues

change as pH is varied.[2] Yoon and Kim (16) have developed a rigorous theory of the free

solution electrophoretic mobility of a weakly charged prolate or oblate ellipsoid of minor axis c,

major axis a, and net charge Q. Their expression for the mobility can be written[32]

$$\mu_{YK} = \frac{qQ}{k_BT}\left(\frac{k_BT}{6\pi\eta R^*}\right)\frac{g(\kappa c)}{(1+\kappa R^*)} \qquad (3-6)$$

where g(κc) is a slowly varying function of κc, and R* is the hydrodynamic radius of the

ellipsoid. The translational diffusion constant of the ellipsoid, D, is related to R* by the Stokes

Einstein relation (Eq. (3-1)). For small ellipsoids such that $\kappa c \leq 1.0$, $g(\kappa c) \approx 1.0$. With minor

rearrangement and the use of the Stokes Einstein relation, Eq. (3-6) can be written

$$Q = \frac{\mu_{YK}(1+C_2/D)}{C_1 D} \qquad (3-7)$$

where $C_1 = q/k_BT = 1.160 \times 10^7/T$ 1/(kV cm), and

$$C_2 = \frac{\kappa k_BT}{6\pi\eta} \qquad (3-8)$$

Eq. (3-7) is strictly valid only for a small, weakly charged ellipsoid. Nonetheless, it does show

in a rigorous way how mobility, charge, and diffusion of a non spherical particle of arbitrary

axial ratio are related to each other. Specifically, Eq. (3-7) is valid whether our particle is a

sphere, needle, or pancake. How well Eq. (3-7) also works for peptides can be examined by comparing Q computed using Eq. (3-7) with model μ's and D's, with Z. Since the model peptides can be large, are not ellipsoids, and the model peptide charge is distributed in complex ways, we do not expect Z and Q to be rigorously equal. The results are shown in Figure 3-5 for all 58 peptides.
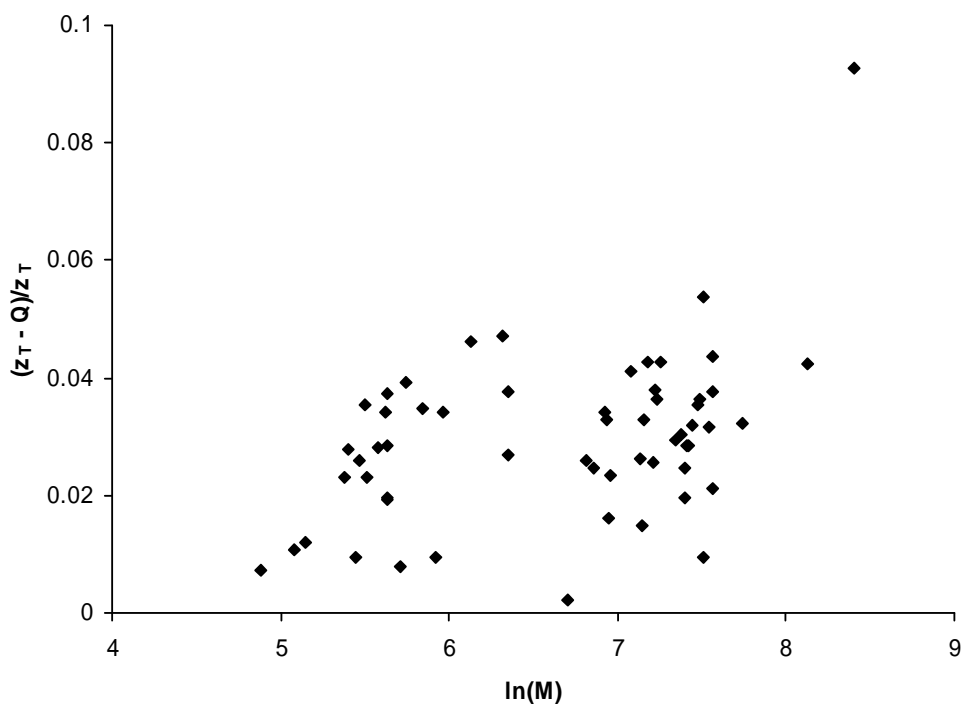
Figure 3-5) Comparison of Q and z_T for Model Peptides. Q is computed using Eq. (3-7) and z_T is the actual average net charge of a particular model peptide. All 58 peptides are included.

With the exception of the largest peptide (# 58) which contains 39 amino acids, $Q \approx z_T$ to a relative accuracy of about 3 %. Specifically, Z exceeds Q by about 1 to 5 %, but the discrepancy

appears to be relatively insensitive with respect to M if we choose to ignore peptide # 58. Finally,

Figure 3-6 shows how Q varies with ln(M) for both model (squares) and experimental (diamonds)

mobility/diffusion data.
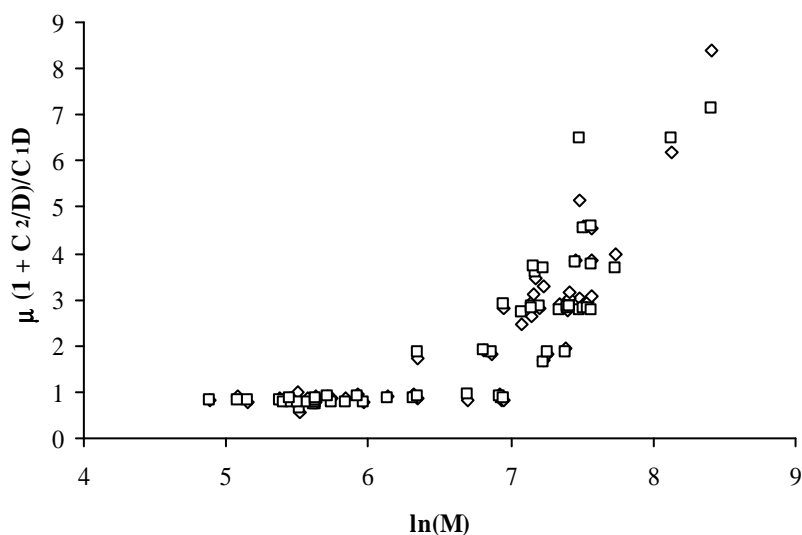
Figure 3-6) Plot of Q versus ln(M) for the 58 Peptides. Experimental and model data points are denoted by diamonds and squares, respectively.

For the "experimental" data in this case, model diffusion constants were used in Eq. (3-7)

since experimental diffusion constants are not available. Note the step like nature of the data

with the most prominent step occurring at Q $\approx$ +1. This corresponds to those peptides which

have a net charge of 1. Other "steps" can also be defined, but become more diffuse as the net

peptide charge increases. It should be emphasized that the net peptide charges do not have to be

integers in general since the average charge of a particular residue at a particular pH is non

integer.

3.4 Summary

Mobilities of peptides can be estimated from the semiempirical approaches of past studies.[7,10,13,59-62] Although net peptide charge, molecular weight or number of amino acids, and (in the case of Ref. 7) the actual peptide sequence are variables in these approaches, their parameterization depended strongly on actual mobility measurements. Under conditions similar to those used in the model parameterizations, these approaches could be used to predict mobilities that are potentially as accurate and in some examples more accurate than could be achieved using the complex methodology developed in the present work. In that case, what is the advantage of the present study?

In the present study, a bead model appropriate for weakly charged peptides is developed and tested against experimental measurements of the electrophoretic mobility. This model should be applicable to weakly charged peptides with an absolute electrophoretic mobility not exceeding approximately 0.20 cm^2/kV sec.[6] Eq. (2-54), or equivalently, Eq. (3-5) can be used to estimate the constraint this places on the upper bound of the absolute total peptide charge, $|Z|$, in protonic units. For a pentapeptide with a molecular weight of about 500 gm/mole, for example, $|Z| \leq 1.90$.   What distinguishes the present work from the semiempirical approaches of past studies summarized in the previous paragraph is that it is structure based, is formally grounded in electrokinetic theory, and its parameterization is totally independent of mobility measurements. With this model, we have shown that overall agreement with experiment[12] is very good on the basis of 58 peptides covering the size range of from 2 to 39 amino acids. Furthermore, this work demonstrates that starting from fundamental considerations of continuum hydrodynamics and electrostatics,

[43]electrophoretic mobilities can be predicted with considerable accuracy when realistic peptide models are employed.

The "structure based" nature of our methodology makes it potentially useful in a number of possible applications. Future studies could include more detailed accounting of peptide conformation. This could be achieved, for example, by selecting conformations from actual structural data bases or molecular dynamics trajectories. In addition, it would be straightforward to predict the mobilities of post-translationally modified peptides.[10] For example, the phosphorylation of serine, an -OH group is replaced with an $-OPO_3H_2$ group which will affect both the size and charge of the peptide. Using the present model, it would be straightforward to account for these structural modifications and predict their effect on peptide mobility. The same approach could be used for other modifications including citrullination or methylation of arginine, deamidation of glutamine, oxidation of methionine, or acetylation of the N-terminal.[10] Also given the strong theoretical foundations of the present work, it can be applied over a wide range of salt, temperature, and pH conditions. In the work of Janini et al., the experiments were carried out at pH = 2.5 where the peptides are largely in their unfolded state. Nonetheless, there is no formal difficulty in applying the present methodology to other salt or pH conditions although folding of the peptides may require more care in modeling peptide conformations prior to the calculation of mobility than employed in the present study. The current methodology could also be used to examine the dependence of mobility on pH for specific peptides.[2] In doing so, it should be possible to examine specific pKa's of charge groups of peptides using experimental mobilities and comparing them with model predictions. At the end of the previous section, we also discussed how complementary measurements of diffusion and mobility could be combined to estimate the net charge of a peptide. An additional and fundamental study involves

a more careful analysis of single amino acid transport and this has been carried out As discussed previously, diffusion constants of some of the amino acids were unknown at the time this work was done and were estimated using the volume increment method of Edward.[68]

The "stand alone" computer program we have developed computes the electrophoretic mobility and translational diffusion constants. It is written in Fortran and requires no auxiliary libraries. As an example of the computation times required, simulations of 100 conformations of dipeptides and a peptide consisting of 39 amino acids required 0.3 sec and 15 minutes, respectively, of single processor time on a Silicon Graphics 4D-380-SX computer. All of 58 peptides summarized in Table 3-2 were done in a single afternoon.

Chapter 4

Improvements in the "Bead Method" to Include Ion Relaxation and "Finite Size Effects"

4.1 Introduction

In the previous chapter, a purely-structure based methodology grounded on fundamental electrohydrodynamic theory is developed. Each amino acid is represented by two beads, one for the backbone of the peptide and one for the side group of the amino acid. The size and charge of each bead are fixed in a way that is entirely independent of electrophoretic mobility measurements, and this greatly limits the number of adjustable parameters available in modeling. However, this methodology is strictly valid for weakly charged peptides in which the beads are small compared to $1/\kappa$, where κ is the Debye-Huckel screening parameter. Specifically, only terms to first order in κa were retained, where a is a typical subunit radius used in modeling. By "weakly charged", we mean the absolute surface or" ζ " potential does not exceed 25mV,[29] or equivalently, the absolute electrophoretic mobility does not exceed approximately 0.20 cm^2 / (kV s).[6] For more highly charged macro-ions, ion relaxation needs to be taken into account. In past work, generally good agreement was obtained between model mobilities and experimental results[12] of 58 peptides ranging in size from 2 to 39 amino acids. For the most part, this particular set of peptides is weakly charged under the conditions of the experiment (pH = 2.5),

and the salt concentration was low enough (35.3 mM monovalent salt) to ensure that κa is small. In this Chapter where ion relaxation and the restriction that $\kappa a \ll 1$ is relaxed are taken in account, all of the peptides studied previously are re-examined. A set of 24 peptides[7,13] which , as a group, tend to be more highly charged than the 58 peptides examined previously.[12] Because of this greater charge, this set is more prone to exhibit substantial ion relaxation effects. In addition, the "charge ladder" of human carbonic anhydrase is examined in which the charge of the protein, which remains in its native conformation, is varied over a wide range.[76] This example clearly shows how ion relaxation influences mobility as charge is varied. It also demonstrates that our procedure of correcting unrelaxed mobilities to account for ion relaxation is effective.

Including ion relaxation complicates the problem substantially because of the coupling of the fluid flow, ion densities, and external electric and /or flow fields[31,41,42,44]. In next section, the procedure used to account for the ion relaxation effect is described in detail. Briefly, we assume

$\dfrac{\mu_r}{\mu_{nr}} = \dfrac{\mu_{rs}}{\mu_{nrs}}$, where $\dfrac{\mu_r}{\mu_{nr}}$ is the ratio of peptide mobility to that without relaxation, and $\dfrac{\mu_{rs}}{\mu_{nrs}}$

represents a similar ratio for a sphere with the same hydrodynamic radius, average electrostatic surface potential and under the same solvent/salt/buffer conditions as our model peptide. The ratio of the spherical model particles is readily determined using the method of O'Brien and White.[31]

4.2   Crystal Structure Approach

Previously, we have developed a bead model to determine the mobility of peptide

assuming the peptide has random coil conformation. However, peptide and protein mobility can also be determined regarding their crystal structure (available at Protein Data Bank). In the crystal structure approach, the backbone beads are placed at the crystallographic coordinates of the α carbons. Let $\mathbf{r}_j$ denote the virtual bond vector extending from the α carbon of the jth amino acid to the α carbon of the $j + 1$ amino acid. Also let $\mathbf{r}_0$ extend from the N of the N-terminus to the first α carbon, and let $\mathbf{r}_N$ extend from the Nth α carbon to the C of the C-terminus. The side beads are initially placed along the vector extending from the α carbon to the β carbon of the side group. The distance of the center of the side bead from the center of the backbone bead is set to the sum of the radii of the two beads. In the event the jth amino acid is glycine, which has no β carbon, the side bead is initially placed along the vector $- (\mathbf{r}_{j-1} + \mathbf{r}_j)$. These positions may have to be modified to avoid bead overlap. If the backbone beads overlap, which occurs if the distance between successive α carbon falls below 0.38 nm, then the radii of the two backbone beads are shrunk by an equal amount to ensure that the beads are just touching. The corresponding distances of side beads from their associated backbone beads are also adjusted to ensure that the side beads and their associated backbone beads just touch. No further adjustment is made regarding the positions or radii of the backbone beads. For the side beads, every interbead distance is checked for possible overlap. If overlap occurs, a new possible position is chosen completely at random, subject to the constraint that the side bead just touches its corresponding backbone bead. If the new position still overlaps another bead, then the position is rejected and the procedure is repeated. If a suitable position can not be found within 100 attempts, then the radius of this side bead is shrunk by 10% and the above procedure is repeated. When a suitable position for a side bead is found, the same procedure is applied to successive side beads until a complete peptide/protein structure is generated.

With regard to macro-ion itself, past work has shown that μ depends primarily on net charge and global structure.[6,17,88] Local structural features or subtle variations in the charge distribution have little effect on μ. At the same time, it is important that the beads making up the model structure do not overlap. The procedure described in the previous paragraph yields structure that both preserve overall conformation and ensure bead overlap does not occur.

Once the structure of the peptide is created, the determination of its charge state of the peptide is next need to be done. The procedure of the assignment of charge to the ionizable residues is the same with that of weakly charge peptide.

4.3   Inclusion of Finite Size Effects and Ion Relaxation

To include the effect of ion relaxation effect, which is important in electrophoresis of highly charged particle, we started from the electrophoretic mobilities without ion relaxation and then made corrections. The relaxation correction, C, is defined

$$C = \frac{\mu_r}{\mu_{nr}} \qquad (4\text{-}1)$$

where μ_{nr} and μ_r are the mobilities of a particular model particle in the absence and presence of ion relaxation,respectively. Also let R denote the hydrodynamic radius of the model particle, which is defined in terms of its translational diffusion constant D_T,

$$R = \frac{k_B T}{6\pi\eta D_T} \qquad (4-2)$$

where k_B is Boltzmann's constant, T is absolute temperature, and η is solvent viscosity. For a model structure, D_T is computed using long established procedures[87,89]. It is shown by previous study[90] that C for a prolate ellipsoid is near identical to that of a sphere with the same R under

conditions of the same solvent temperature, salt concentration and composition, and average zeta potential. It should be emphasized that this is independent of the axial ratio of the ellipsoid. Based on this study, we shall simply assume that C for an arbitrary irregular structure is equal to that of an equivalent sphere.

$$C \cong \frac{\mu_{rs}}{\mu_{nrs}} \qquad (4\text{-}3)$$

The advantage of Eq. (4-3) is that relaxed and unrelaxed mobilities of spheres are relatively easy to determine using available procedures.[31] The reduced potential, y, is defined

$$y = \frac{q\zeta}{k_B T} \qquad (4\text{-}4)$$

where ζ represents the electrostatic potential averaged over the surface of the model particle. On the physical grounds, C varies continuously as y varies and has its maximum value of 1.0 at y = 0. This is because ion relaxation always acts to reduce the absolute electrophoretic mobility and vanishes in the limit of zero ζ potential. Also, dC/dy = 0.0 at y = 0. At small |y|, C can be related to y

$$C = 1 + a_1 y^2 + a_2 y^3 + a_3 y^4 \qquad (4\text{-}5)$$

The a_j coefficients in Eq. (4-5) will depend on salt concentration, ion type, and R. All of peptide mobility measurements (but not the protein charge ladder results[76]) reported in this work were carried out in 35.3 mM $Na^+ HPO_4^-$ buffer system at $pH = 2.5$ and 22 °C.[7,12] We examined model spheres of variable y in the size range 0.5 nm ≤ R ≤ 2.0 nm and obtained the following coefficients in this particular salt/buffer system (R is in nanometers).

$$a_1 = -0.005 - 0.021R \qquad (4\text{-}6a)$$

$$a_2 = -0.0021 + 0.0024R \qquad (4\text{-}6b)$$

$$a_3 = 0.00013 + 0.00008R \qquad (4-6c)$$

Once the hydrodynamic radius of a peptide and y are determined, Eqs. (4-6a, b, c) can be used to estimate C. Once the unrelaxed mobility, μ_{nr} is determined, the relaxed mobility is simply $\mu_r = C\mu_{nr}$.

For the charge ladder of human carbonic anhydrase,[76] the temperature was 25 °C, pH = 8.4, and the salt consisted of 7.9 mM Tris$^+$glycine$^-$. Under these conditions

$$a_1 \quad = \quad -.0152 - .0066\,R \qquad (4-7a)$$

$$a_2 \quad = \quad -.0006 + .0003\,R \qquad (4-7b)$$

$$a_3 \quad = \quad +.00011 + .0001\,R \qquad (4-7c)$$

It is important to emphasize that these coefficients depend strongly on ionic strength as well as the specific ion composition of the buffer.

Since peptides are irregularly shaped, it can be argued that the relaxation correction may be more complicated than for axisymmetric prolate ellipsoids. As a preliminary consideration of this issue, we shall first consider the case of hen eggwhite lysozyme that was studied by a Boundary Element (BE) procedure using an atomically detailed surface model derived from the crystal structure of the protein.[35] This protein has a hydrodynamic radius of 2.02 nm, and at 0 °C in 0.15 M NaCl at pH = 3, the average reduced surface potential, y, is approximately 1.35. From BE modeling, the ratio μ_r/μ_{nr} under these conditions is 0.952 (see Figure 6 of reference (35)). The corresponding ratio using spheres is 0.956. Consequently, the simple procedure used to account for the relaxation effect is quite accurate but not exact in this particular case. Nonetheless, the correction does succeed in properly accounting for much of the effect. A more complete analysis of the accuracy of the relaxation correction is given at the end of the next section by the example of the charge ladder of human carbonic anhydrase.

4.4   Results and Discussion

To check the accuracy of the procedure discussed in section 4.2 and 4.3 which included the ion relaxation and finite size effect, we have examined two sets of peptides where experimental data is available. The first set of 50 consists of peptides ranging in size from 2 to 39 amino acids that, for the most part, are weakly charged.[12] Consequently, neglect of ion relaxation should be a good approximation for many of the peptides in this set. The second set of 24 peptides ranges in size from 2 to 42 residues, and these tend to be more highly charged than the first set.[7] The second set serves as a more stringent test of our procedure to account for ion relaxation that the first set. In addition, other investigators[13] have analyzed this second set in terms of several different semi empirical models that shall be discussed. The experiments[7,12] were carried out at 22 °C in a buffer system consisting of 50 mM phosphoric acid that was adjusted to pH 2.5 with triethylamine. Using a $pK_a = 2.12$ for the first acid dissociation constant of phosphoric acid, the ion strength, I, is estimated to be 35.3mM, which also equals the concentration of $H_2PO_4^-$. The solvent dielectric constant and solvent viscosity, η, are taken to be 80 and 0.955 cp, respectively. The Debye-Huckel screening parameter, κ, equals 0.622 nm^{-1} under the conditions of the experiment.

Table 4-1

Transport Properties of Set 1 (50 Peptides)

Peptide	Sequence	z_T	μ_{exp}	μ_{nr} [a]	μ_{nr} [b]	μ_r [c]
1	DD	0.694	.103	0.121	.122	0.120
2	FD	0.773	.130	0.119	.121	0.119
3	EE	0.769	.125	0.118	.120	0.118
4	GG	0.818	.217	0.204	.205	0.197
5	AA	0.818	.193	0.172	.174	0.168
6	PG	0.818	.184	0.181	.182	0.176
7	VV	0.817	.154	0.122	.124	0.122
8	FG	0.818	.152	0.143	.145	0.142
9	FA	0.817	.149	0.136	.138	0.135
10	FV	0.817	.139	0.118	.120	0.118
11	MM	0.817	.139	0.140	.142	0.139
12	YY	0.817	.121	0.108	.111	0.109
13	AAA	0.888	.154	0.152	.154	0.150
14	SSS	0.884	.132	0.146	.148	0.144
15	AAAA	0.913	.139	0.133	.135	0.132
16	AAAAA	0.921	.123	0.120	.122	0.120
17	YGGFM	0.921	.095	0.094	.096	0.095
18	RPPGF	1.888	.184	0.199	.203	0.193
19	AAGIGILTV	0.936	.065	0.073	.076	0.075
20	YMDGTMSQV	0.882	.060	0.062	.064	0.063
21	VLQELNVTV	0.918	.066	0.061	.063	0.063

22	RPPGFSPFR	2.777	.197	0.207	.213	0.200
23	AFLPWHRLF	2.831	.166	0.191	.196	0.184
24	VISNDVCAQV	0.895	.058	0.059	.061	0.061
25	KLVVVGADGV	1.882	.131	0.128	.132	0.128
26	KLVVVGAAGV	1.923	.141	0.133	.137	0.133
27	NSFCMGGMNRR	2.718	.183	0.182	.184	0.178
28	RPKPQQFFGLM	2.904	.170	0.182	.189	0.178
29	ACLGRDRRTEE	3.602	.210	0.230	.235	0.213
30	DAEKSDICTDEY	1.644	.099	0.099	.101	0.100
31	TTIHYNYICNSS	1.926	.106	0.115	.118	0.115
32	PHRERCSDSDGL-ace	2.739	.195	0.173	.176	0.167
33	ACPGTDRRTGGGN	2.796	.151	0.182	.186	0.175
34	ACPGKDRRTGGGN	3.717	.191	0.239	.243	0.219
35	MGGMNWRPILTIIT	1.926	.102	0.109	.112	0.110
36	SPALNKMFCELAKT	2.838	.157	0.161	.166	0.159
37	HMTEVVRHCPHHER	6.323	.264	0.335	.344	0.279
38	LAKTCPVRLWVDSTPP	2.857	.151	0.146	.15	0.144
39	LGRNSFEVCVCACPGRD	2.81	.137	0.142	.148	0.143
40	KLVVVGAGDVGKSALTI	2.855	.137	0.139	.144	0.139
41	TPPPGTRVQQSQHMTEV	2.878	.142	0.139	.143	0.137
42	YKLVVVGAAGVGKSALT	2.903	.142	0.142	.147	0.141
43	YGLVVVGACGVGKSALT	2.907	.143	0.140	.146	0.140
44	YNYMCNSSGMGGMNRRP	2.824	.143	0.143	.148	0.143
45	YKLVVVGAVGVGKSALT	2.903	.151	0.139	.144	0.138
46	YKLVVVGARGVGKSALT	3.883	.178	0.185	.191	0.178

47	PPPGTRVRVMAIYKQSQ	3.887	.182	0.185	.191	0.177
48	DGLAPPQHRIRVEGNLR	4.496	.195	0.222	.227	0.205
49	VPYEPPEVGSVYHHPLQLHV	3.753	.153	0.157	.161	0.152
50	HQIINMWQEVGKAMYAPPISGQ IRRIHIGPGRAFYTTKN	7.762	.175	0.206	.213	0.189

(a) finite bead size effects not included and no relaxation correction

(b) finite bead size effects included, but no relaxation correction

(c) finite bead size effects included plus ion relaxation

Table 4-2

Transport Properties of Set 2 (24 Peptides)

Peptide	Sequence	z_T	μ_{exp}	$\mu_{nr}^{(a)}$	$\mu_{nr}^{(b)}$	$\mu_r^{(c)}$
1	FF	0.817	0.128	0.113	0.115	0.113
2	FL	0.817	0.133	0.12	0.123	0.120
3	LL	0.817	0.146	0.128	0.131	0.128
4	WW	0.817	0.110	0.111	0.114	0.112
5	FFF	0.886	0.104	0.097	0.0998	0.0982
6	KKKK	4.380	0.330	0.43	0.439	0.341
7	KKKKK	5.315	0.330	0.461	0.472	0.346
8	YGGFL	0.918	0.0975	0.091	0.0934	0.0921
9	ACHGRDRRT	4.467	0.265	0.33	0.336	0.285
10	VVRRYPHHE	4.628	0.274	0.307	0.315	0.265
11	CRHRRRHRRGC	8.480	0.297	0.532	0.546	0.317
12	CRHHRRRHRRGC	9.456	0.297	0.559	0.573	0.309
13	HMTEVRRYPHHER	6.290	0.264	0.342	0.351	0.282
14	HMTEVRHCPHHER	6.287	0.264	0.355	0.363	0.290
15	HRSCRRRKRRSCRHR	11.20	0.303	0.562	0.579	0.310
16	RTHCQSHYRRRHCSR	8.423	0.290	0.427	0.440	0.306
17	YAEDGVHATSKPARR	4.441	0.214	0.241	0.247	0.224
18	VVRRCPHQRCSDSGL	4.734	0.208	0.236	0.241	0.212
19	DGLAPPQHRIRVFGNLR	4.532	0.190	0.223	0.228	0.206
20	NHQLLSPAKTGWRIFHP	4.772	0.194	0.231	0.239	0.216
21	RTHGQSHYRRRHCSRRRLHRIHRRQ	15.29	0.290	0.532	0.543	0.262
22	FLTPKKLQCVDLHVISNDVCAQVHPQKVTK	6.478	0.187	0.202	0.209	0.189
23	KQIINMWQEVGKAMYAPPISGQIRRIHIGPGRAFYTTKN	7.775	0.178	0.204	0.209	0.186
24	DRVIEVVQGAYRAIRHIPRRIRGQLERRIHIGPGRAFYTTKN	12.17	0.208	0.295	0.292	0.218

(a) finite bead size effects not included and no relaxation correction

(b) finite bead size effects included, but no relaxation correction
(c) finite bead size effects included plus ion relaxation

Shown in Tables 4-1 and 4-2 are the sequences, experimental mobilities, μ_{exp}, and three different model mobilities for these two sets of peptides. The first model mobilities listed, $\mu_{nr}^{(a)}$, ignore ion relaxation and assume $\kappa a \ll 1$ (where a is a typical bead size). The second set of model mobilities, $\mu_{nr}^{(b)}$, relax this approximation. It is clear from both Tables that taking more accurate account of the finite size of the model subunits produces a change in model mobility of approximately 1 %. Under the conditions of the experiment and taking a typical bead radius of 0.25 nm, $\kappa a = 0.16$. Under the conditions of the experiments, the "small bead approximation" is a reasonable assumption. We now turn to the effect of including ion relaxation in the model calculations and the overall accuracy of the model mobilities. The error E defined in previous chapter is used to evaluate the difference between experimental and model mobilities. Including the finite size correction, for set 1, $\langle E_{nr} \rangle = -.041$, $\langle E_{nr}^2 \rangle^{1/2} = .110$, $\langle E_r \rangle = .0039$, and $\langle E_r^2 \rangle^{1/2} = .080$. Brackets indicate an average over all peptides in the data set. The more negative value of $\langle E_{nr} \rangle$ is due to the fact that ion relaxation, present in an actual experiment, produces absolute mobilities that are lower than they would be in its absence. On average, including ion relaxation brings model and experimental mobilities into better agreement. For the Set 1 peptides, model (with relaxation) and experimental mobilities, on average, agree to better than 1 %. The low value of $\langle E_r \rangle$ indicates there are no significant systematic errors in our modeling. This, in turn, suggests that our modeling captures the essential physics of the phenomenon of electrophoresis.

Also from some highly charged peptides of set 2, it is clear that inclusion the ion relaxation improved the modeling a lot. For example, Peptide no. 43 is one of most highly charged peptides in this data set with model mobility exceeded 0.2 cm^2/(kV s). Including the

ion relaxation improved the modeling a lot and E goes from 0.268 to 0.0250. No. 55 with net charge of 4.52 and E goes from 0.138 to 0.0256. No. 58 with net charge of 7.79 and E goes from 0.175 to 0.0468.

Nonetheless, substantial discrepancies do persist for particular peptides, as evidenced by the fairly large $<E^2>^{1/2}$ values. As discussed previously[88], this is probably due to errors in estimating the charge of the peptides in specific cases. Error in estimating charge in specific cases, which could be due to underestimating or overestimating the pK_a of specific residues, could very well be responsible for the "scatter" seen in a comparison of μ_{expt} and μ_r. The importance of including ion relaxation is made even more evident by Set 2, where the peptides tend to be more highly charged than Set 1. For Set 2, $<E_{nr}> = -.294$, $<E_{nr}^2>^{1/2} = .430$, $<E_r> = -.013$, and $<E_r^2>^{1/2} = .069$. Not surprisingly, neglect of ion relaxation produces even greater error for this set of peptides. Including ion relaxation results in overall accuracy that is comparable to that of Set 1. Plotted in Figure 4-1 are E_{nr} and E_r for all 74 peptides versus the net charge to size ratio, Z/N.
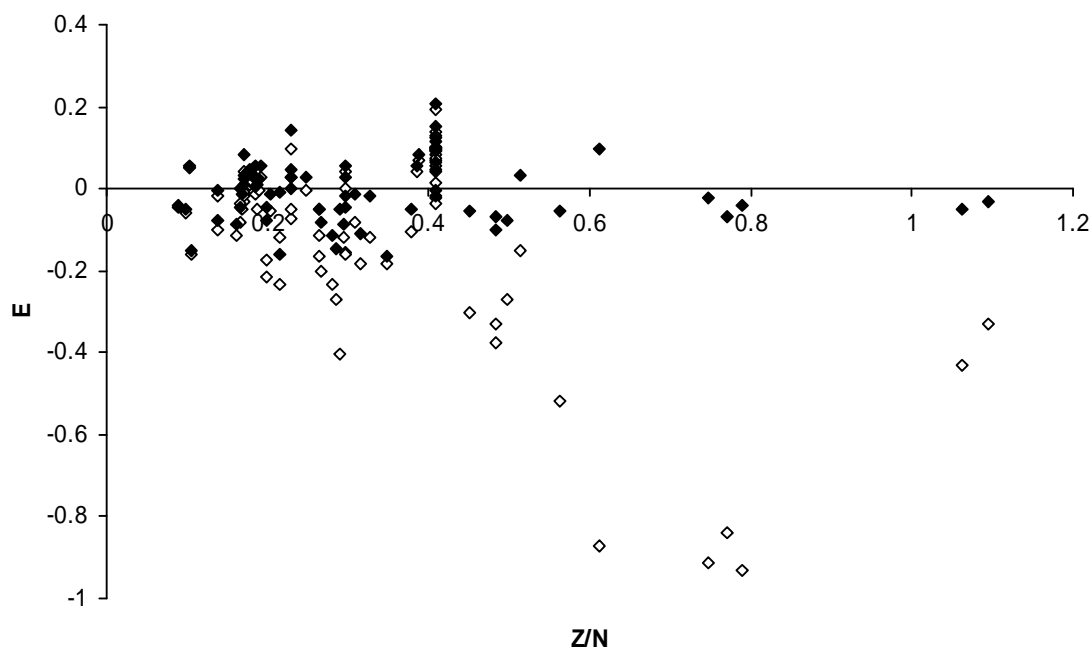
Figure 4-1) E versus Z/N for Model Mobilities. Results of 74 peptides (Sets 1 and 2) are included. Unfilled and filled diamonds correspond to model mobilities without and with the ion relaxation correction, respectively.

As Z/N increases and the effects of ion relaxation on mobility increase, E_{nr} tends to deviate more strongly from 0 as expected. It is worth noting that for E_r, the greatest "scatter" occurs at low Z/N. This can be explained as follows. When the net absolute charge, |Z|, of the peptide is low, a small absolute error in estimating Z can produce a large relative error in Z and hence E. Thus, inaccuracy in estimating peptide charge is likely to be a principal cause of error in predicting peptide mobilities. On the basis of Figure 4-1, this error is about 12 % in the worst cases. The random scatter seen argues against systematic error in our modeling procedure. Another possible source of error involves inaccurate sampling of peptide conformations. In previous work[88], mobility was shown to depend on conformation, but that dependence is fairly weak. The mobility of the pentapeptide, AAAAA, was shown to vary from .111 (fully extended) to .125 (compact) in a study of 5000 independent conformations.

If a peptide was trapped in a single conformation (fully compact, for example, with μ = .125 cm^2/kV sec), it is conceivable that a predicted mobility, based on conformations selected at random (giving $\langle\mu\rangle$ = .119 cm^2/kV sec in the above example) would produce error (5% in the above example).

Other investigators have developed sophisticated semi-empirical models that can be quite accurate under specific conditions. These include the multi-variable (MV) model by Janini and co-workers,[7] multiple linear regressions (MLR) model and artificial neural network (ANN) by Jalali-Heravi.[13] Listed in Table 3, along with experimental mobilities, are the corresponding "bead method" mobilities of the present work as well as predicted MV, MLR, and ANN mobilities.

Table 4-3

Comparison of Different Models with Experiment (Peptide Set 2)

No.	Y	μ(expt)[a]	μ(BM)[c]	μ(BM)[d]	μ(MV)[a]	μ(MLR)[b]	μ(ANN)[b]
1	1.072	0.128	0.115	0.113	0.1318	0.1399	0.1306
2	1.135	0.133	0.123	0.120	0.1391	0.143	0.1351
3	1.194	0.146	0.131	0.128	0.1458	0.1473	0.1461
4	1.064	0.11	0.114	0.112	0.1091	0.1323	0.128
5	0.967	0.104	0.0998	0.0982	0.1076	0.1248	0.1192
6	3.509	0.33	0.439	0.341	0.3353	0.3517	0.3188
7	3.784	0.33	0.472	0.346	0.3318	0.3645	0.3176
8	0.867	0.0975	0.0934	0.0921	0.097	0.1176	0.1058
9	2.717	0.265	0.336	0.285	0.2854	0.2439	0.269
10	2.712	0.274	0.315	0.265	0.2546	0.2324	0.2555
11	4.693	0.297	0.546	0.317	0.2975	0.3325	0.3072
12	4.960	0.297	0.573	0.309	0.2961	0.3454	0.3089
13	2.918	0.264	0.351	0.282	0.2711	0.2492	0.2654

14	2.984	0.264	0.363	0.290	0.2507	0.2535	0.2636
15	4.826	0.303	0.579	0.310	0.3141	0.3557	0.3068
16	3.684	0.29	0.440	0.306	0.2639	0.2872	0.2764
17	1.946	0.214	0.247	0.224	0.2194	0.2004	0.2215
18	2.188	0.208	0.241	0.212	0.1922	0.1844	0.2092
19	1.959	0.19	0.228	0.206	0.2049	0.181	0.204
20	1.949	0.194	0.239	0.216	0.1885	0.184	0.2028
21	4.872	0.29	0.543	0.262	0.2832	0.3429	0.2857
22	1.736	0.187	0.209	0.189	0.1983	0.1635	0.1865
23	1.796	0.178	0.209	0.186	0.1771	0.1691	0.1839
24	2.782	0.208	0.292	0.218	0.2179	0.2213	0.218

[a] data comes from Ref. 5. [b] data comes from Ref. 33.

[c] bead model without ion relaxation

[d] bead model with ion relaxation

Plotted in Figure 4-2 are the corresponding E values for the four models. (Values for the bead

model in the absence of the ion relaxation correction are not included.) The corresponding

$<E^2>^{1/2}$ values are: .069 (bead model with relaxation correction), .045 (MV), .118 (MLR),

and .058 (ANN). Although the bead model is not better than the semiempirical models, it is

competitive with all of them. Furthermore, there is considerable advantage to a structure

based model grounded in fundamental electrokinetic theory as discussed in the Conclusions

section.
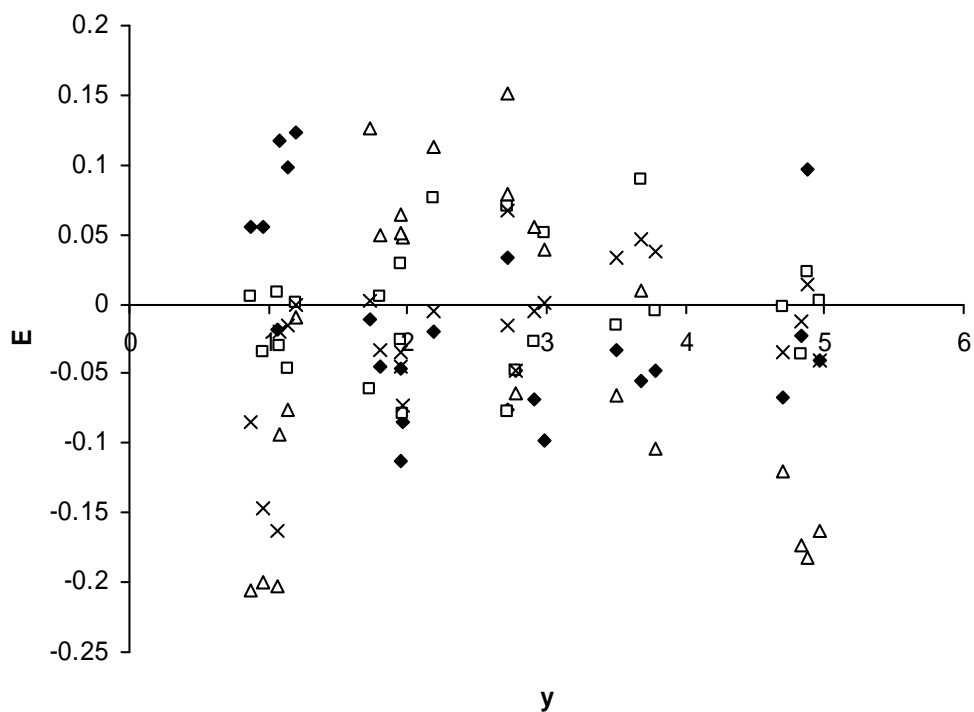
Figure 4-2) Comparison of Several Models with Experiment versus y. Results are for
Peptide set 2. Bead Model with ion relaxation (diamonds), MV (squares), MLR (triangles),
and ANN (crosses).
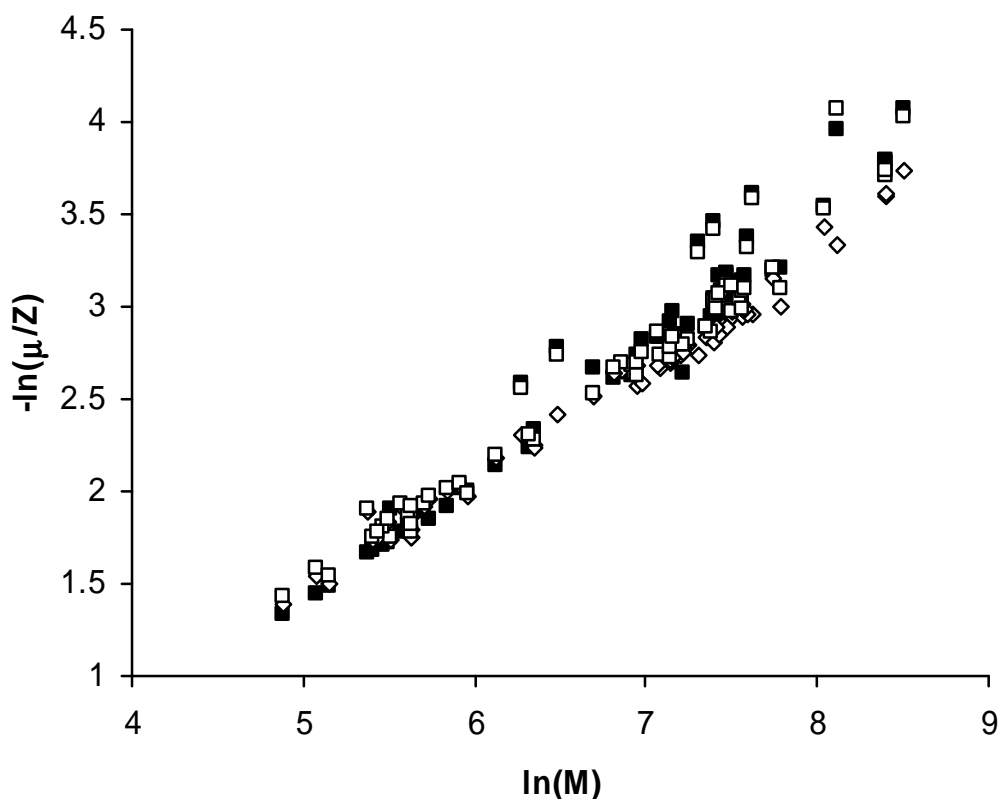
Figure 4-3) Correlation of Experimental and Model Mobilities with Net Charge, Z, and molecular weight, M. Results of 74 peptides (Sets 1 and 2) are included. Experimental data points are represented by filled squares. Model results without and with the ion relaxation correction are indicated by unfilled diamonds and squares, respectively.

Plotted in Figure 4-3 are the $-\ln(\mu/Z)$ versus $\ln(M)$ for all 74 peptides (sets 1 and 2) listed in Tables 4-1 and 4-2. In this way, the bead modeling can be compared with the simple Offord model indicated in Eq. (2-54) and (2-55). Experimental points are indicated by filled squares. Model results without and with the ion relaxation correction are indicated by unfilled diamonds and squares, respectively. As can be seen, there is considerable scatter in the results. Plotted in this way, model results with ion relaxation always lie below those without ion relaxation. More highly charged peptides tend to lie above their more weakly

charged counterparts.

   Next, we shall consider the case of a protein charge ladder.[76] The reason for presenting this analysis is to address two issues. First, it shows that the ralxation correction works well for globular proteins. Second, the simple bead models used in the present work yield electrophoretic mobilities that are comparable to those using BE modeling that accounts more accurately for the actual surface of hydrodynamic shear. Protein charge ladders are collections of protein derivatives where the number of charge group is varied by partial acylation of lysine residues or by amidation of glutamic and aspartic acid residues.[6,45,76] Modified proteins which have the same number of acylated sites have approximately the same charge and migrate with approximately the same mobility. In this work, we consider the example of human carbonic anhydrase II.[76] The charge ladder was formed by partial acylation of a variable number of the 23 lysines present in the protein. For modeling, bead coordinates were genetated from the crystal structure available through Protein Data Bank (PDB code 1CA2).

   It was assumed that the conformation of the protein remains unchanged as it is acylated. To examine, in a systematic manner, the importance of ion relaxation, mobilities are plotted versus the number of lysine residue modified (n). The unmodified protein is negatively charged and as n increases, the net charge of protein increases. Figure 4-5 summarizes the principal results. Experimental results are indicated with asterisks and bead model results without and with the relaxation correction are indicated weak and heavy solid lines, respectively. As n increases, the absolute charge of the protein increases and ion relaxation becomes progressively more important. From this example, it is clear that ion relaxation becomes important when $|\mu|$ exceeds approximately 0.2 cm^2/kV sec. The good agreement between modeling (with ion relaxation) and experiment confirms the accuracy of the bead methodology in a situation quite different from the peptides considered previously. Also

included in Figure 4-5 are results from an earlier Boundary Element, BE, modeling study[6] indicated by the thick, shaded line. In BE modeling, the macroion is modeled as an irregularly shaped rigid body with charges distributed within.[6,91] Also, ion relaxation is included in this case and its inclusion is determined by direct numerical solution of the coupled electrokinetic field equations.[33,34,91] Although the BE results are expected to be accurate, they also require much more computation time than the bead model results of the present study.

human carbonic anhydrase II
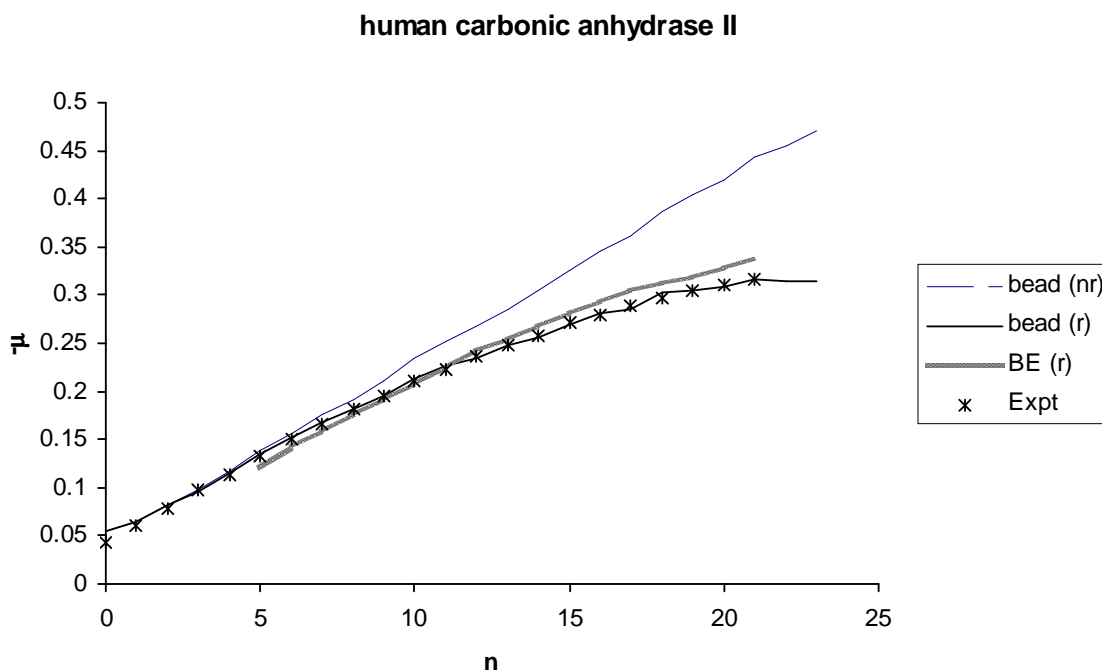
Figure 4-4) Mobilities vs n for human carbonic anhydrase II. The studies are carried out in 25 mM Tris base plus 192 mM glycine at 25 C and pH = 8.4.

4.5 Summary

The bead methodology, described in Chapter 2 and 3, differs from semi-empirical approaches[7,13] in three significant ways. First, it is structure based. Second, it is formally

grounded in electrokinetic theory. Third, its parameterization is totally independent of mobility measurements. Consequently, it can be applied to a broad range of flexible biomolecules under a wide range of experimental conditions and it can potentially be used to extract charge and structural information. The principal objectives of the present study involve the analysis of two assumptions of our earlier work and generalizing the methodology to deal with them. These two assumptions and how they impact present and future work are summarized below.

First, the restriction that $\kappa a \ll 1$ (where κ is the Debye Huckel screening parameter and "a" is a typical subunit radius in our model) has been removed. For the peptides under the conditions examined in this paper, $\kappa a \cong 0.16$, and the assumption of small κa is shown to yield accurate mobilities. It should be emphasized, however, that this is specific to the system of interest. For peptides, for example, the assumption becomes progressively worse as the salt concentration increases. For another example, suppose we wish to model duplex DNA as a semi-flexible string of touching beads of radius of 1.59 nm.[92] In this case, $\kappa a \cong$ 0.58 in a monovalent salt solution of 20 mM at room temperature, and finite bead effects can be expected to be much more significant than they are in the peptide systems examined in the present work. This is a subject under investigation in our laboratory at the present time.

Second, the effect of ion relaxation is accounted for in the present study. Ion relaxation becomes important when the local charge density, becomes large. Provided the absolute elctrophoretic mobility of a peptide does not exceed approximately 0.2 $cm^2/(kV\ s)$, ion relaxation can be ignored.[6,29] The direct inclusion of ion relaxation in electrophoresis theory is challenging due to the coupling of the electrodynamic, fluid flow, and ion transport field equations.[30,31,33,34,42,44,91] The approach used here is much simpler and is based on the observation that the relaxation effect is similar for irregularly shaped particles and spheres under similar conditions.[90] Thus, mobilities that do not account for ion relaxation are

corrected using a correction factor derived from mobility studies of spheres under similar conditions. It should be emphasized that this approach is approximate and may not work well for highly asymmetrical particles. Also, the equilibrium potential is calculated at the level of the linearized Poisson-Boltzmann equation in this work. When the charge on the macroion is high, the non-linear Poisson-Boltzmann equation should really be solved and this will influence the relaxation correction. We have tested the algorithm by it applying it to two sets of peptides (74 total) from the work of Janini and co-workers.[7,12] Some of the peptides in this data set are highly charged and ion relaxation is predicted to have an effect on their mobilities. The model mobilities are in good agreement with experiment when corrected for ion relaxation. It is also shown that the accuracy of the bead model methodology is competitive with the semiempirical methods developed by a number of investigators. As a final application, the bead model methodology is applied to the "charge ladder" of human carbonic anhydrase II.[76] In this example, the charge on the protein is varied in a systematic way and also protein conformation does not change significantly as the charge is varied. When the charge of the protein is low, it is demonstrated that ion relaxation has little effect on mobility. When the charge is large, however, ion relaxation is important in reducing the absolute mobility relative to the "no relaxation" value. When corrected for ion relaxation, model and experimental mobilities are found to be in excellent agreement.

In the future, we plan to extend this work in several directions. First of all, we are now in a position to study other biomolecules such as single stranded DNA, RNA, and duplex DNA. These tend to be more highly charged than peptides and thus the relaxation effect is expected to be significant. Also, the model "building blocks" for these systems[92] will be larger than for peptides making it more important to account for the finite size of the model subunits

Chapter 5

Electrokinetic Transport of a Spherical Gel-layer Model Particle

5.1 Introduction

The combined and complementary techniques of electrophoresis and viscosity are potentially useful in the quantitative characterization of charge, size, and other structural features of highly charged colloidal particles in solution.[21] The colloidal particle which we were interested is polystyrene sulfonate coated with sodium polystyrene sulfonate. The structure of sodium polystyrene sulfonate is shown in Figure 5-1. This colloidal particle is a typical model for the 'soft' particle with a hard inner core surrounded by a porous gel layer which has an unusual behavior of mobility and viscosity compared to 'hard' surface particle.
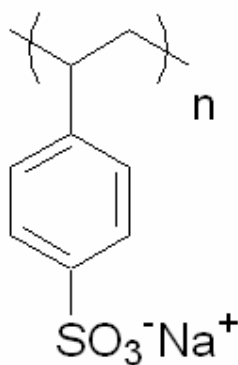
Figure 5-1) Structure of sodium polystyrene sulfonate.

In past works, a number of investigators have noted "anomalies" in the electrophoresis and viscosity results of polystyrene latex particles. These include electroviscous effects (Ion

relaxation also causes the viscosity of a suspension of dilute hard particles to be higher that that of a corresponding suspension of equivalent, but uncharged particles and this is called the primary electroviscous effect.[44]) that are difficult to reconcile with "hard sphere" modeling,[22,95] and a significant dependence of mobility on pH.[96,97]

 Ohshima has developed a detailed theory of the electrophoresis of spherical colloid particles containing a gel layer.[98-101] This work is of considerable value in enabling scientists to understand the essential physics of colloid electrophoresis when a gel layer is present. On the other hand, this theory is only applicable when the colloidal particle is weakly charged, since the ion relaxation effect is not accounted for. Hill et al.[102] accounted for the relaxation effect in modeling the electrophoresis of spherical particles containing a gel layer. Recently, we developed a spherical gel layer model that numerically determines both the electrophoretic mobilities and viscosity of highly charged particles of arbitrary size.[21] Basically, this model extends the "hard sphere" model of O'Brien and White[31](electrophoresis) and Watterson and White[103](viscosity) to include the presence of a gel layer of uniform composition.

 In the present work, we shall apply this model to the polystyrene sulfonate latex studied by Garcia-Salinas and de las Nieves.[22,95] Another factor that is dealt with in the present work is accounting how environmental considerations influence the pK_a of charged groups in the gel layer. This effect is examined using free energy arguments and solution of the Poisson-Boltzmann equation.

5.2   Method

5.2.1   Model System

 The colloidal particle considered in the present work is a generalization of the model

considered previously.[21] The model consists of an unhydrated core particle of radius a made up of "segments" of volume v_c per segment. The gel layer, which lies outside of the core and may be hydrated, is made up of potentially different material. Let v_{gl} denote the volume of an individual (unhydrated) segment in the gel layer. It is assumed that the segment density within the gel layer, ρ_s, is uniform and that it drops abruptly to 0 at a distance, b, from the center of the colloidal sphere. If the gel layer were fully collapsed, then $b = b*$. The number of segments making up the core, N_c, and gel layer, N_{gl}, are then

$$N_c = \frac{4\pi a^3}{3v_c} \qquad (5-1)$$

$$N_{gl} = \frac{4\pi(b*^3 - a^3)}{3v_{gl}} \qquad (5-2)$$

Also let f denote the fraction of segments in the gel layer, which equals $N_{gl}/(N_c+N_{gl})$. It is straightforward to show

$$a = \frac{b*(1-f)^{1/3}}{(1+\Delta f)^{1/3}} \qquad (5-3)$$

where

$$\Delta = \frac{v_{gl} - v_c}{v_c} \qquad (5-4)$$

If V_t* and V_t denote the total volumes of the unhydrated and hydrated particle, respectively, the degree of hydration, S_V, is

$$S_V = \frac{V_t - V_t*}{V_t*} \qquad (5-5)$$

and it then follows,

$$b = b*(1+S_V)^{1/3} \qquad (5-6)$$

Due to hydration, there is partial fluid flow within the gel layer.[93,94,104,105] In a reference frame stationary with respect to the core of the particle, the solution of the

Brinkman and solvent incompressibility equations is

$$\eta_0 \nabla^2 \underline{v} - \underline{\nabla} P \;=\; -\underline{s_e} + \eta_0 \lambda^2 \underline{v} \qquad (5-7)$$

$$\underline{\nabla} \cdot \underline{v} \;=\; 0 \qquad (5-8)$$

where η_0 is the solvent viscosity, **v** is the local fluid velocity, P is the pressure, s_e is the local external electric force/volume on the fluid, and λ is the Brinkman screening parameter with units of length^{-1} that is related to the segment density within the gel layer.[93,94,104,105] Let ζ and ρ_s denote the friction factor/segment and the segment density in the gel layer, respectively, then

$$\rho_s \zeta \;=\; \eta_0 \lambda^2 \qquad (5-9)$$

Setting $\zeta = 6\pi\eta_0\sigma$ where σ is an effective hydrodynamic radius in the gel layer. If we simply take $\sigma = v_{gl}^{1/3}$, it then follows that

$$\lambda^{*2} \;=\; \frac{6\pi}{\sigma^2} \qquad (5-10)$$

where λ^* is the Brinkman parameter of a unhydrated gel layer. For styrene, for example, the partial molar volume is 99 cm^3/mole[106] and hence $v_{gl} = 1.645 \times 10^{-22}$ cm^3, $\sigma = .548$ nm, and $\lambda^* = 7.92$ nm^{-1}. For the hydrated particle, the previous relations can be combined to yield

$$\lambda^2 \;=\; \lambda^{*2} \frac{(1+\Delta)}{\left(\dfrac{S_V}{f} + 1 + \Delta(1+S_V)\right)} \qquad (5-11)$$

This is a generalization of Eq. (6) of reference 21 where it was assumed $v_{gl} = v_c$ and hence $\Delta = 0$.

We now come to the charge characteristics of the particle. It shall be assumed that the total charge resides in a potentially charged "halo" that comprises at least part of the gel layer. This is shown schematically in Figure 5-2 where the charge halo lies within the spherical shell, $a' < r < b'$. Also shown is the core radius, a, and the outer radius of the gel layer, b. It

should be emphasized that ρ_s (segment density) within the entire gel layer ($a < r < b$) is assumed uniform. The density of monovalent acidic groups within this halo is assumed to be uniform and let γ denote the average number of acidic groups per segment. If every segment within the halo carried a single acidic group, for example, $\gamma = 1$. If Q_t^0 denotes the total titration charge (in protonic units) of a single colloid particle and N_{cgl} is the number of segments in the charge halo,

$$N_{cgl} = -\frac{Q_t^0}{\gamma} \quad (5-12)$$

Since the entire gel layer has a uniform segment density

$$N_{cgl} = \left(\frac{b'^3 - a'^3}{b^3 - a^3}\right) N_{gl} \quad (5-13)$$

It will prove convenient to define a new parameter, Φ, by

$$\Phi \equiv -\frac{3 v_{gl} Q_t^0}{4\pi\gamma b*^3} = \left(\frac{b'^3 - a'^3}{b^3 - a^3}\right)\left(1 - \left(\frac{a}{b*}\right)^3\right) \quad (5-14)$$

The second equality on the rhs of Eq. (5-14) follows from Eq. (5-2). For the polystyrene sulfonates of interest in this work, $Q_t^0 = -3.6 \times 10^5$, $b* = 144.5$ nm, and v_{gl} has been previously given. If we also make a reasonable assumption regarding γ, then Φ is determined. Assuming all segments in the gel layer carry a single acidic group, $\gamma = 1$ and $\Phi = 4.69 \times 10^{-3}$. We shall also assume $b' = b$ (the outermost portion of the gel layer contains potential charge sites), $\Delta = 0$ (segment volumes of core and gel layer are equal), and $b - a \ll b$ (the thickness of the gel layer is small relative to the overall size of the particle), then Eq. (5-14) reduces to

$$a = b*\left(1 - \left(\frac{b-a}{b-a'}\right)\Phi\right)^{1/3} \quad (5-15)$$

From Eq. (5-3),

$$f = \left(\frac{b-a}{b-a'}\right)\Phi \qquad (5-16)$$

The degree of hydration, S_V, and hence b, can be deduced from viscosity studies. For a dilute suspension of spheres, the coefficient, p', is defined[21,107]

$$\frac{\eta}{\eta_0} - 1 = \frac{5}{2}(1+p')\phi^* \qquad (5-17)$$

where η is the viscosity of the suspension, η_0 is the solvent viscosity, and ϕ^* is the volume fraction of the colloid particles in the solution if hydration is ignored. In modeling, it is convenient to define shape factors, ξ and ξ_0, for the hydrated charged and uncharged model particles respectively,

$$\frac{\eta}{\eta_0} - 1 = \xi\phi = \xi_0(1+p)\phi \qquad (5-18)$$

where ϕ is the volume fraction of the hydrated particle and p is the primary electroviscous coefficient. The shape factors and p are determined numerically using electrokinetic modeling.[21,103] It is straightforward to show that

$$p' = \frac{2\xi_0}{5}(1+p)(1+S_V) - 1 \approx S_V + p(1+S_V) \qquad (5-19)$$

The second equality on the rhs of Eq. (5-19) holds for colloidal particles with thin gel layers since $\xi_0 \approx 5/2$. Also, p is only significant at low salt[103] and hence p' $\approx S_V$ under these conditions.[21,107] At high salt, p' is dominated by solvation and this gives S_V.

We can now outline a procedure to make reasonable parameter assignments for the model. If we have b* and can estimate S_V from viscosity data, Eq. (5-6) yields b. From Eq. (5-14), Φ is known provided Q_t^0, v_{gl}, and γ are specified. A value for the ratio, (b – a)/(b – a'), can be assumed and then a and f follow from Eqs. (5-15) and (5-16). Also, Eq. (5-11) yields λ.
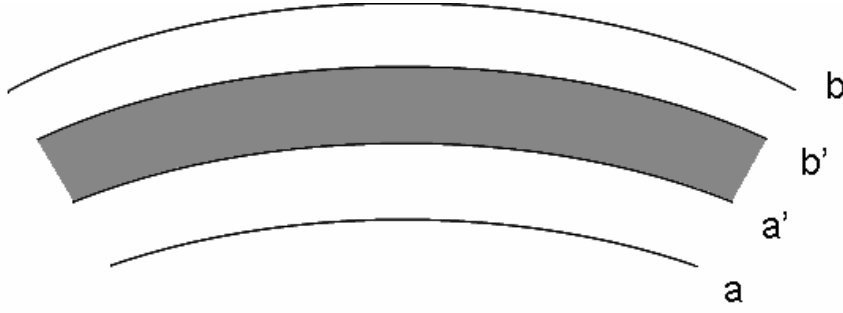
Figure 5-2) Schematic of the Spherical Gel-Layer Model. The solid core of the spherical particle has radius a. The gel layer, assumed to have a uniform segment density, extends from a < r < b, where r is the radius. The potentially charged portion of the gel layer extends from a' < r < b'.

5.2.2 Using Free Energy Cycle and Poisson-Boltzmann Theory to Determine Charge and Electrostatic Potential

For the spherical colloid model described in the Model section, the electrostatic potential, Λ_0, is a function of the radial variable, r. Also let $y(r) = q\Lambda_0(r)/k_BT$ denote a reduced (dimensionless) potential, k_B is Boltzmann's constant, and T is absolute temperature. The charge of the colloidal particle is assumed to arise from deprotonation of acidic groups that are present at uniform concentration, $\rho_s\gamma$, in the gel layer for a' < r < b'. Let $pKa(r) = -log_{10}(Ka(r))$ where $Ka(r)$ is the local acid dissociation constant at position r in the gel layer. At r, the fraction of acidic groups that are deprotonated, $\chi(r)$, is

$$\chi(r) \quad = \quad \frac{1}{1 + 10^{pKa(r) - pH_{loc}(r)}} \qquad (5-20)$$

where $pH_{loc}(r)$ is the local pH of the solution. It is important to distinguish this from the ambient pH of the solution which shall simply be denoted "pH" in this work. Because of the unusual electrostatic environment of a highly charged gel layer, local concentrations of H^+ as well as other ions can be very different from their bulk values.[97] It is straightforward to show

$$pH_{loc}(r) \;\;=\;\; pH + 0.434\, y(r) \qquad (5-21)$$

Because of "charge regulation", $(0 < \chi(r) < 1)$, the actual charge of the colloidal particle, Q_t (in protonic units), will be different from the titration charge, Q_t^0. The actual charge of the model particle can be written

$$Q_t \;\;=\;\; \frac{3Q_t^0}{b'^3 - a'^3} \int_{a'}^{b'} r^2 dr\, \chi(r) \qquad (5-22)$$

From Eq. (5-20), we need to know the local pKa before we can compute $\chi(r)$ and this, in turn, can be very different from the dissociation constant of the free acid, pKa^0, due to environmental conditions at a particular charge site.[74] In the field of Biophysics, atomically detailed models based on the continuum dielectric/linear Poisson-Boltzmann equation have been developed to compute pKa's of charge groups of biomolecules, particularly proteins.[77-81] For highly charged gel layers, it is necessary to go beyond the linear Poisson-Boltzmann equation upon which these methodologies are based. Starting from a general expression for the electrostatic free energy at the level of the continuum primitive model,[108] we derive an approximate expression for pKa(r) in Appendix A, Eqs. (A13-A14). These simple expressions relate the local pKa to the characteristics of the gel layer as well as y(r) and $\chi(r)$.

The Poisson-Boltzmann equation for the spherical colloid particle beyond the surface of the core, $r > a$, can be written

$$\frac{1}{r^2}\frac{d}{dr}\left(r^2 \frac{d\Lambda_0(r)}{dr}\right) \;\;=\;\; -\frac{X\gamma q}{\varepsilon}\rho_s(r)\chi(r) - \frac{Xq}{\varepsilon}\sum_j c_{j0} z_j \omega(r) e^{-qz_j\Lambda_0(r)/k_BT} \qquad (5-23)$$

where $X = 4\pi$ (in CGS units) or $1/\varepsilon_0$ where ε_0 is the permittivity of free space (in MKSA units), ε is the dielectric constant of the solution (assumed uniform), c_{j0} is the ambient concentration of mobile ion j of valence z_j, $\omega(r)$ is the ion exclusion parameter (assumed uniform for all ions), and the sum extends over all mobile ion species present. The concentration of gel fragments, $\rho_s(r)$, is equal to zero for $r > b$ and equal to $3N_{gl}/4\pi(b^3-a^3)$ for

$a < r < b$ where N_{gl} is given by Eq. (5-2). The ion exclusion parameter is given by

$$\omega(r) \;=\; 1 - \rho_s(r)\,v_{gl} \qquad (5-24)$$

Let $x = 1/\kappa r$ where κ is the Debye-Huckel screening parameter of the solution (see Eq. (B9)). Eqn. (5-23) can then be written

$$x^4 \frac{d^2 y(x)}{dx^2} \;=\; -\frac{\gamma}{2I}\rho_s(x)\chi(x) - \sum_j \left(\frac{c_{j0}}{2I}\right) z_j\,\omega(x)e^{-z_j y(x)} \qquad (5-25)$$

where I is the ionic strength of the solution. In the applications of interest in the present work, the core of the particle is uncharged and excluded to penetration by mobile ions. Consequently, we have the following boundary condition,

$$\left(\frac{d\,y(r)}{dr}\right)_{r=a} \;=\; 0 \qquad (5-26)$$

For small x or large r ($r > b + 6/\kappa$, for example), y approaches the linear Poisson-Boltzmann form

$$y(x) \;=\; Axe^{-1/x} \qquad (5-27)$$

where A is an undetermined constant. If our particle was a weakly charged solid sphere of radius a and total charge Q_t (in protonic units), then $A = X\kappa q^2 Q_t e^{+\kappa a}/(4\pi\varepsilon(1+\kappa a))$. This value might serve as a reasonable initial estimate of A, but in general, it must be chosen in an iterative approach to simultaneously satisfy Eq. (5-25) and the boundary condition, Eq. (5-26).

An outline of the procedure used to calculate y and χ can now be given. One begins with and initial estimate of χ. For example, if the colloid is assumed to be fully charged (all acidic groups deprotonated), then $\chi = 1$ for a' $< r <$ b' and equal to 0 otherwise. A is then estimated and Eq. (5-25) solved by a 4th order Runge-Kutta algorithm[109] starting from small x (large r). If y begins to diverge or Eq. (5-26) is not satisfied, A is adjusted. This procedure is repeated until y converges and Eq. (5-26) is satisfied to within a specified tolerance level.

When converged, we only have an <u>approximate</u> reduced potential since it is based on approximate χ's. By specifying the pH and pKa^0 of the charge group, Eqs. (A13-A14) are used to estimate pKa(r) using approximate χ's and y's. Then, Eqs. (5-20 and 5-21) are used to re-estimate the χ's over the gel layer domain. At this point, the entire cycle is repeated until the y's and χ's converge.

5.3   Results

Past theoretical/modeling work has extensively studied the electrophoresis of weakly[98-101] and highly[102] charged spherical colloid particles containing a gel layer. In the present work, we shall focus on a particular polystyrene sulfonate latex[95,110] since both electrophoresis and viscosity studies have been carried out on that particular system. The viscosity studies provide valuable information about the presence of a gel layer that compliments measurements of electrophoresis.[21,107] These latex particles have a diameter of 289 nm and a surface charge density of -22 μC/cm^2.[110] This surface charge density, σ_c, determined by conductometric titration, can be related to the titration charge of the particle, Q_t^0 (in protonic units), by

$$Q_t^0 \;=\; 0.7844\,\sigma_c\,b*^2 \qquad (5-28)$$

where σ_c is in μC/cm^2 and b* is in nm. Assuming b* = 144.5 nm, Q_t^0 = -3.6 x 10^5. The experiments were carried out at 25 °C (η_0 = 0.89 cP) at pH = 5.5 in monovalent NaCl solutions with concentrations varying from 10^{-6} to 10^{-1} moles/liter. We shall set $v_c = v_{gl}$, σ = 0.548 nm, λ* = 7.92 nm^{-1}, γ = 1.0, and Φ = 4.69 x 10^{-3} (see the Model section of this chapter). Since the relaxation effect is included in this work, it is necessary to account for the mobilities of co- and counterions present.[30,31] As discussed previously,[105] the hydrodynamic

radius, r_j, of a mobile ion is estimated from limiting molar conductivities, λ_j^∞, and the Nernst-Einstein relation. If z_j is the ion valence, then

$$r_j \quad = \quad 9.201 \frac{z_j^2}{\lambda_j^\infty} \qquad (5-29)$$

where r_j is in nm and λ_j^∞ is reported at 25 °C in 10^{-4} S m^2/mole. From tables of λ_j^∞, r_j = .0263, .1837, and .1206 nm for H$^+$, Na$^+$, and Cl$^-$, respectively.[111]

In order to illustrate the importance of ion relaxation in the present application, we shall first consider the example of a uniformly charged gel layer model (Eqs. (5-15) and (5-16) yield a = 144.27 nm and f = Φ = 4.69 x 10^{-3}), with S$_V$ =0.30 (Eq. (5-6) yields b = 157.71 nm and Eq. (5-11) yields λ = 0.982 nm^{-1}). In order to insure that Eq. (5-12) on p. 253 of Ohshima[100] is applicable, we shall also choose a NaCl concentration of 10^{-2} moles/liter.
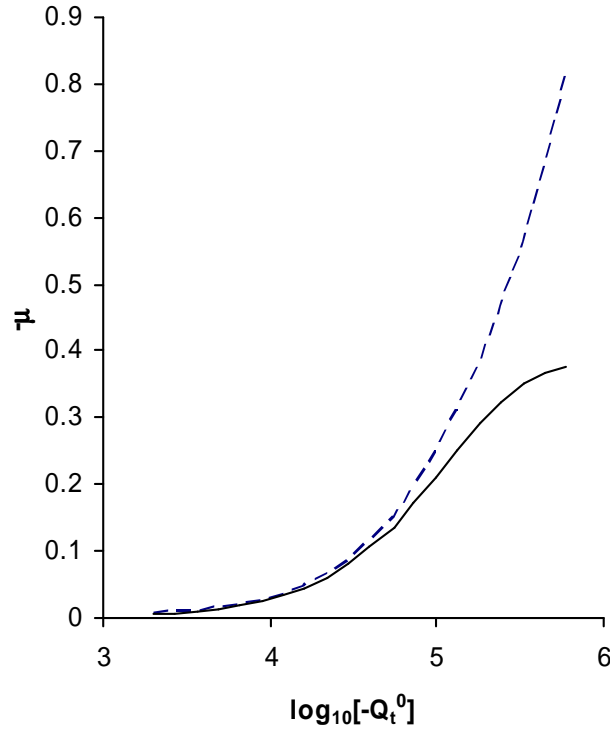
Figure 5-3) Mobility, μ, versus Net Charge, Q_t^0, for a Particular Uniformly Charged Gel-Layer Model. In this example, T = 25 °C, η_0 = 0.89 cP, [NaCl] = 0.01 moles/liter, σ = .548 nm, a = a' = 144.27 nm, b = b' = 157.71 nm, λ = .982 nm^{-1}, and μ's are in cm^2/kV sec. The solid line represents mobilities that include the relaxation effect (calculated using the numerical procedure of ref. 21 and the present work), and the dashed line represents mobilites that do not include the relaxation effect (calculated using Eq. (12) of ref. 100).

Plotted in Figure 5-3 is the electrophoretic mobility, μ, in cm^2/kV sec, over a wide range of different Q_t^0. The solid line represents the numerical mobilities of the present work that include the relaxation effect, and the dashed line is from Ohshima,[100] which does not account for the relaxation effect. If the absolute charge of the colloidal particle is low, the two results are in excellent agreement with each other. If the absolute charge is high, however, the absolute mobility predicted by Ohshima exceeds the numerical value by a significant amount. Since the actual polystyrene sulfonate latex particles contain a titration charge that occurs near the high (absolute) charge end of Figure 5-3, it is important to include the relaxation effect in this case. Shown in Figure 5-4 is the absolute reduced potential at r = a (dashed line), and r = b (solid line). Comparing Figures. 5-3 and 5-4, it is clear that the relaxation effect becomes significant when the reduced absolute potential in the gel layer exceeds 1-2.
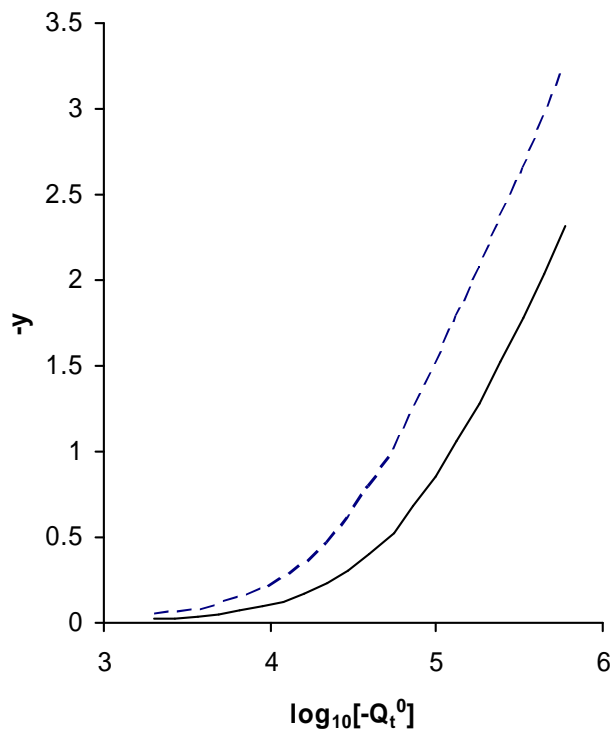
Figure 5-4) Reduced Potential, y, versus Net Charge, Q_t^0, for a Particular Uniformly Charged Gel-Layer Model. Parameters are the same as in Figure 5-2. The solid line represents y evaluated at r = b, and the dashed line represents y evaluated at r = a.

Under the conditions of the above example, the primary electroviscous coefficient, p in Eq. (5-18) is small (< 0.003) even at the highest absolute charge considered. The primary electroviscous effect is only significant when there is significant distortion of the ion atmosphere by a shear field.[103,112] Conditions of a thin gel layer (b – a << b*), low $|Q_t^0|$, and high salt all act to reduce p. However, p' (Eqs. (5-17) and (5-19)), may be significant due to solvation of the particle.[21] In the example considered in the previous paragraph, p' ≈ 0.28 and is nearly independent of Q_t^0.
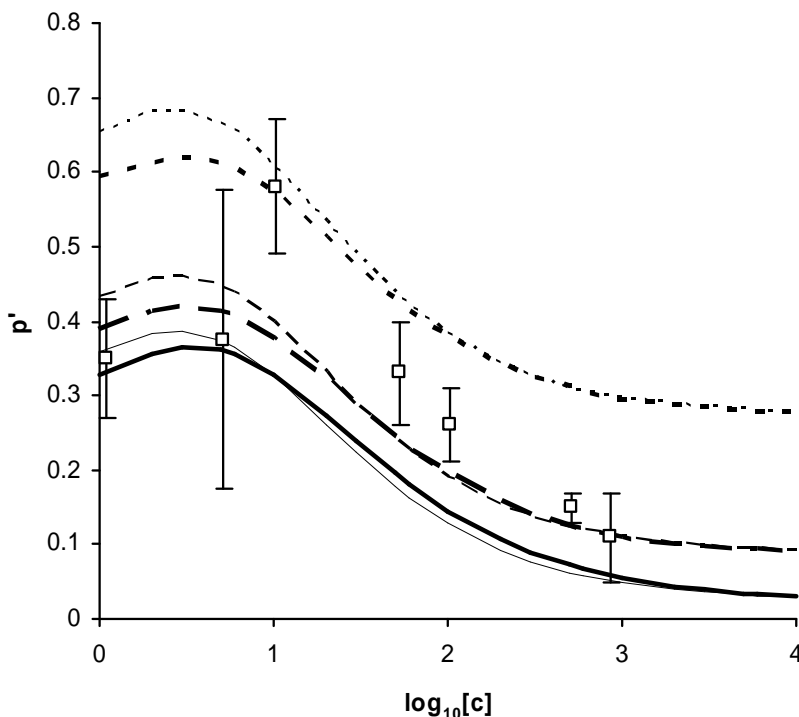
Figure 5-5) p' versus $\log_{10}[c]$ for Models with a Uniform Concentration of Acidic Residues in the Gel-Layer. Solid, dashed, and dotted lines correspond to $S_V = 0.03$, 0.10, and 0.30, respectively. Bold lines correspond to the inclusion of charge regulation (variable Q_t), and non-bold lines correspond to leaving charge regulation out ($Q_t = Q_t^0$). See the text for more details about model parameters.

Shown in Figure 5-5 are experimental p's[110] versus $\log_{10}[c]$ where c is the ambient NaCl concentration in μmoles/liter. Experimental points are squares with error bars. Also shown are model studies of uniformly charged gel layers with $S_V = 0.03$ (solid line, a = 144.27 nm, b = 145.93 nm, λ = 2.91 nm^{-1}), $S_V = 0.10$ (dashed line, a = 144.27 nm, b = 149.16 nm, λ = 1.68 nm^{-1}), and $S_V = 0.30$ (dotted line, a = 144.27 nm, b = 157.71 nm, λ = 0.982 nm^{-1}). Parameters are otherwise the same as before. In the model studies, the concentration of H$^+$ is taken to be 3 x 10^{-6} appropriate for a solution at pH = 5.5. Although the H$^+$ ions have little effect on results at high salt, they can have a significant effect at low salt.[110] For each of the three model studies shown with different S_V, separate studies are presented with and without

charge regulation. Studies without charge regulation (thin solid, dashed, and dotted lines) all have $Q_t = Q_t^0 = -3.6 \times 10^5$. For studies with charge regulation (thick solid, dashed, and dotted lines, $Q_t^0 = -3.6 \times 10^5$, but Q_t can be substantially different from Q_t^0 as discussed in the section entitled Charge and Electrostatic Potential. For the model studies with charge regulation, we assume $pKa^0 = 0.7$, consistent with the acid dissociation constant of benzene sulfonic acid.[111] Comparing these particular model results with the experimental p' in Figure 5-5, it is concluded that $S_V \approx 0.10$ at 0.001 mole/liter NaCl (the highest salt measured) but that $S_V \approx 0.30$ around 10^{-5} mole/liter NaCl. The behaviour at the very lowest salt is more complicated and shall be considered near the end of the Summary. For now, we shall focus on the data above approximately 10^{-5} moles/liter NaCl. For the uniformly charged gel layer models considered, charge regulation has only a modest effect on p' and then only at low salt concentration.
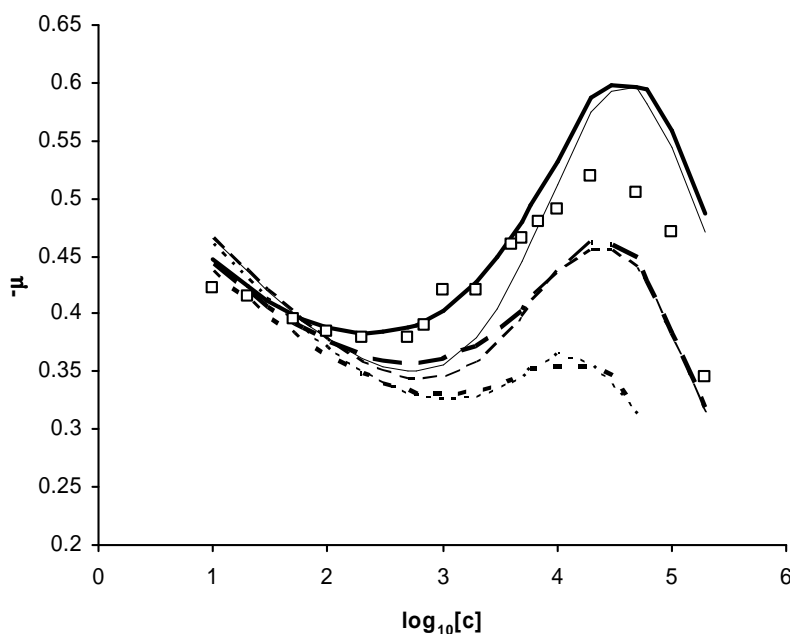
Figure 5-6) μ versus $\log_{10}[c]$ for Models with a Uniform Concentration of Acidic Residues in the Gel-Layer. Solid, dashed, and dotted lines correspond to S_V = 0.03, 0.10, and 0.30, respectively. Bold lines correspond to the inclusion of charge regulation (variable Q_t), and non-bold lines correspond to leaving charge regulation out ($Q_t = Q_t^0$). See the text for more details about model parameters.

Similar to Figure 5-5, shown in Figure 5-6 are experimental electrophoretic mobilities (squares) versus $\log_{10}[c]$. Mobilities are in cm^2/kV sec and as in the case of p', experimental mobilities come from reference 13. Also shown are model studies for the same three uniformly charged gel layer models considered in the previous paragraph with and without charge regulation. For a NaCl concentration below 0.01 mole/liter, the model with S_V = 0.03 and charge regulation included is in best agreement with experiment. At higher salt concentration, a model with S_V between .03 and .10 is most consistent with experimental mobility. An obvious problem with this interpretation is that the viscosity and mobility data lead to different model interpretations when the gel layer is assumed to be uniformly charged with the viscosity data consistent with a thicker gel layer than the mobility data.

Consider next a "halo" model in which only the outermost portion of the gel layer is charged. It is assumed that $(b - a)/(b - a') = 4$ so Eq. (5-15) yields a = 143.59 nm and Eq. (5-16) yields f = .01875. For a particular S_V, b is given by Eq. (5-6), λ by Eq. (5-11), and a' from the assumed ratio of $(b - a)/(b - a')$. The same S_V values considered previously using a uniformly charged gel layer are used in the "halo" model results presented in Figures 6 and 7. The specific parameters are: S_V = 0.03 (solid line, a' = 145.34 nm, b = 145.93 nm, λ = 4.91 nm^{-1}), S_V = 0.10 (dashed line, a' = 147.77 nm, b = 149.16 nm, λ = 3.15 nm^{-1}), and S_V = 0.30 (dotted line, a' = 154.18 nm, b = 157.71 nm, λ = 1.92 nm^{-1}). Otherwise, parameters are the same as before.
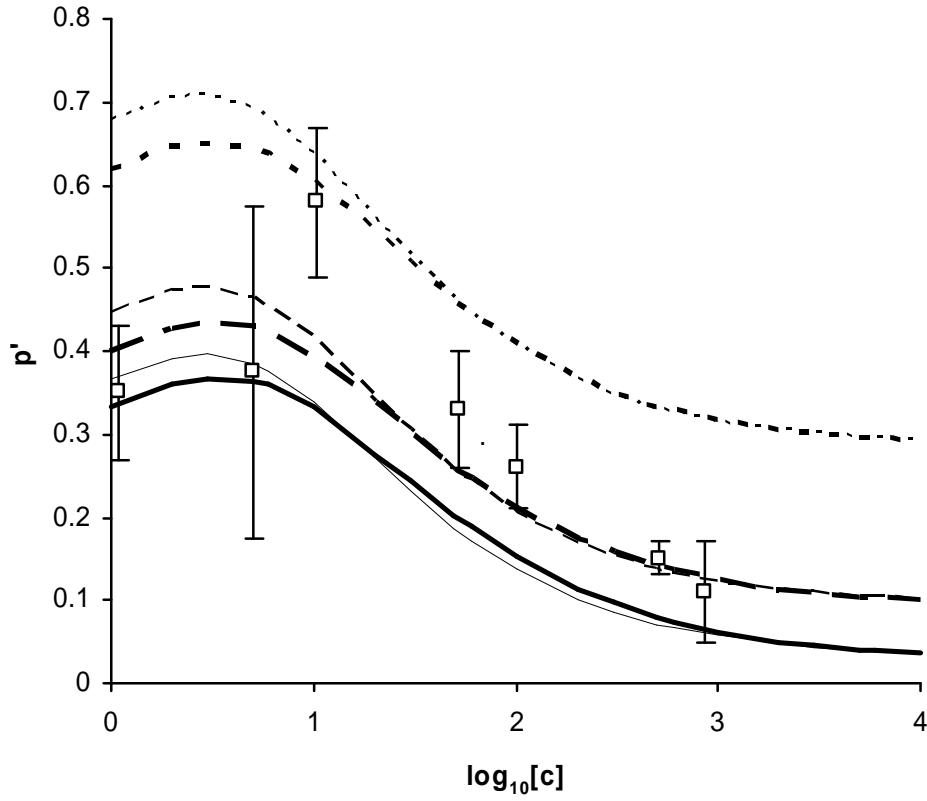
Figure 5-7) p' versus $\log_{10}[c]$ for Charged "Halo" Gel-Layer Models. Solid, dashed, and dotted lines correspond to S_V = 0.03, 0.10, and 0.30, respectively. Bold lines correspond to the inclusion of charge regulation (variable Q_t), and non-bold lines correspond to leaving charge regulation out ($Q_t = Q_t^0$). See the text for more details about model parameters
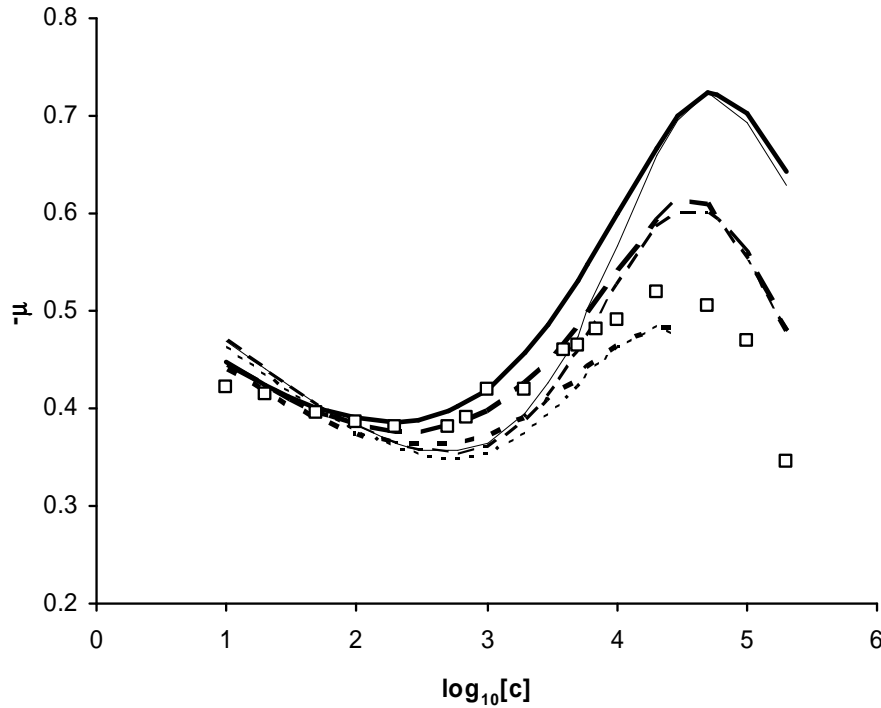
Figure 5-8) μ versus $\log_{10}[c]$ for Charged "Halo" Gel-Layer Models. Solid, dashed, and dotted lines correspond to $S_V = 0.03$, 0.10, and 0.30, respectively. Bold lines correspond to the inclusion of charge regulation (variable Q_t), and non-bold lines correspond to leaving charge regulation out ($Q_t = Q_t^0$). See the text for more details about model parameters.

Comparing Figs. 5-5 and 5-7, the detailed structure of the gel layer (whether it is uniformly charged or not) appears to have little effect on p' except at the lowest salt where charge regulation effects can be significantly different in the two cases. The mobility data of the halo model is especially interesting. The halo model with $S_V = 0.03$ and 0.10 are in good agreement with experiment at intermediate salt concentration. Also, including charge regulation improves quantitative agreement between model and experiment. Without charge regulation, it is simply not possible to find a gel layer model thick enough to give $S_V \geq 0.10$ (consistent with the viscosity data). For thick gel layers with $Q_t \approx -3.6 \times 10^{-5}$, model studies invariably yield $|\mu| \leq 0.36$ cm^2/kV sec at intermediate salt concentrations. Reducing $|Q_t|$ by the mechanism of charge regulation yields mobilities in better agreement with experiment.

Table 5-1

Charge regulation in the halo model with $S_V = 0.10$

$\log_{10}[c]^a$	$-\langle y \rangle_{gl}^{ncr}$	$-\langle y \rangle_{gl}^{cr}$	Q_t/Q_t^0
0	12.49	7.17	.0326
.30	12.26	7.12	.0355
.48	12.06	7.08	.0397
.70	11.78	7.01	.0454
1.0	11.33	6.88	.0548
1.48	10.41	6.75	.0719
2.0	9.25	6.35	.147
2.48	8.16	6.03	.231
3.0	6.98	5.63	.400
3.48	5.89	5.16	.615
4.0	4.68	4.44	.857
4.48	3.59	3.53	.972
5.0	2.44	2.41	.994

a – c is the NaCl concentration in μmoles/liter

In Table 5-1, the effects of charge regulation are illustrated in detail for the halo model considered in the previous paragraph with $S_V = 0.10$ as a function of salt concentration. Along with the ratio, Q_t/Q_t^0, are listed the averaged reduced potential in the charged portion of the gel layer in the absence, $\langle y \rangle_{gl}^{ncr}$, and presence, $\langle y \rangle_{gh}^{cr}$ of charge regulation. At low salt in the absence of charge regulation, the absolute reduced potential is very large and this causes the local pKa's to be much larger than the free solution value (taken to 0.7). This, in turn, causes the charged gel layers to become largely uncharged (by protonating the acidic sites) at low salt. Even with charge regulation, however, the reduced absolute potentials in

the charged portion of the gel layer exceed 7 at low salt. Above a NaCl concentration of about 10^{-2} moles/liter, charge regulation is insignificant.

Under high salt conditions of 0.10 mole/liter NaCl, model studies indicate the presence of a gel layer. A solid sphere model predicts $\mu = -0.80$ cm^2/kV sec under these conditions. A gel layer of at least 1 nm thickness is necessary in modeling to account for the experimental mobility of -0.47 cm^2/kV sec.

On the basis of the experimental data coupled with modeling, we conclude the polystyrene sulfonate latex particles contain a gel layer that shrinks from roughly $S_V = 0.3$ to 0.10 as the NaCl concentration is raised from 10^{-5} to 10^{-3} moles/liter on the basis of the viscosity data. The mobility data is consistent with this model provided charge regulation is included and only the outer portion of the gel layer is charged. This could occur, for example if the sulfonated polystyrenes were largely relegated to the outside of the particle, and there was a uncharged, but hydrated layer between the core surface and the charged portion of the gel layer. In order to account for the experimental mobilities, it is concluded that a gel layer of at least 1 nm thickness persists even at high salt.

5.4   Summary

In this chapter, an electrokinetic model of a spherical colloid particle containing a gel layer introduced previously[21] is developed further. The gel layer may be solvated, but is assumed to be of uniform segment density. It is also assumed that a portion of the gel layer bears acidic groups and that the charge of the particle results from deprotonation of these acidic groups. The actual charge state of the particle depends on the local pKa's of the charge groups and the local pH of the solution. In Appendices A and B, free energy considerations and Poisson-Boltzmann electrostatics are used to estimate the charge state of the colloidal

particle. This modulation of colloidal charge, which depends on the geometry of the charged gel layer, the intrinsic pKa of the acidic groups, the salt concentration, salt type, and pH is called charge regulation. This methodology is then applied to the viscosity and electrophoretic mobility of a particular polystyrene sulfonate latex over a broad range of monovalent salt concentration. Using realistic model parameters, it is straightforward to identify models which are consistent with experiment. The viscosity data strongly supports a model with a fairly thick gel layer at low salt in which S_V drops from approximately 0.30 to 0.10 as the concentration of NaCl is raised from 10^{-5} to 10^{-3} moles/liter. Even at high salt (0.10 moles/liter), the mobility data indicate the presence of a gel layer at least 1nm in thickness. The electrophoresis data in general can be accounted for by a halo model in which only the outer portion of the gel layer is charged. It is also necessary to include charge regulation in modeling. Modeling with charge regulation indicates that the colloidal particle becomes more highly protonated (lower absolute net charge) as the salt concentration is reduced. This may at first seem surprising since the intrinsic pKa of the benzene sulfonic acid groups are around 0.7[81] and the pH of the solution is 5.5.[110] Nonetheless, due to the large absolute electrostatic potential present in the charged gel layer at low ambient salt, significant protonation of even strong acid groups is predicted to occur.

The model considered here could be generalized in several ways. First of all, the concentration of segments in the gel layer probably is not uniform, and this could be modified by replacing a gel layer of uniform density with a variable density model. Second, it is possible that the charge of the colloidal particle could be further reduced by specific binding of counterions to the deprotonated acidic groups. Generalizing the model to account for these two factors as well as a number of others would be straightforward, but would have the disadvantage of introducing additional parameters into the model. These generalizations can be included as more experimental data becomes available. Finally, the viscosity data at

extremely low salt ($\leq 10^{-5}$ moles/liter) deserves comment. As pointed out by Garcia-Salinas and le las Nieves ,[110] the low values for p' seen in Figures. (5-5) and (5-7) below a salt concentration of about 10^{-5} moles/liter can be attributed to the presence of low, but finite concentrations of H^+. This is accounted for in the present work using an ion mobility estimated from limiting molar conductivities as discussed previously. This may overestimate the mobility of H^+ at the lowest salt concentrations considered.[95,113] However, this phenomenon appears to be limited to H^+ at very low salt and does not alter our primary conclusions.

Appendix A – The approximate pKa(r) of an acidic group in a gel layer surrounding a large colloidal particle.

Assume we have a gel layer of uniform segment density surrounding a large colloidal particle as discussed in the Model section. The colloidal charge is assumed to arise from deprotonation of acidic groups that are present in uniform concentration between a' < r < b', where r is the distance from the center of the colloidal particle. The acidic groups are considered to be monovalent and of a single type. (With minor modifications, this analysis could be modified to treat multiple acid types or deprotonation of basic groups. For the sake of brevity and clarity, this shall not be done in the present work.) Let pKa^0 denote the pKa of the free acid in dilute aqueous solution. This pKa is related to the single molecule free energy change, $\Delta G^0(HX \rightarrow X^-)$, by

$$pKa^0 = \frac{1}{2.303 k_B T} \Delta G^0 (HX \rightarrow X^-) \qquad (A1)$$

where k_B is Boltzmann's constant and T is absolute temperature. In general, pKa^0 will depend on concentration of acid and concentration of added salt and salt type. In practice,

however, these variations are small relative to the substantial charge-charge interactions present in a highly charged gel layer. Consequently, the dependence of pKa^0 on concentration and the characteristics of added salt shall be ignored. It shall also be assumed that electrostatic interactions between neighboring charge residues within the gel layer are responsible for the departure of pKa from pKa^0.
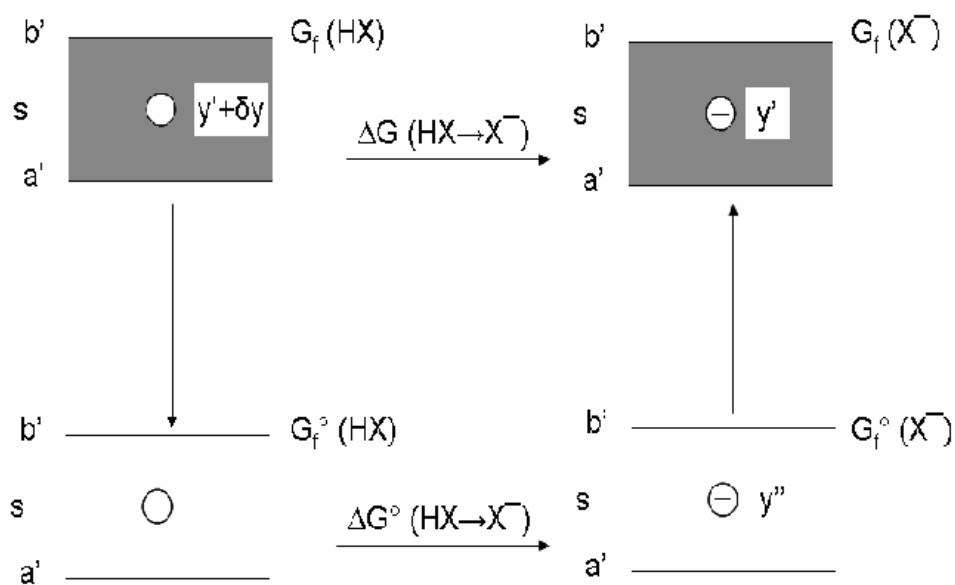
Figure 5-9) Free Energy Diagram of the Deprotonation of a Particular Acidic Residue in the Gel-Layer. The (potentially) charged portion of the gel layer lies between a' < r < b' and the residue site of interest, represented as a small spherical cavity, is at r = s. The surroundings are represented as a charged (shaded) or uncharged (unshaded) continuum. Reduced electrostatic potentials for the various states are represented by, y' + δy, y', and y", respectively. G's represent free energies.

Consider a single residue at r = s. In the actual environment of this residue in the gel layer, it is surrounded by neighboring charge sites that alter the electrostatic potential and ionic atmosphere relative to the environment of a "free" residue. In the present work, we shall approximate the discrete neighborhood of the residue with a uniformly charged continuum that reflects the average environment at that particular position in the gel layer. The residue of interest is modeled as a cavity of radius σ that is uncharged in the protonated state and carries a single -1 charge (in protonic units) in the discharged state. The free energy of dissociation, $\Delta G(HX \rightarrow X^-)$, may be substantially different from $\Delta G^0(HX \rightarrow X^-)$. With the help of Figure 8, we can write

$$\Delta G(HX \rightarrow X^-) \;\; = \;\; \Delta G^0(HX \rightarrow X^-) + [G_f^0(HX) - G_f(HX) + G_f(X^-) - G_f^0(X^-)] \quad (A2)$$

where the G_f's represent molecular free energies of formation. The quantities y', y'+δy, and y'' in Fig. 8 denote dimensionless electrostatic potentials which vary with distance from the center of the cavity which is located at r = s. It shall be assumed that the free energy differences appearing in brackets in Eq. (A2) are dominated by charge-charge interactions. The electrostatic free energy of a particular charged system, G^{el}, can be written[108]

$$G^{el} \;\; = \;\; \int dV[\rho_f \Lambda - k_B T \sum_j c_{j0} \omega (e^{-z_j \Lambda / k_B T} - 1) - \frac{1}{2X} \underline{E} \cdot \underline{D}] \qquad (A3)$$

where the volume integration is carried out over all space, ρ_f is the fixed charge density, Λ is the electrostatic potential, the sum over j is over all mobile ion species present of valence z_j and ambient concentration c_{j0}, ω is the ion exclusion parameter (assumed the same for all mobile ions), $\mathbf{E}$ ($= - \nabla \Lambda$) is the electric field, $\mathbf{D}$ ($= \varepsilon \mathbf{E}$) is the electric displacement, ε is the (local) dielectric constant, and $X = 4\pi$ (in CGS units), or $1/\varepsilon_0$ where ε_0 is the permittivity of free space (in MKSA units). Making use of the Poisson-Boltzmann equation and the divergence theorem in dealing with the $\mathbf{E} \cdot \mathbf{D}$ term, it is straightforward to show that Eq. (A3) can be written

$$G^{el} \quad = \quad \frac{k_B T}{2} \int dV \left[\frac{\rho_f}{q} \phi - h(\phi) \right] \qquad (A4)$$

where q is the protonic charge, and

$$\phi \quad = \quad \frac{q \Lambda}{k_B T} \qquad (A5)$$

$$h(\phi) \quad = \quad \omega \sum_j c_{j0} [e^{-z_j \phi} (2 + z_j \phi) - 2] \qquad (A6)$$

The term in brackets in Eq. (A2) can be written

$$\Delta\Delta G^{el} \quad = \quad [G_f^0(HX) - G_f(HX) + G_f(X^-) - G_f^0(X^-)]$$

$$= \quad \frac{k_B T}{2} \left\{ -[y'(\underline{s}) - y''(\underline{s})] + \int_{V_{sol}} dV \left[-\frac{\rho_g}{q} \delta y + h(y'') + h(y' + \delta y) - h(y') \right] \right\} \qquad (A7)$$

where y'(**s**) and y''(**s**) represent the reduced potentials at the surface of the cavity containing a

single – charge in the presence of a charged and uncharged gel layer background, ρ_g ($= \rho_s \gamma \chi$)

is the charge density due to fixed charges embedded in the gel layer, and V_{sol} represents the

fluid domain.

In Eq. (A7), we can replace y'(**s**) – y''(**s**) with y(**s**), where y(**s**) represents the reduced

mean field potential at r = |**s**| of our charged gel layer. Next consider the h-terms in Eq. (A7).

At low ϕ, the exponential in Eq. (A6) can be expanded and the leading terms in Eq. (A6) are

of order ϕ^3 in the case of polyvalent salt, and of order ϕ^4 if only monovalent mobile ions are

present. For small $|\phi|$, it is clear that the h-terms in Eq. (A7) can be ignored. On this basis,

we can ignore h(y'') appearing in Eq. (A7) to a good approximation. For the remaining terms,

we make the reasonable approximation valid at large |y|,

$$h(y' + \delta y) - h(y') \quad \approx \quad \delta y \frac{\partial h(\phi)}{\partial \phi} \bigg]_{\phi = y} \quad = \quad -\omega \delta y \sum_j c_{j0} z_j (1 + z_j y) e^{-z_j y}$$

$$\approx \quad -\omega \delta y \, c_{j0} * z_j * (1 + z_j * y) e^{-z_j * y} \qquad (A8)$$

where "*" denotes the principal counterion(s) present in solution. Now, δy appearing in Eq. (A8) represents the reduced "perturbed" potential at some point in space, **x,** due to a cavity centered at **s**. This potential is derived in Appendix B and is given by Eqs. (B12-14). It then follows from Eqs. (B8-B14) and Eq. (A8), that

$$\int_{V_{sol}} dV[h(y'')+h(y'+\delta y)-h(y')] \;\approx\; -y(\underline{s}) - \frac{1}{z_j{}^*} \qquad (A9)$$

To a good approximation then, Eq. (A7) can be written

$$\Delta\Delta G^{el} \;\approx\; \frac{k_B T}{2}\left\{ -2y(\underline{s}) \;-\frac{1}{z_j{}^*} - \int_{V_{sol}} \frac{\rho_g(\underline{x})}{q}\delta y(\underline{x},\underline{s})\, dV_x \right\} \qquad (A10)$$

From Eqs. (A1, A2, A10),

$$pKa(\underline{s}) \;=\; pKa^0 - 0.217\left\{ 2y(\underline{s}) +\frac{1}{z_j{}^*} + \int_{V_{sol}} \frac{\rho_g(\underline{x})}{q}\delta y(\underline{x},\underline{s})\, dV_x \right\} \qquad (A11)$$

The potential δy falls off rapidly with distance from the cavity and hence the integrand on the lhs of Eq. (A9) will be dominated by terms near the cavity. Consequently

$$\frac{\rho_g(\underline{x})}{q} \approx \frac{\rho_g(\underline{s})}{q} \;=\; \frac{Q_t^0}{V_{cgl}}\chi(\underline{s}) \qquad (A12)$$

where Q_t^0 is the titration charge of the colloid, V_{cgl} is the volume of the potentially charged portion of the gel layer, and $\chi(\mathbf{s})$ is the fraction of acidic sites at $\mathbf{x} = \mathbf{s}$ that are deprotonated. From the defininition of the charged gel layer, $V_{cgl} = 4\pi(b'^3-a'^3)/3$. Integrating over the charged gel layer domain,

$$pKa(s) \;=\; pKa^0 - .217\left\{ 2y(s)+\frac{1}{z_j{}^*} + (4\pi B(s))\left(\frac{Q_t^0\chi(s)}{\alpha(s)^2 V_{cgl}} \right)h(\alpha,s,a',b') \right\} \qquad (A13)$$

where s is the distance of the cavity from the center of the colloidal particle, $\alpha(s)$ is given by Eq. (B8), B(s) is given by Eq. (B14), and

$$h(\alpha, s, a', b') = 1 - \frac{1}{2\alpha(s)s}[e^{-\alpha(s)(b'-s)}(\alpha(s)b'+1) + e^{-\alpha(s)(s-a')}(\alpha(s)a'-1)$$

$$- e^{-\alpha(s)(b'+s)}(\alpha(s)b'+1) + e^{-\alpha(s)(a'+s)}(\alpha(s)a'+1)] \qquad (A14)$$

It is straightforward to generalize Eq. (A13) to include a surface charge on the core of the particle. Since a surface charge is not included in the present study, however, this generalization shall not be given here.

As an illustration of charge regulation discussed above that is also relevant to the polystyrene sulfonate sample studied in the present work, consider a model with a = 143.59 nm, a' = 147.77 nm, b = b' = 149.16 nm, and λ = 3.15 nm^{-1}. For the most part, this corresponds to the "halo" model discussed in the Results section with S_V = 0.10. It is also assumed that pKa^0 = 0.7 (appropriate for benzene sulfonic acid[111]), the ambient pH of the sample is 5.5[110], and the ambient concentration of Na$^+$ ions is 10^{-4} moles/liter. At this salt concentration, substantial charge regulation is predicted to occur when Q_t^0 = -3.6 x 10^5, which corresponds to the experimental titration charge of the colloidal particle. In the present example, however, Q_t^0 is varied holding other parameters constant.

Table 5-2

Charge regulation versus $|Q_t^0|$ for a particular gel layer model

$-10^{-5}Q_t^0$	$-<y>_{gel}$	$<pKa>_{gel}$	$<pH_{loc}>_{gel}$	Q_t/Q_t^0
0.049	2.58	1.82	4.38	0.997
0.090	3.53	2.24	3.97	0.982
0.164	4.36	2.63	3.61	0.906
0.299	4.98	2.91	3.39	0.732
0.544	5.42	3.11	3.15	0.530
0.942	5.74	3.25	3.01	0.357
1.81	6.02	3.38	2.89	0.233
3.29	6.32	3.50	2.77	0.153
6.00	6.55	3.62	2.66	0.098

For a particular Q_t^0; y, χ, and pKa are calculated over a range of different s-values within the gel layer following the iterative procedure discussed in the "Charge and Electrostatic Potential" section of this paper. Equations (A13-A14) play a prominent role in this procedure. Summarized in Table 5-2 are relevant quantities averaged over the charged portion of the gel layer (a' ≤ s ≤ b') for different Q_t^0's. The ratio of the actual charge, Q_t, to Q_t^0 is given in the final column. For a fully deprotonated or protonated particle, this ratio should equal 1 or 0, respectively. Since pKa^0 is much lower than the ambient pH of 5.5, we might expect $Q_t/Q_t^0 \approx 1.0$ and that is indeed true when $|Q_t^0|$ is low as shown in Table 5-2. As $|Q_t^0|$ is raised, however, $-\langle y \rangle_{gel}$ increases and also $\langle pKa \rangle_{gel}$ increases due to a buildup of charge-charge repulsion in the gel layer. Furthermore, as $-\langle y \rangle_{gel}$ increases, $\langle pH_{loc} \rangle_{gel}$ decreases following Eq. (5-21). (The local concentration of H^+ in the gel layer increases due to the negative charges on the deprotonated acidic sites.) Provided $\langle pKa \rangle_{gel}$ is substantially smaller than $\langle pH_{loc} \rangle_{gel}$, the degree of charge regulation remains small ($Q_t/Q_t^0 \approx 1.0$). However, as $|Q_t^0|$ increases, $\langle pKa \rangle_{gel}$ increases, $\langle pH_{loc} \rangle_{gel}$ decreases, and at some point, the two approach each other and eventually become equal. In the present example, this occurs around $Q_t^0 \approx -60,000$. About 50% of the charge groups in the gel are protonated at this point ($Q_t/Q_t^0 \approx 0.5$). Increasing $|Q_t^0|$ further leads to still greater charge regulation. This particular case illustrates the charge regulation phenomenon in a way that is clear and straightforward to understand.

Appendix B – Cavity potential, δy.

The purpose of this appendix is to outline the derivation of an expression for the reduced "cavity" potential, δy(**x**,s), for a field point, **x**, of a cavity of radius σ centered at

position **s**. From Figure 8 and the Poisson-Boltzmann equation

$$\nabla^2 \delta y(\underline{x}, \underline{s}) \;=\; \nabla^2 ((y'(\underline{x}, \underline{s}) + \delta y(\underline{x}, \underline{s})) - y'(\underline{x}, \underline{s}))$$

$$=\; -\frac{Xq^2}{\varepsilon k_B T}[\delta(\underline{x} - \underline{s}) - \sum_j c_{j0} z_j \omega_j e^{-z_j y'(\underline{x}, \underline{s})}(1 - e^{-z_j \delta y(\underline{x}, \underline{s})})] \qquad (B1)$$

where ∇^2 is the Laplacian operator which acts on the field variable, **x**, $X = 4\pi$ (in CGS units) or $1/\varepsilon_0$ where ε_0 is the permittivity of free space (in MKS units), q is the protonic charge, ε is the relative dielectric constant of the solution (taken to be 78.3 for water at 25 °C[111]), k_B is Boltzmann's constant, T is absolute temperature, δ(**x-s**) is the delta-function, the sum over j is over all mobile ion species present of valence z_j, ω_j is the (spatially dependent) ion exclusion parameter, and y'(**x**, **s**) is the reduced potential at **x** due to a negatively charged cavity centered at **s**. Integrating Eq. (B1) over a sphere of radius σ that just encloses the cavity centered at **x** = **s** gives the normal derivative on the surface, S*, of the cavity

$$\delta y'(\underline{s}*, \underline{s}) \;\equiv\; \underline{\nabla} \delta y(\underline{x}, \underline{s})|_{S*} \cdot \underline{n}(\underline{s}*) \;\approx\; -\frac{X q^2}{4\pi \varepsilon \sigma^2 k_B T} \qquad (B2)$$

where **s*** is a point on S* and **n(s*)** is a local outward normal to S*. In general, we need to consider the effect of S_p (colloid surface) on δy as depicted in Figure 5-10.
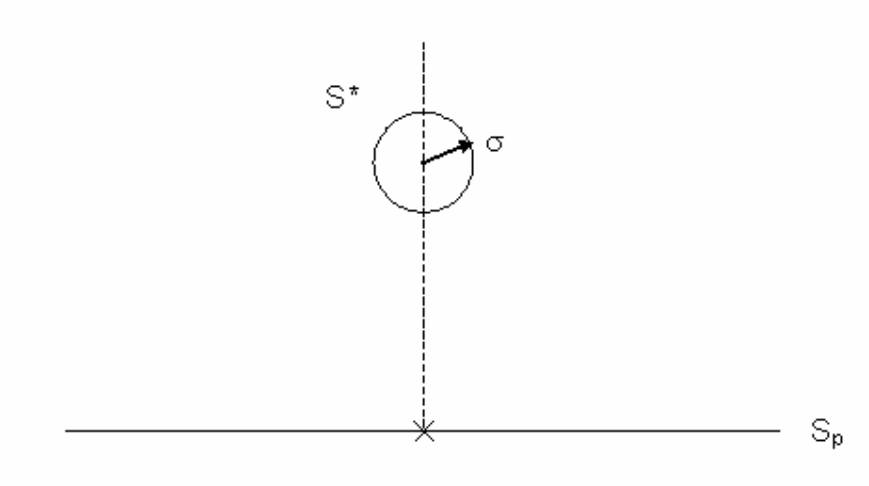
Figure 5-10) Cavity Near the Surface of the Core Particle. The acidic residue of interest is represented as a spherical cavity of radius σ and surface S*. The surface of the core particle is S_p. The origin of the local frame of reference is denoted by an X.

This effect shall be ignored for the present and reconsidered near the end of this Appendix. Applying Green's Theorem to the fluid domain, V_f, and ignoring the contribution of S_p (see, for example, reference 105)

$$\delta y(\underline{x}', \underline{s}) = -\int_{V_f} F_\alpha(\underline{x}, \underline{x}')[\nabla^2 \delta y(\underline{x}, \underline{s}) - \alpha^2 \delta y(\underline{x}, \underline{s})]\, dV_x$$

$$-\int_{S*} [F_\alpha(\underline{x}, \underline{x}')\delta y'(\underline{x}, \underline{s}) - F_\alpha'(\underline{x}, \underline{x}')\delta y(\underline{x}, \underline{s})]\, dS_x \qquad (B3)$$

where

$$F_\alpha(\underline{x}, \underline{x}') = \frac{1}{4\pi r} e^{-\alpha r} \qquad (B4)$$

$$F_\alpha'(\underline{x}, \underline{x}') = -\frac{(1+\alpha r)}{4\pi r^3} \underline{n} \cdot \underline{r} e^{-\alpha r} \qquad (B5)$$

$$\underline{r} = \underline{x} - \underline{x}' \qquad (B6)$$

$r = |\mathbf{r}|$, $\mathbf{n}$ is the local outward unit normal to the bounding surface, and α is an arbitrary

constant we are free to choose provided it is real and positive. In practice, we want to choose α so that $\nabla^2\delta y - \alpha^2\,\delta y$ vanishes throughout as much of the fluid volume as possible. We anticipate that δy falls off with distance moving away from the cavity and that $y'(\mathbf{x},\mathbf{s}) \to y(\mathbf{s})$ where $y(\mathbf{s})$ is the mean field reduced potential at $\mathbf{s}$. (This is the reduced potential corresponding to the same charge distribution as y', but the negatively charged cavity replaced with a continuum charge distribution.) The calculation of y is discussed in the main body of this work. Assume the ion exclusion parameter is the same for all atoms, $\omega_j = \omega$, and that the mean field potential depends only on the distance, $s = |\mathbf{s}|$. Expanding the exponential of $z_j\delta y$ in Eq. (B1) and retaining the leading term in δy,

$$\nabla^2\,\delta y - \alpha^2\,\delta y \;\approx\; \frac{X\omega q^2}{\varepsilon k_B T}\,\delta y \sum_j c_{j0}\,z_j^{\,2}\,e^{-z_j y(s)} - \alpha^2\,\delta y \qquad (B7)$$

Consequently, we want to choose

$$\alpha^2(s) \;=\; \frac{\omega\kappa^2}{2I}\sum_j c_{j0}\,z_j^{\,2}\,e^{-z_j y(s)} \qquad (B8)$$

where

$$\kappa^2 \;=\; \frac{2X\,q^2\,I}{\varepsilon k_B T} \qquad (B9)$$

is the square of the Debye-Huckel parameter, and

$$I \;=\; \frac{1}{2}\sum_j c_{j0}\,z_j^{\,2} \qquad (B10)$$

is the ionic strength. Eq. (B3) can be reduced to the form

$$\delta y(\underline{x}',\underline{s}) \;=\; \delta y^{(0)}(s,r') - \frac{\alpha(s)\omega\kappa^2}{2I}\sum_j c_{j0}z_j\,e^{-z_j y(s)}\int_{\sigma}^{\infty} x^2 dx\, f(\alpha,\sigma,x,r) \qquad (B11)$$

where

$$\delta y^{(0)}(s,r') \;=\; \frac{B(s)}{r'}\,e^{-\alpha(s)r'} \qquad (B12)$$

$$r' = |\underline{x}' - \underline{s}| \;, \quad and \quad r = |\underline{x} - \underline{x}'| \quad (B13)$$

$$B(s) = \frac{Xq^2}{4\pi\varepsilon k_B T(1+\alpha(s)\sigma)}e^{\alpha(s)\sigma} \quad (B14)$$

$$f(\alpha,\sigma,x,r) = \frac{i_1(\alpha\sigma)}{k_1(\alpha\sigma)}k_0(\alpha r)k_0(\alpha x) + i_0(\alpha r_<)k_0(\alpha r_>)[1-e^{-z_\alpha\delta y(\underline{x}',\underline{s})} - z_\alpha\delta y(\underline{x}',\underline{s})] \quad (B15)$$

$r_<$ and $r_>$ are the lesser and greater of x and r, respectively, and the i's and k's are modified spherical Bessel functions. In Eq. (B15), f depends implicitly on s through the dependence of α on s and $i_0(x) = \sinh(x)/x$, $i_1(x) = \cosh(x)(1/x + 1/x^2)$, $k_0(x) = e^{-x}/x$, and $k_1(x) = e^{-x}(1/x + 1/x^2)$.

The difficulty with Eq. (B11) is that the integral on the lhs of the equation contains the reduced potential that we are trying to determine. Fortunately, under the conditions of interest in the present work, the integral term in Eq. (B11) turns out to be small compared to the leading term, $\delta y^{(0)}(r')$. To illustrate this, consider the example of a monovalent salt with $c_{\alpha 0} = 10^{-3}$ moles/liter, $\sigma = .548$ nm, T = 25 °C, y(s) = -5, and $\lambda = 1.0$. These are typical parameters for the polystyrene sufonate latex particles considered in the present work. Under these conditions $\kappa = 0.10$ nm^{-1} (the Debye-Huckel parameter of the ambient salt solution), and $\alpha = 1.22$ nm^{-1} (an effective screening parameter characteristic of the "local" salt solution in the vicinity of the cavity). Approximating $\delta y(\mathbf{x},\mathbf{s})$ with $\delta y^{(0)}(|\mathbf{x}-\mathbf{s}|)$ in the integral on the lhs of Eq. (B11), it is straightforward to show that the integral term amounts to 1.1 % of $\delta y^{(0)}(r')$. Thus, to a good approximation

$$\delta y(\underline{x}',\underline{s}) = \delta y^{(0)}(s,r') \quad (B16)$$

Where $\delta y^{(0)}$ is given by Eqs. (B12-B14). In other words, the reduced "cavity" potential decays, to a good approximation, exponentially with a Debye-Huckel screening parameter that reflects the local ion concentration rather than the ambient salt concentration. Although the ambient salt concentration may be very low, the local concentration can be quite large due

to the high |y| values that are possible.

As discussed at the beginning of this appendix, the boundary element derivation given above has ignored the effect of the boundary surface of the colloidal particle itself, S_p. Including this effect, surface integrals over S_p entirely analogous to the surface integrals over S* should be included in Eq. (B3). Generalizing Eq. (B3) to include these new terms and also approximating the solution of Eq. (B3) with Eq. (B16)

$$\delta y(\underline{x}',\underline{s}) \approx \delta y^{(0)}(s,r') - \int_{S_p}[F_\alpha(\underline{x},\underline{x}')\delta y'(\underline{x},\underline{s}) - F_\alpha'(\underline{x},\underline{x}')\delta y(\underline{x},\underline{s})]dS_x \qquad (B17)$$

It is straightforward to estimate the relative size of the new terms by approximating δy and $\delta y'$ appearing in the surface integral on the lhs of Eq. (B17) with $\delta y^{(0)}$ and $\delta y'^{(0)}$. For the case $y = -5$, $\alpha = 1.22$, and approximating S_p with an infinite flat plane, numerical integrations over a large number of possible $\{x',s\}$ configurations has shown that the surface integral terms make a contribution that is at most 2 % of $\delta y^{(0)}(s, r')$ even when s lies very close to S_p. On this basis, it can be concluded that $\delta y^{(0)}$ given by Eqs. (B12-B14) constitutes a good approximation of the reduced "cavity" potential.

Chapter 6

Electrokinetic Transport of Large Rigid Macroions in the Thin Double Layer Limit

6.1   Introduction

The objective of this chapter is to develop a simplified numerical BE procedure that utilizes ideas of O'Brien and his coworkers applicable to spherical and spheroidal particles and apply them to large model particles of arbitrary shape. Dukhin[115] and later O'Brien and coworkers[31,116,117] and others[118,119] have explored this "thin double layer", or TDL, regime in depth. Dukhin[115], and O'Brien and Hunter[31] derived simple analytical formulas for a spherical macroion of uniform surface, or "zeta" potential, that are accurate for κa greater than approximately 30 where κ is the Debye-Huckel screening parameter and a is the sphere radius. O'Brien and Ward[117] subsequently derived an approximate analytical formula (Eq. (5.16) in reference 117) applicable to prolate and oblate spheroids of arbitrary axial ratio. The O'Brien and Ward formula appears to be quite accurate for κa as small as 20 where a, in this case, denotes the minor axis of the spheroid. Thus, for spherical or spheroidal particles of uniform zeta potential, accurate analytical formulas are available for κa greater than about 20. For smaller, highly charged particles whether they are spheres or particles of arbitrary shape, it is necessary to resort to numerical results summarized in the previous paragraph.

The motivation for the development of such a procedure is primarily practical in nature. By reducing the computation time of BE calculations and reducing the complexity of

the code, it will hopefully become more accessible to a larger audience. As developed, the procedure is applicable to large particles of uniform "zeta" potential, but no assumption needs to be made about its actual shape. The principal advantage of the new approach is that the time consuming volume integrations that must be carried out in the general BE procedure[34,106,120] are eliminated. Numerical surface integrations remain, but their computation is rapid relative to the volume intergrations.

The outline of this chapter is as follows. The Methods section first discusses the continuum primitive model and introduces the fundamental field equations that must be solved in order to compute an electrophoretic mobility. Then, we restrict the treatment to "thin double layer" particles (particles that are large relative to the thickness of the ionic double layer that surrounds them). The main features of the BE procedure as applied to computing the electrophoretic mobility of a model polyion in the thin double layer limit are then summarized. In the Results section, the procedure is first applied to spheres and compared with independent theory. Subsequently the procedure is applied to the electrophoretic transport of high molecular weight duplex DNA complexed with the trication, spermidine. We end with a Summary of our major findings. The technical aspects of this manuscript are largely relegated to four appendices since this material will undoubtedly be of interest to a limited audience. For the sake of completeness as well as those investigators who may be interested in applying the procedures to their own problems, however, we feel it is essential to include this material. The appendices treat: (A) the BE approach as applied to scalar fields; (B) the BE approach as applied to the velocity field of a thin double layer particle; (C) thin double layer approach to the calculation of ion relaxation (distortion of the ion atmosphere from its equilibrium distribution); and (D) computing the net forces on model particles.

6.2   Modeling

6.2.1   Continuum Primitive Model and Overview of the Field Equations

Consider a suspension of monodisperse particles (macroions or colloids) widely dispersed in a fluid at temperature T. The suspension is assumed to be sufficiently dilute that interparticle direct and hydrodynamic interactions are, on average, negligible. In modeling the individual macroion particle and surrounding fluid, the continuum primitive model, CPM, is employed.[121]   In the CPM, the macroion is represented as low dielectric rigid body of arbitrary shape. Within the macroion or on its surface, a well defined, but arbitrary charged distribution is placed.[6,34]   Alternatively, one can define the electrostatic potential, or "zeta" potential over the entire macroion surface, or to be more precise, the surface of hydrodynamic shear, S_p. This shear surface, S_p, separates the rigid macroion from the continuum Newtonian fluid that is incompressible, has a viscosity coefficient of η, and a dielectric constant of ε_s. In the present work, the "gel" layer[21,103,106] shall be ignored. In addition, mobile ions in the solvent are modeled as a continuum, and local ion concentrations are assumed to obey the Poisson equation,

$$\underline{\nabla} \cdot (\varepsilon(\underline{x}) \underline{\nabla} \Lambda(\underline{x})) \;\; = \;\; -\mathrm{X}\, \rho(\underline{x}) \qquad (6-1)$$

for the general non-equilibrium case or the Poisson-Boltzmann equation,

$$\underline{\nabla} \cdot (\varepsilon(\underline{x}) \underline{\nabla} \Lambda_0(\underline{x})) \;\; = \;\; -\mathrm{X}\, q \sum_\alpha c_\alpha z_\alpha \exp(-\beta q z_\alpha \Lambda_0(\underline{x})) \qquad (6-2)$$

for systems at equilibrium. In Eqs. (6-1 and 6-2), $\mathrm{X} = 4\pi$ (in CGS units), or $1/\varepsilon_0$ where ε_0 is the permittivity of free space (in MKSA units), Λ and Λ_0 denote the nonequilibrium and equilibrium electric potentials, respectively, at point $\mathbf{x}$ in a local frame of reference, ε is the local dielectric constant, ρ is the local charge density, q is the protonic charge, c_α is the ambient concentration of the α-th mobile ion present in solution and z_α is its valence, the sum extends over all ionic species present, and $\beta = 1/k_\mathbf{B}T$ where k_B is Boltzmann's constant, and T

is absolute temperature.

In order to determine a transport property such as the electrophoretic mobility of a model particle, it is necessary to know the forces or stresses acting on it. This, in turn, requires knowledge of various field quantities such as the local fluid velocity, $\mathbf{v}_T$, ion concentrations, and electric potentials. In the present work, we shall be interested in a model particle that is stationary, but placed in a constant electric field, $\mathbf{e}$, or translating with velocity $\mathbf{u}$, without an electric field, through a fluid that is otherwise at rest. It is convenient to define a perturbation potential, ψ, through

$$\Lambda(\underline{x}) = \Lambda_0(\underline{x}) + \psi(\underline{x}) - \underline{e} \cdot \underline{x} \qquad (6-3)$$

where Λ and Λ_0 are the local nonequilibrium and equilibrium electric potentials, in the presence and absence of an electric or flow field, respectively. Far from the particle, $\Lambda \approx -\mathbf{e} \cong \mathbf{x}$, $\Lambda_0 \approx 0$, and therefore $\psi \approx 0$.

Following O'Brien and White, [31] additional potentials, Φ_α, are also introduced to represent the departure of local ion concentrations, n_α, from their equilibrium value, $n_{\alpha 0}$. Retaining terms to first order in the perturbing electric or flow field,

$$n_\alpha(\underline{x}) = n_{\alpha 0}(\underline{x})\left[1 - \beta q z_\alpha[\psi(\underline{x}) + \Phi_\alpha(\underline{x})]\right] \qquad (6-4)$$

$$n_{\alpha 0}(\underline{x}) = c_\alpha \exp\left[-\beta q z_\alpha \Lambda_0(\underline{x})\right] \qquad (6-5)$$

where the various quantities have been defined previously. In general the potentials, Φ_α, are obtained by solving a steady state ion transport equation for each ion species present. The equation of continuity requires (in a frame of reference stationary with respect to the particle)

$$\underline{\nabla} \cdot \underline{j}_\alpha(x) = 0 \qquad (6-6)$$

where $\mathbf{j}_\alpha$ is the local current density of ion α. To first order in the perturbing electric or flow field[34]

$$\underline{j}_\alpha(x) = n_{\alpha 0}(\underline{x})\left[\underline{v}_T(\underline{x}) + \beta q z_\alpha D_\alpha[\underline{\nabla}\Phi_\alpha(\underline{x}) + \underline{e}]\right] \qquad (6-7)$$

where $\mathbf{v}_T$ is the local fluid velocity, D_α is the diffusion constant of ionic species α.

Substituting (6-7) into (6-6) and assuming the solvent is incompressible ($\nabla \cong \mathbf{v}_T = 0$), yields

$$\nabla^2 \Phi_\alpha(\underline{x}) \quad = \quad f_\alpha(\underline{x}) \qquad (6-8)$$

where f_α represents the "source" term of Φ_α and is given by

$$f_\alpha(\underline{x}) \quad = \quad \left[\frac{1}{D_\alpha}\underline{v}_T(\underline{x}) + \beta q z_\alpha (\underline{\nabla}\Phi_\alpha(\underline{x}) + \underline{e})\right] \cdot \underline{\nabla}\Lambda_0(\underline{x}) \qquad (6-9)$$

Since Λ_0 falls off rapidly moving away from the particle surface, f_α is only significant near S_p. This feature shall be useful in the present analysis. It is assumed that S_p is impermeable to the passage of ions which requires $\mathbf{j}_\alpha$ A $\mathbf{n} = 0$ where $\mathbf{n}$ represents the local outward unit normal to S_p. In addition, "stick" hydrodynamic boundary conditions are assumed to hold that requires $\mathbf{v}_T = \mathbf{0}$ on S_p. From Eq. (6-7), we then can identify the boundary condition for the outward normal derivative of Φ_α on S_p

$$\left(\frac{\partial \Phi_\alpha(\underline{x})}{\partial n}\right)_{S_p} \quad = \quad -\underline{e}\cdot\underline{n}(\underline{x}) \qquad (6-10)$$

In order to obtain $\mathbf{v}_T$, it is necessary to solve the linear steady state Navier-Stokes equation, which can be written (6-2-6-6, 6-22)

$$\eta\nabla^2\underline{v}_T(\underline{x}) - \underline{\nabla}p(\underline{x}) \quad = \quad -\underline{w}(\underline{x}) \qquad (6-11)$$

$$\underline{\nabla}\cdot\underline{v}_T \quad = \quad 0 \qquad (6-12)$$

where p is a local pressure and $\mathbf{w}$ represents an effective local external force/volume on the fluid,

$$\underline{w}(\underline{x}) \quad = \quad q\sum_\alpha z_\alpha\left[n_{\alpha 0}(\underline{x}) - c_\alpha\right]\underline{\nabla}\Phi_\alpha(\underline{x}) + \underline{e}] \qquad (6-13)$$

Moving away from the particle surface, the local ion concentration, $n_{\alpha 0}$, approaches its ambient value, c_α. For a large particle, $\mathbf{w}$ vanihes except for a thin layer of fluid near S_p. This is called the electric "double layer".

In summary, it is necessary to solve Eqs. (6-1,2,8 and 11) in order to determine a transport property such as the electrophoretic mobility. In general, these equations are coupled to each other and must be solved simultaneously. Different investigators and investigations may have followed somewhat different pathways to achieve this and have employed different computational strategies, but the underlying problem has basically been the same.[21,31,34,103] For a general model particle, it has been necessary to employ BE procedures,[34,106,120] which is outlined in the next subsection.

6.2.2 BE procedure for calculating the electrophoretic mobility of a rigid model polyion in the thin double layer limit

In order to calculate an electrophoretic mobility, it is necessary to determine the total force exerted by the particle on the fluid, $\mathbf{z}_T$, for two transport cases,[31,34] which shall be called Case 1 and 2, respectively. In the present work, the analysis shall be restricted to model particles that are large compared to the thickness of the ion atmosphere, b, that surrounds them. The quantity b will be comparable to κ^{-1} (Eq. (A15)). If L represents the smallest linear dimension of the model particle, the present treatment is restricted to $\kappa L \gg 1$. Appendix D explains how the total force is related to the fundamental fields, Λ_0, Φ_α, and $\mathbf{v}_T$ defined previously. (A surface, S_{dl} is defined which is displaced outward from S_p by the distance b. The force, $\mathbf{z}_T$ can be computed once $\mathbf{v}_T$ on S_{dl} is known. However, $\mathbf{v}_T$ depends in a rather complex way on Λ_0 and Φ_α as discussed in Appendices B and C.)

In Case 1, the particle is translated with velocity $\mathbf{u}$ in the absence of an electric field and $\mathbf{z}_T^{(1)}$ is related to $\mathbf{u}$ by Ref. 92

$$\underline{z_T^{(1)}} = \underline{\underline{\Xi}}_t \cdot \underline{u} \qquad (6-14)$$

where Ξ_t is the translational friction tensor. The components of Ξ_t are obtained by translating

the particle along three orthogonal directions, computing $\mathbf{z}_T^{(1)}$ (as discussed in Appendix D) and then simply identifying the components of Ξ_t. For axisymmetric particles, only two orthogonal directions need to be considered and for a sphere, only a single direction needs to be considered. In Case 2, the particle is held stationary, but it is subjected to a constant external electric field, $\mathbf{e}$. In this case,

$$\underline{z_T^{(2)}} = -\underline{\underline{Q}} \cdot \underline{e} \qquad (6-15)$$

where $\mathbf{Q}$ is the effective charge, or "tether force" tensor.[20] In general, 3 calculations with $\mathbf{e}$ oriented along three orthogonal directions are required in order to determine the components of $\mathbf{Q}$. For symmetric particles, however, this number is reduced.

Once Ξ_t and $\mathbf{Q}$ are known, the electrophoretic mobility, μ is readily obtained. Consider our model particle oriented in a particular way and subjected to a constant external electric field, $\mathbf{e}$. The particle migrates with steady state velocity $\mathbf{u}$. Under steady state conditions, the net force on the particle must vanish and we can view the transport as a superposition of Cases 1 and 2,

$$\underline{0} = \underline{\underline{\Xi}}_t \cdot \underline{u} - \underline{\underline{Q}} \cdot \underline{e} \qquad (6-16)$$

Solving for $\mathbf{u}$,

$$\underline{u} = \underline{\underline{\Xi}}_t^{-1} \cdot \underline{\underline{Q}} \cdot \underline{e} = \underline{\underline{M}} \cdot \underline{e} \qquad (6-17)$$

where "-1" denotes inverse and $\mathbf{M}$ is the electrophoretic mobility tensor. Under conditions of weak applied fields where all particle orientations are equally probable, μ can be equated to the isotropic average of $\mathbf{M}$,

$$\mu = \frac{1}{3} Tr[\underline{\underline{M}}] \qquad (6-18)$$

where Tr denotes the trace of the mobility tensor. Attention shall now be turned to the calculation of the fields Λ_0, Φ_α, and $\mathbf{v}_T$ needed in order to calculate μ.

In addition to the TDL assumption that $\kappa L \gg 1$, it shall be assumed that the electrostatic potential on S_p, ζ, is uniform. For a simple two component salt of absolute valence z, the electrostatic potential at distance x from S_p is given by[122]

$$\Lambda_0(x) \quad = \quad \frac{2k_BT}{qz} \ln\left[\frac{1+Ae^{-\kappa x}}{1-Ae^{-\kappa x}}\right] \qquad (6-19)$$

where

$$A \quad = \quad \tanh\left[\frac{qz\zeta}{4k_BT}\right] \qquad (6-20)$$

The other special case of interest is that of a highly charged large particle with a surface charge density of σ in the presence of a more complex salt solution. Near S_p, the ion density in solution is dominated by the contribution of counterions with maximum absolute valency, $|z^*|$. This shall be called the "principal counterion" (or "principal counterions" to be more precise, since several species of the same absolute valence may be present) and let the ambient concentration be denoted by c^*. The charge density is related to the reduced zeta potential, $y_0 = q\zeta/k_BT$, by the relation[29]

$$\sigma^2 \quad = \quad \frac{2k_BT}{X}\sum_\alpha c_\alpha(e^{-z_\alpha y_0} - 1) \qquad (6-21)$$

The right hand side (rhs) of Eq. (6-21) is dominated by the principal counterion. In this case it is convenient to write

$$e^{-z^*y_0} \quad = \quad \frac{X\sigma^2}{2k_BT\,c^*} + 1 - \sum_\alpha{}' \frac{c_\alpha}{c^*}(e^{-z_\alpha y_0} - 1) \qquad (6-22)$$

where the sum on the rhs of Eq. (6-22) is over all ions excluding the principal counterion. In practice, this term is small. Given the charge density, σ, and salt conditions, Eq. (6-22) can be used to determine y_0. As a first approximation, the summation on the rhs of Eq. (6-22) is ignored and y_0 estimated. This estimate is then used in the summation on the rhs of Eq. (6-22)

to obtain a better estimate. This procedure can be repeated until y_0 converges. Beginning with the Poisson-Boltzmann equation, Eq. (6-1), it is possible to derive a first order differential equation for reduced potential, $y = q\Lambda_0/k_BT$,[29]

$$\frac{dy}{dx} = \pm\kappa\sqrt{\sum_\alpha \frac{c_\alpha}{I}(e^{-z_\alpha y} - 1)} \qquad (6-23)$$

where the + root is taken if $y_0 < 0$ and the – root is taken if $y_0 > 0$. Standard procedures are available to solve first order differential equations, such as the Euler Method[123] and this is done in the present work for large particles in a complex salt solution. Far from the particle, $y(x) = c\, e^{-\kappa x}$ where c is a constant. This behavior coupled with the boundary condition $y(0) = y_0$ is used to solve Eq. (6-23) numerically. For particles not large compared to κ^{-1} or large particles of nonuniform surface potential, numerical alternatives such as the BE approach outlined in Appendix A could be used.

A major feature of the BE procedure is the discretization of S_p into a series of N interconnected platelets where N is typically in the range of 100 to N_{max} given by Eq. (B23). A representative example of a toroidal particle studied later in the present work is shown in Figure 6-1. The approximation is made that field quantities such as Φ_α, and $\mathbf{v}_T$ (and, in general, Λ_0) are uniform over individual platelets. It is straightforward to test this approximation by varying N and extrapolating to the $N \rightarrow \infty$ limit. In the present work on thin double layer particles, discritization in the direction normal to S_p is avoided as explained in Appendices B and C.
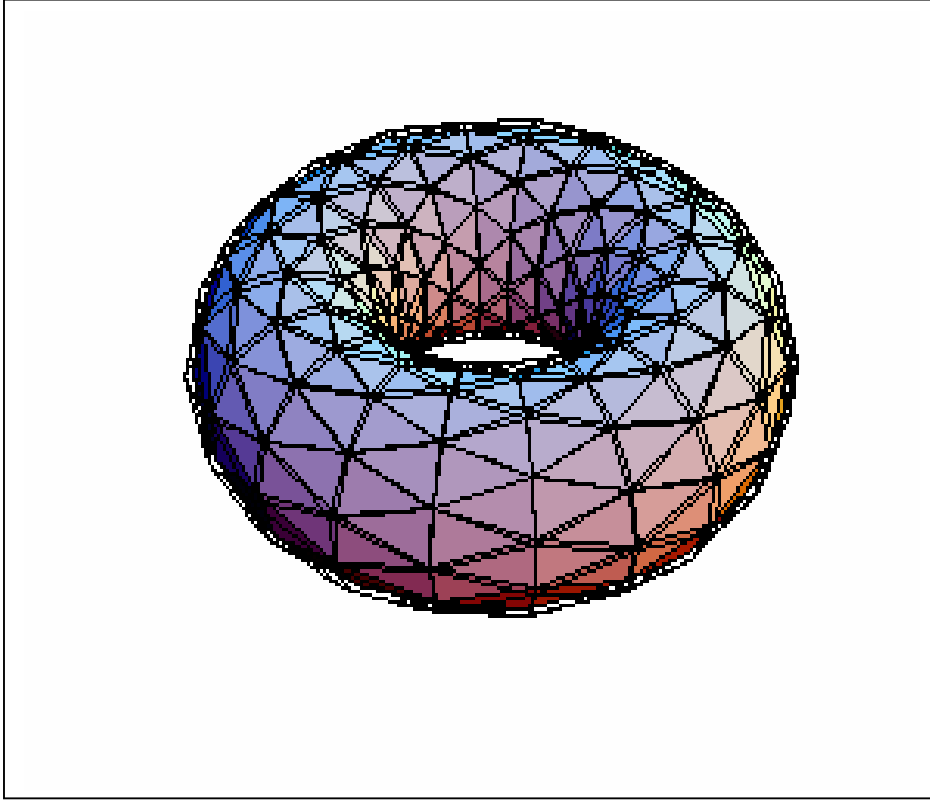
Figure 6-1) Toroid Consisting of 480 Platelets.   The "inner" toroidal radius, r, equals 100 nm and the outer toroidal radius, R, equals 200 nm. The solid surface represents S_p. Displaced slightly outward from S_p lies the surface S_{dl}, which is indicated by the transparent (wireframe) structure.   In this example, S_{dl} lies at a distance of $8/\kappa$ from S_p.

The calculation of $\mathbf{v}_T$ is carried out following the procedures of Appendix B culminating in Eq. (B32).   This, in turn, requires the scalar potentials, Φ_α, which are determined following the procedures of Appendix C.   Since the transport equations for Φ_α and $\mathbf{v}_T$ are coupled together, it is necessary to adopt an iterative procedure in order to determine them.[34]   We begin by ignoring ion relaxation and approximate the local ion

densities in the fluid near the model particle with their equilibrium ion densities. This requires setting $\Phi_\alpha = -\psi$ where ψ is the correction potential of a low dielectric cavity in a constant external electric field. (See discussion in Appendix A following Eq. (A16).) The flow field $\mathbf{v}_T$ is computed as described in Appendix B, and then $\mathbf{z}_T$ is determined. At this point, we now have estimates of $\mathbf{v}_T$ and can obtain better estimates of Φ_α and $\nabla\Phi_\alpha$ by employing the procedures of Appendix C. This whole process is repeated until $\mathbf{z}_T$ converges to within a predefined tolerance level (typically 0.1 %).

6.3 Results and Discussion:
6.3.1 Spheres in KCl

The BE-TDL methodology described in the previous section and the appendices is first applied to a spheres of radius a. The solvent is taken to be water at 20 °C ($\eta = 1$ centipoise, $\varepsilon_s = 80.36$) and the salt is taken to be KCl at an ionic strength equal to 0.3725 M. The Debye-Huckel screening parameter, κ equals 2 nm^{-1} under these conditions (Eq. (A15)) and a is set to 10, 25, or 50 nm to give $\kappa a = 20$, 50, or 100, respectively. The small ion diffusion constants, D_α, or the hydrodynamic ion radius, r_α ($r_\alpha = k_B T/6\pi\eta\, D_\alpha$), is estimated from limiting molar ionic conductivities, λ_α^∞, and the Nernst-Einstein relation. The λ_α^∞'s (in 10^{-4} S m^2/mole at 25 °C) are related to r_α (in nm) by[49]

$$r_\alpha \;=\; 9.201\frac{z_\alpha^2}{\lambda_\alpha^\infty} \qquad (6-24)$$

where z_α is the valence of the α-ion. Since λ_α^∞ is similar for K$^+$ and Cl$^-$ ions, an average radius of .1229 nm is used for both. The reduced zeta potential, y_0, defined by

$$y_0 \;=\; \frac{q\,\zeta}{k_B T} \qquad (6-25)$$

(ζ is the actual zeta potential) is varied from +1 to +6 and $\Lambda_0(x)$ is estimated using Eq. (6-20).

The plated sphere models are generated using a procedure described in detail elsewhere.[6,34,49] For each case examined, several different model spheres are considered with the number of platelets, N, varied. A dimensionless electrophoretic mobility, E, is computed for each case[30,31]

$$E \;=\; \frac{3X\eta q}{2\varepsilon_s k_B T}\mu \quad (6-26)$$

where $X = 4\pi$ (in CGS units) or $1/\varepsilon_0$ (ε_0 = permittivity of free space, in MKSA units), q is the protonic charge, μ is the electrophoretic mobility, and other quantities have been defined previously in this section. The resulting E's are extrapolated versus 1/N and the $1/N \rightarrow 0$ limit is estimated. This "extrapolated shell" procedure[92] is carried out to correct, at least approximately, for the discretization error that results from replacing a "smooth", continuous model with a discrete one. In general, b (the double layer thickness) needs to be set large enough that $y(b)/y_0 \ll 1$ which insures that equilibrium charge densities are negligible for r > b. This result is satisfied if b is set in the range of $4/\kappa$ to $8/\kappa$. As the surface zeta potential increases, the value of b can actually be reduced. Shown in Table 6-1 are (extrapolated shell) E's for a wide range of cases. In addition to reduced mobilities that include ion relaxation, E_r, results are also included that leave ion relaxation out, E_{nr}. The E_{nr} and E_r BE-TDL results are compared with the independent theory of Henry[28] (for E_{nr}) and O'Brien and White[31] (for E_r). It is evident from the results of Table 6-1 that the methodology works best when κa is large. This, however, is expected on the basis of the approximations involved. For $\kappa a > 50$, the BE-TDL yields mobilities that are within a few percent of independent theory. It is appropriate at this point to discuss the similarities and differences of the BE-TDL approach used here with the related approaches of O'Brien and coworkers[116,117] and Dukhin and Shilov[124] applied to spheres, prolate, and oblate ellipsoids.

Table 6-1

Unrelaxed (E_{nr}) and Relaxed (E_r) for Spheres in KCl at 20 °C

κa	y_o	$E_{nr}(BE)$	$E_{nr}(H)^{(a)}$	Error[b]	$E_r(BE)$	$E_r(OW)^{(c)}$	Error[b]
20	1	1.34	1.387	3.5	1.32	1.447	9.6
"	2	2.68	2.77	3.4	2.50	2.738	9.5
"	3	4.02	4.148	3.2	3.40	3.720	9.4
"	4	5.36	5.517	2.9	3.92	4.260	8.7
"	5	6.70	6.872	2.6	4.04	4.360	7.9
"	6	8.04	8.203	2.0	3.88	4.171	7.5
50	1	1.42	1.431	0.8	1.48	1.429	-3.4
"	2	2.84	2.860	0.7	2.75	2.776	-0.9
"	3	4.27	4.283	0.3	3.89	3.945	1.4
"	4	5.69	5.700	0.2	4.77	4.822	1.1
"	5	7.11	7.106	-0.1	5.19	5.271	1.6
"	6	8.53	8.490	-0.5	5.20	5.324	2.4
100	1	1.46	1.446	1.0	1.48	1.426	-3.6
"	2	2.92	2.892	-1.0	2.86	2.808	-1.8
"	3	4.39	4.332	-1.3	4.23	4.085	-3.4
"	4	5.85	5.767	-1.4	5.30	5.172	-2.4
"	5	7.31	7.191	-1.6	5.98	5.933	-0.8
"	6	8.78	8.591	-2.2	6.36	6.305	-0.9

(a) from Henry[28], (b) Error = 100*(E(BE)/E(H or OW) – 1)

(c) from O'Brien and White[31]

Outside the double layer, Φ_α satisfies Laplace's equation (Eq. (6-8) with f_α set to 0). For simple geometries, the general solution of Φ_α can be written as an infinite, but convergent sum of "product functions" which are, individually, solutions of Eq. (6-8). The individual "product functions", in turn, are products of known functions of the individual orthogonal coordinates. (For a spherical particle, for example, the orthogonal coordinates are the radial variable, r, and two angular variables, θ and ϕ, respectively. The "product functions" involve simple polynomials in r, times spherical harmonics involving the angular variables. For prolate and oblate ellipsoids as well as a few other geometries,[125] the same approach can be used.) Although the individual "product functions" satisfy Laplace's equation, they do not satisfy the boundary condition on S_{dl} appropriate in the special case of interest here, Eq. (C8), but an infinite series can be constructed which does. (See discussion centered around Eq. (3.9) of reference 117). Dukhin and Shilov[124] and O'Brien and Ward[117] have shown that approximating this infinite series with the leading term yields accurate conductivities and electrophoretic mobilities[117] as well as induced electric dipole moments[124] under most conditions. By truncating the series in this manner, analytical expressions for electrophortic mobilities as well as other transport properties have been derived.[117,124]

For simple geometries such as spheres, prolate, and oblate ellipsoids, these alternative approaches[116,117,124] are simpler and more efficient that the BE-TDL approach used here. The advantage of the BE-TDL approach is that it can be applied to models of arbitrary shape. It is applied to spheres in the present work in order to verify the method as well as assess its range of validity. Another difference between the present method and the alternative approaches[116,117,124] is the inclusion of finite size effects on the velocity field, $\mathbf{v}_T$, as summarized by Eq. (B32). Including finite size effects in $\mathbf{v}_T$ also introduces a small velocity component normal to the local surface, S_p, and this also contributes to Φ_α (the $\mathbf{h}_j$ term in Eq. (C9)). Although size effects in $\mathbf{v}_T$ can be ignored for κa greater several hundred, our

observation has been that they should be included for smaller particles.

6.3.2 DNA-Spermidine Complexes

As an application of the BE-TDL procedure, we shall consider high molecular weight duplex DNA in the presence of the trication, spermidine ($NH^+(CH_2)_4N^+(CH_2)_3NH^+$). There has been considerable interest in the DNA-spermidine system over the past 25 years since it is ubiquitous in nature and mimics, in vitro, the compaction of DNA in living systems.[126,127] Under most salt conditions, purified high molecular weight duplex DNA exists in solution in an unfolded, random coil configuration. Under low salt conditions and in the presence of spermidine or other polycations, however, DNA undergoes a collapse to a compact, possibly toroidal shaped particle.[126,128-130] It is now believed that spermidine (a counterion) binds to DNA and is capable of forming crosslinks between strands of duplex DNA. When, for example, the butyl moiety of spermidine is replaced with propyl through octyl moieties, the interhelical strand separation varies in a systematic way that is readily explained in terms of a crosslinking model.[131] By examining, directly, the free solution electrophoretic mobility of compact DNA-spermidine complexes, we shall be able to draw some firm conclusions about the nature of spermidine – DNA interaction. Yamasaki et al.[132] have examined the complex of viral T4 DNA (166,000 base pairs) with spermidine in a buffer solution of 50 mM sodium maleate at pH = 6.0 and 20 °C. (At this pH, spermidine exists in solution as a +3 cation.) In the absence of spermidine, DNA exists in solution as an extended random coil and the free solution electrophoretic mobility, μ is measured to be -.328 cm^2/kV sec.[132] Although the random coil or wormlike chain structure of DNA is not amenable to the BE-TDL modeling developed in this work, it is worthwhile to consider closely related modeling grounded on the same principles of the CPM model before considering the DNA-sperimidine complex.

Stigter[33] has written a program which solves the coupled transport equations for an infinitely

long rod in monovalent salt and computes μ. Modeling DNA as a infinitely long rod of

diameter 2 nm and line charge density –2q per base pair (which yields an equivalent surface

charge density, σ, of -.150 coul/m^2 assuming a rise per base pair of .34 nm), Stigter's

program predicts μ = -.449 cm^2/kV sec. A detailed BE study of the length dependence of

DNA has shown that curvature of DNA can reduce $|\mu|$ below its "straight long rod" value by

approximately 20%.[20] This brings the experimental and model mobility into good agreement.

Thus, for DNA in the unfolded, random coil-wormike chain state, the CPM-electrokinetic

model yields free solution electrophoretic mobilities in good agreement with experiment.

Moving on to the DNA-spermidine complex , we shall consider a solution containing

12 mM of spermidine in addition to 50 mM sodium maleate buffer. At this spermidine

concentration, T4 DNA is present in the form of compact structures that are approximately

600 nm in diameter.[132] On the basis of the work of Yamasaki et al., we cannot say anything

about the shape of the particles, but independent study suggests a toroidal shape.[126-130] For

purposes of modeling, we shall consider two different shaped structures to illustrate the

dependence of mobility on particle shape. The first considered is a sphere (radius = a). For

a sphere of with a = 300 nm in aqueous solvent at 20 °C, the translational diffusion constant,

D_t, should be equal to .717 x 10^{-8} cm^2/sec. The second and physically more realistic model is

a toroid with "inner" toroidal radius, r, equal to 100 nm, and "outer" toroidal radius, R, equal

to 200 nm. (One can imagine generating a toroid by starting with a circle of radius, r, the

center of which is at distance R from some convenient origin. The symmetry axis lies

perpendicular to the line connecting the origin to the center of the circle. The toroid is

generated by rotating the circle about the symmetry axis by 2π radians.) For this toroid, D_t =

.874 x 10^{-8} cm^2/sec.[133,134] Plated structures with N varying between 128 and 512 are

generated for both the sphere and toroid models. Shown in Figure 6-1 is an example of a

toroid with R/r =2 consisting of 480 platelets. All of the plated structures are designed to

reproduce the D_t's mentioned previously. As a charge model, first assume σ is simply that of

duplex DNA (σ = -.150 coul/m^2).   The DNA phosphate charges inside the surface of the

complex are presumed to be neutralized by entrapped counterions. The net charge of the

complex arises from the surface charge density which is taken to be the same as that of

duplex DNA. It is also assumed that the charge distribution of mobile ions is described by

the Poisson-Boltzmann equation, Eq. (6-1). With this charge distribution with 12 mM

spermidine –trichloride plus 50 mM sodium maleate, Eq. (6-22) gives y_0 = -2.10.

Table 6-2

Mobilities[a] of Model DNA-Spermidine Complexes

Model	$f^{[b]}$	$-y_0$	$-\mu_{nr}{}^{[c]}$	$-\mu_r{}^{[d]}$
Sphere	0	2.10	.369	.335
Toroid	0	"	.354	.309
Sphere	0.92	0.505	.089	.087
Toroid	0.92	"	.086	.087
Sphere	0.95	0.335	.059	.057
Toroid	0.95	"	.057	.056
Sphere	0.97	0.208	.037	.036
Toroid	0.97	"	.036	.035

(a) mobilities are reported in cm^2/kV sec

(b) fraction of DNA phosphates neutralized by counterions

(c) ion relaxation not included

(d) ion relaxation included

Shown in Table 6-2 are the mobilities, computed by the TDL-BE procedure, for both models in the presence and absence of ion relaxation. As discussed previously, the mobilities are extrapolated to the $1/N \rightarrow 0$ limit. It is evident from these results that the mobilities are similar for the two model structures and yield an average mobility of about $-.32$ cm^2/kV sec if ion relaxation is included. The experimental mobility, on the other hand, is $-.050$ cm^2/kV sec, which, in absolute terms, is less than 1/6 the model mobility. The actual complex is behaving as though its absolute charge was much smaller than expected on the basis of the strict CPM model. A simple way of reconciling model and experimental mobilities is to reduce the (absolute) surface charge density used in modeling to the point that model and experimental mobilities are in agreement. Physically, this corresponds to a certain fraction of the DNA phosphates "specifically bound", by spermidine counterions. In the present interpretation, one can define "specifically bound" counterions as those trapped within the surface of hydrodynamic shear, S_p. There is no significant exchange of "specifically bound" counterions (inside S_p) and counterions in the fluid domain (outside of S_p) that are assumed to obey the Poisson-Boltzmann equation, Eq. (6-1). Table 6-2 gives mobilities in which the fraction of "specifically bound" DNA phosphates, f, is taken to be 0.92, 0.95, and 0.97, respectively. In order to bring experimental and model mobilities into agreement, approximately 95 % of the DNA phosphates must be "specifically bound" by spermidine. How do the findings of the present work compare with other studies?

There exists an extensive literature[135] on salt-linear polyelectrolyte interactions in general, and the compact form of DNA induced by polyvalent cations in particular.[125] Counterion "binding" can be defined in thermodynamic terms through the preferential interaction coefficient, Γ.[135,136] In particular, $1 + 2\Gamma$ can be interpreted as the average degree of "thermodynamic counterion association" per structural charge on the polymer.   The

preferential interaction coefficient has been examined in terms of counterion condensation theory,[137] PB theory,[138] and Monte Carlo simulation.[136] Counterion condensation theory[137,139] offers a particularly simple view of polyion-counterion interactions. According to this theory,[137,139] a certain fraction, f*, of counterions "condense" on a linear polyelectrolyte provided the absolute linear charge density exceeds a certain threshold, as it does for duplex DNA. Also,

$$1 + 2\Gamma \quad = \quad \frac{1 + f*}{2} \qquad (6-27)$$

For DNA in the presence of single monovalent, divalent, or trivalent counterions, f* = 0.76, 0.88, 0.92, respectively. Extensive past work on the compact form of DNA in the presence of spermidine as well as other polycations ($3 \leq$ valence charge) has convincingly shown that the compact structure of DNA is formed when f* exceeds about 0.90 when interpreted in terms of counterion condensation theory.[125] It is inappropriate to equate our f = .95 with f* (or possibly $1 + 2\Gamma$) as defined above. First of all, since we are inferring f from a transport property, it will depend, in principle at least, on non-equilibrium variables such as the relative counterion mobilities. In the strictest sense, our f cannot be related to a true equilibrium binding constant. Second, for unfolded DNA in the presence of monovalent salt, the model mobility with f = 0 (not 0.76 as one might expect on the basis of counterion condensation theory) agrees with experiment.

6.4 Summary

The Boundary Element methodology, BE-TDL, developed in the present work yields accurate electrophoretic mobilities of spheres provided κa exceeds approximately 50. For particles with a smallest linear dimension equal to L, the BE-TDL is limited to those with L

greater than $50/\kappa$. In addition, alternative methods are available and preferable for large spherical or spheroidal (prolate or oblate ellipsoid) model particles.[116,117,124] The BE-TDL method should be useful in modeling large particles of arbitrary shape. In the present work, the example of compact, high molecular weight DNA-spermidine complexes has been examined.

For native, unfolded DNA in the presence of monovalent salt, the CPM model of electrophoresis is able to account for the observed mobility without the need of "specific binding" of a certain fraction of DNA phosphates by Na^+ counterions. For DNA-spermidine complex, on the other hand, it is necessary to assume that 95% of the spermidine as "specifically bound" to DNA in order to reconcile experimental and model mobilities. It should be emphasized, however, that this is based on the assumed validity of the CPM model. As discussed in Section II.A, one component of the CPM model is the assumption that the Poisson-Boltzmann, PB, equation accurately describes the ion distribution within the double layer of the model macroion. For monovalent salt, the PB equation does indeed accurately describes the ion distribution around the DNA provided the counterion is not very large.[140] For more complex systems, such as the one involving the trication spermidine, on the other hand, the PB approximation suffers severe deficiencies.[141] Consequently, the inability of the CPM model to account for the experimental mobility of the DNA-spermidine complex without invoking "specific binding" may be due, in part at least, to a breakdown of the CPM model. In this case, alternatives exist such as triple layer modeling,[142] or more formal theoretical approaches such as functional expansion techniques[143] and dressed ion theory.[141] This, however, is beyond the scope of the present work.

Appendix A: Boundary Element Method for Scalar Fields

The Boundary Element (BE) approach for the scalar fields of interest in this work are described in detail elsewhere.[34,144,147] The main features of the method as applied to scalar fields are summarized below. This is followed with several illustrative examples that are relevant to the present work. Consider a scalar field, ψ, associated with a particle enclosed by shear surface S_p and let **n** denote the local outward unit normal to S_p. It is assumed that ψ goes to zero far from S_p, and satisfies

$$\nabla^2 \psi(\underline{x}) \;=\; h'(\underline{x}) \qquad (A1)$$

where h' represents the source terms for the scalar field and **x** represents any point in space. It is also convenient to define the outward normal derivative at a point **x** on S_p

$$p(\underline{x}) \;=\; \underline{\nabla}\psi(\underline{x}) \cdot \underline{n}(\underline{x}) \qquad (A2)$$

It is important to distinguish whether the normal derivative indicated by Eq. (A2) is taken just inside, p^i, or just outside, p^e, S_p. In the BE approach, the solution of ψ is written as an integral equation over the surface, S_p, as well as a bounding volume that can be chosen to correspond to the particle interior, or the volume exterior to the particle. The assumption is made that the scalar field varies sufficiently slowly over S_p that ψ and its normal derivative is constant, to a good approximation, over a small region of S_p. Consequently, S_p is approximated as a series of N interconnected triangular plates, or platelets, and ψ and its normal derivative are assumed constant over a single platelet. Let $\mathbf{x}_k$ denote the centroid of platelet k and also let ψ_k, p_k^i, and p_k^e denote $\psi(\mathbf{x}_k)$, $p^i(\mathbf{x}_k)$, and $p^e(\mathbf{x}_k)$, respectively. For   an arbitrary "field" point, **s**, in the fluid domain exterior to S_p, the potential can be written[34]

$$\psi(\underline{s}) \;=\; v^e(\underline{s}) - \sum_k I_1(\omega,k,\underline{s})\psi_k - \sum_k I_2(\omega,k,\underline{s})\,p_k^e \qquad (A3)$$

where the sum over k extends over all N platelets, ω is an arbitrary constant,

$$v^e(\underline{s}) \;=\; -\int_\Omega F(\omega,\underline{x},\underline{s})[h'(\underline{x}) - \omega^2\psi(\underline{x})]dV_x \qquad (A4)$$

$$I_1(\omega,k,\underline{s}) \;=\; -\int_{S_k} F'(\omega,\underline{x},\underline{s})\,dS_x \qquad (A5)$$

$$I_2(\omega,k,\underline{s}) \;=\; \int_{S_k} F(\omega,\underline{x},\underline{s})\,dS_x \qquad (A6)$$

$$F(\omega,\underline{x},\underline{s}) \;=\; \frac{e^{-\omega|\underline{x}-\underline{s}|}}{4\pi|\underline{x}-\underline{s}|} \qquad (A7)$$

$$F'(\omega,\underline{x},\underline{s}) \;=\; \underline{\nabla}_x F(\omega,\underline{x},\underline{s})\cdot\underline{n}(\underline{x}) \qquad (A8)$$

In Eq. (A4), the integration is over the entire fluid domain and in Eqs. (A5-A6), the domain of integration is the surface of platelet k, S_k. The unknowns in Eq. (A3) are the ψ_k's and p_k's, and possibly the "h' - $\omega^2\,\psi$" terms appearing in Eq. (A4) for $v^e(\mathbf{s})$. The latter terms, if present, can be approximated with initial estimates or results from previous iterations.[34,147] The 2N ψ_k's and p_k's can be determined by considering field points, $\mathbf{s}$, to correspond to the centroids of the individual plates. In general, the 2N unknowns can be obtained by simultaneous solution of[34]

$$\frac{1}{2}\psi_j \;=\; v_j^e - \sum_k D_{jk}\,p_k^e - \sum_k B_{jk}\psi_k \qquad (A9)$$

$$\frac{1}{2}\psi_j \;=\; v_j^i + \sum_k C_{jk}\,p_k^i + \sum_k A_{jk}\psi_k \qquad (A10)$$

where

$$A_{jk} = I_1(0,k,\underline{x}_j), \quad B_{jk} = I_1(\omega,k,\underline{x}_j), \quad C_{jk} = I_2(0,k,\underline{x}_j), \quad D_{jk} = I_2(\omega,k,\underline{x}_j) \qquad (A11)$$

and

$$v_j^i = -\int_{\Omega_i} F(0,\underline{x},\underline{x}_j)h'(\underline{x})dV_x \qquad (A12)$$

In Eq. (A12), the domain of integration, Ω_i, is the volume interior to S_p. Once a model has been defined, the $4N^2$ surface integrals represented by Eq. (A11) can be determined numerically. The source terms, v_j^i and v_j^e, are also known or can be approximated.   In the general case, the ψ_k's and p_k's are solved by numerical solution of the 2N equations given by (A9) and (A10) above. Several specific examples are considered below.

As a first example, consider the equilibrium electrostatic potential in the vicinity of a model macroion that obeys Eqs. (6-1,2) in the text. It is assumed that the dielectric constant is equal to ε_i inside of the macroion, $\rho_{fixed}(\mathbf{x})$, and ε_s outside of the macroion. If we also specify the charge distribution inside the macroion, then for h'($\mathbf{x}$) in Eq. (A12), Eq. (6-1) gives h'($\mathbf{x}$) = -X $\rho_{fixed}(\mathbf{x})/\varepsilon_i$ where X = 4π (in CGS units), or $1/\varepsilon_0$ where ε_0 is the permittivity of free space (in MKSA units), and $\mathbf{x}$ is a point in the macroion interior.   The normal derivatives are related to each other by the electrostatic boundary condition

$$\varepsilon_s \, p_k^e = \varepsilon_i \, p_k^i \qquad (A13)$$

Thus, Eq. (A12) can be solved once the charge distribution inside of the macroion is defined. For the exterior source terms given by Eq. (A4), we have from Eq. (6-2)

$$h'(\underline{x}) \quad = \quad -\frac{Xq}{\varepsilon_s}\sum_{\alpha}c_{\alpha}z_{\alpha}\,e^{-qz_{\alpha}\Lambda_0(\underline{x})/k_BT} \qquad (A14)$$

For ω appearing in Eq. (A4) and (A11) for B_{jk} and D_{jk}, it is convenient to choose the Debye

screening length, κ, defined by

$$\kappa^2 \quad = \quad \frac{Xq^2}{\varepsilon_s k_B T}\sum_{\alpha}c_{\alpha}z_{\alpha}^{\,2} \qquad (A15)$$

The reason for this choice becomes clear when Eq. (A14) is substituted in Eq. (A4).

Provided the potential, $\Lambda_0(\mathbf{x})$ is small in the fluid domain. The exponential in Eq. (A14) can

be expanded and only the linear term in $\Lambda_0(\mathbf{x})$ retained. This truncation yields the "linear"

Poisson-Boltzmann, PB, equation. For the choice $\omega = \kappa$, h' - $\kappa^2\Lambda_0 = 0$ everywhere, and $v^e(\mathbf{s})$

vanishes. In this case, Eqs. (A9) and (A10) can be solved for the ψ_k's and p_k's. Then Eq. (A3)

can be used to solve for $\Lambda_0(\mathbf{s})$ for arbitrary field points. When the macroion is highly charged,

however, the linear PB equation is no longer valid and one is forced to return to the full form

given by Eq. (A14). The difficulty this creates, however, is that the potential, which we wish

to obtain, appears in the source term, $v^e(\mathbf{s})$. This can be dealt with by first assuming $v^e(\mathbf{s}) = 0$,

which is equivalent to assuming $\Lambda_0(\mathbf{x})$ obeys the linear PB equation, solving for the initial

ψ_k's and p_k's, and then using Eq. (A3) to determine $\Lambda_0(\mathbf{s})$ for a large number of field points in

the fluid domain near the model macroion. Then choosing $\mathbf{s} = \mathbf{x}_j$ in Eq. (A4), revised source

terms can be computed using either the full exponential form, or expanding the exponential

an truncating the sum after a finite number of terms. Then the whole procedure is repeated

until the potentials converge to a finite value. This is basically the procedure proposed by

Zhou[147] and which we have employed in our lab for the last eight years.[34,106,120]

As a variation of the approach considered in the previous problem, consider the

equilibrium electrostatic potential again but instead of specifying the charge distribution of the macroion, specifying the surface potential, Λ_{0k}. This case is simpler than the previous one since we now only need to consider Eq. (A9). Eq. (A9) can be written in more compact "supermatrix" form

$$\left[\frac{1}{2}\underline{\underline{I}} + \underline{\underline{B}} \right] \cdot \underline{\Lambda}_0 \quad = \quad \underline{v}^e - \underline{\underline{D}} \cdot \underline{p}^e \qquad (A16)$$

where $\mathbf{\Lambda_0}$, $\mathbf{v^e}$, and $\mathbf{p^e}$ denote N by 1 column vectors; and $\mathbf{B}$ and $\mathbf{D}$ represent N by N matricies where the j-k element are B_{jk} and D_{jk}, respectively. Also, $\mathbf{I}$ denotes the N by N identity matrix with diagonal components equal to 1 and off-diagonal components equal to 0. Provided we have estimates of the source terms, $\mathbf{v^e}$, Eq. (A16) can be inverted to obtain the N unknown components of $\mathbf{p^e}$. For problems in which the surface potential $\mathbf{\Lambda_0}$ contains components that are large in absolute magnitude, it is necessary to carry out an iterative solution as described in the previous paragraph.

Next consider the correction potential, ψ, defined by Eq. (6-3), for the special case of a low dielectric cavity in a high dielectric medium subject to a constant external electric field, $\mathbf{e}$. In this case, the surface of the cavity is taken to be S_p. This potential is useful in the present work in defining the initial estimate of the Φ_α defined by Eqs. (6-8)-(6-10). In order to calculate the components of $\mathbf{\psi}$, (ψ_k is the correction potential at the centroid of surface platelet k), it is convenient to set $\omega = 0$ in Eq. (A11) which yields $B_{jk} \rightarrow A_{jk}$ and $D_{jk} \rightarrow C_{jk}$. Also, the dielectric boundary condition corresponding to Eq. (A13) appropriate for the correction potential becomes

$$\varepsilon_s (p_k^e \; - \; a_k) \quad = \quad \varepsilon_i (p_k^i \; - \; a_k) \qquad (A18)$$

where the "s" and "i" subscripts on ε indicate external (solvent) and internal dielectric

constants, respectively, and $a_i = \mathbf{e} \cdot \mathbf{n}_i$ ($\mathbf{n}_i$ is the outward unit normal to surface platelet i). With this boundary condition, making use of the supermatrix and column vector notation introduced in the previous paragraph, and assuming $\varepsilon_i \ll \varepsilon_s$, Eqs. (A8-A9) can be manipulated to yield

$$\underline{p}^e = \underline{a} \qquad (A19)$$

$$\underline{\psi} = -\left[\frac{1}{2}\underline{\underline{I}} + \underline{\underline{A}}\right]^{-1} \cdot \underline{\underline{C}} \cdot \underline{a} \qquad (A20)$$

Once the components of $\boldsymbol{\psi}$ are determined, the correction potential at arbitrary point $\mathbf{s}$ in the fluid is given by

$$\psi(\underline{s}) = -\sum_k \left[I_1(0,k,\underline{s})\psi_k + I_2(0,k,\underline{s})a_k\right] \qquad (A21)$$

For the potentials, Φ_α, it is again convenient to choose $\omega = 0$ in Eq. (A11). In this example, it is only necessary to solve the "exterior" problem (Eq. (A9)) with the boundary condition from Eq. (6-10)

$$\underline{p}^e_\alpha = -\underline{a} \qquad (A22)$$

Eq. (A9) reduces to

$$\underline{\Phi}_\alpha = \left[\frac{1}{2}\underline{\underline{I}} + \underline{\underline{A}}\right]^{-1} \cdot \left[\underline{v}^e_\alpha + \underline{\underline{C}} \cdot \underline{a}\right] \qquad (A23)$$

where $(\mathbf{v}_\alpha^e)_k = v_\alpha^e(\mathbf{x}_k)$, and

$$v_\alpha^e(\underline{s}) = -\int_\Omega F(0,\underline{x},\underline{s}) f_\alpha(\underline{x}) dV_x \qquad (A24)$$

where Ω denotes the fluid external to S_p, and f_α is given by Eq. (6-9). Once the surface potential components are computed from Eq. (A23), Eq. (A3) can be used to compute $\Phi_\alpha(\mathbf{s})$ for arbitrary points in the fluid. Since the source terms, f_α, contain the potentials that we are attempting to determine, it is necessary to follow an iterative approach analogous to that employed for Λ_0. Initially, ion distributions are approximated by their equilibrium values and from Eq. (6-4), this requires setting $\Phi_\alpha = -\psi$ with a similar relationship for the gradient. This is iterated until Φ_α converges.[34]

A disadvantage of this approach is the necessity of computing the volume integrals throughout the fluid domain as defined by Eq. (A24). Volume integrations of this kind are straightforward, but computationally time consuming. An alternative discussed in Appendix C circumvents this computational bottleneck and results in a substantial speedup in computation time.
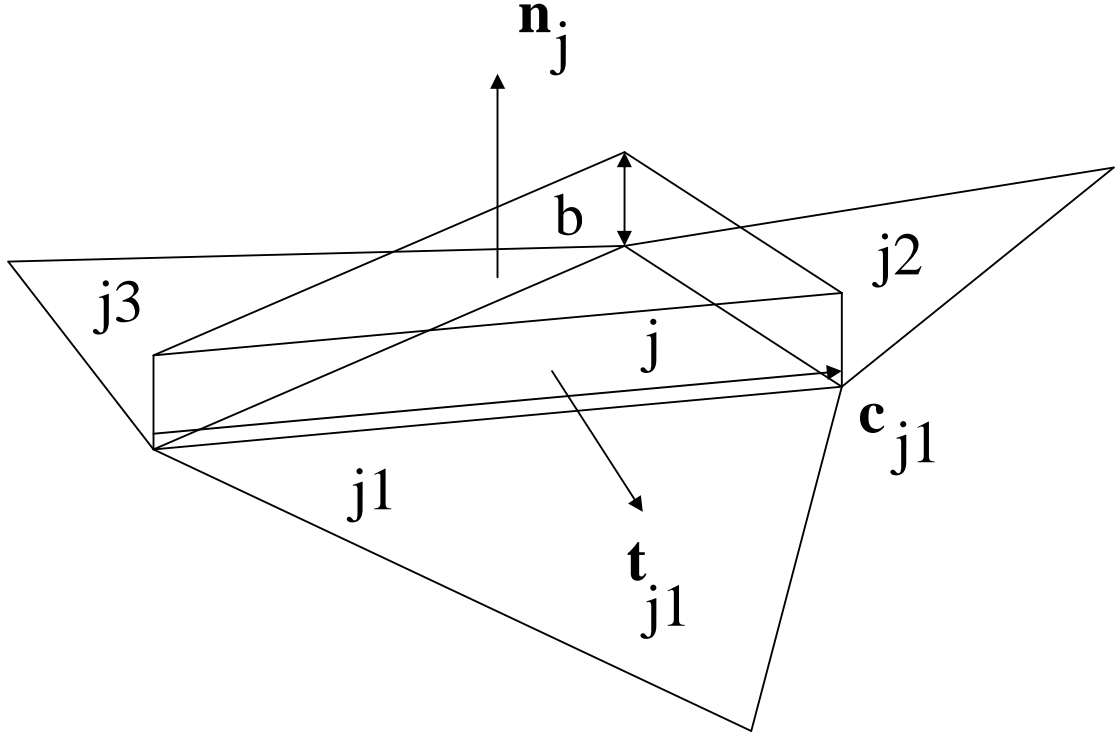
Figure 6-2) **Volume Element and Associated Variables.** Volume V_j is the wedge-shaped structure at the center of the figure. Shown is plate j and neighboring plates j1, j2, and j3. The unit vectors $\mathbf{n}_j$ and $\mathbf{t}_{j1}$ denote outward normals to plate j and side 1 of plate j, respectively. The $\mathbf{c}_{j1}$ vector is the first side vector of plate j and b denotes the thickness of V_j.

Appendix B: Fluid Velocity in the TDL Regime, a Boundary Element Analysis

The Boundary Element representation of the velocity field, $\mathbf{v}_T$, is well described elsewhere[92,106,120] and we begin by writing down the integral equation

$$\underline{v}_T(\underline{s}) \;=\; \underline{v}_\infty(\underline{s}) - \int_{S_p} \underline{\underline{U}}(\underline{x},\underline{s})\cdot\underline{f}_T(\underline{x})\,dS_x - \int_\Omega \underline{\underline{U}}(\underline{y},\underline{s})\cdot\underline{w}(\underline{y})\,dV_y \qquad (B1)$$

where $\mathbf{v}_\infty(\mathbf{s})$ denotes the fluid velocity at $\mathbf{s}$ if the particle were absent, S_p denotes the surface of hydrodynamic shear, Ω is the fluid domain exterior to S_p, $\mathbf{f}_T(\mathbf{x})$ is the (effective) hydrodynamic stress on S_g at point $\mathbf{x}$, $\mathbf{w}(\mathbf{y})$ is the (effective) external force per unit volume at point $\mathbf{y}$ in the fluid defined by Eq. (6-12),

$$\underline{\underline{U}}(\underline{x},\underline{s}) \;=\; -\frac{1}{8\pi\eta r}\left[\underline{\underline{I}} + \frac{\underline{\underline{rr}}}{r^2}\right] \qquad (B2)$$

where η is the solvent viscosity, $\mathbf{r} = \mathbf{x} - \mathbf{s}$, $r = |\mathbf{r}|$, $\mathbf{I}$ is the 3 by 3 identity matrix, and $\mathbf{rr}$ is the 3 by 3 position dyadic with components $(\mathbf{rr})_{nm} = (\mathbf{r})_n(\mathbf{r})_m$. In Eq. (B1), $\mathbf{x}$ denotes the domain of integration over surface points of S_p and $\mathbf{y}$ denotes the domain of integration over the fluid volume external to S_p. The reason for this subtle distinction is to distinguish between "surface" and "volume" points. Stick hydrodynamic boundary conditions are assumed which means the fluid and particle velocities match on S_p. For a particular point, $\mathbf{s} = \mathbf{x}_j$ on S_p and in a reference frame stationary with respect to the particle, Eq. (B1) can be written

$$\underline{0} \;=\; \underline{v}_\infty(\underline{x}_j) - \int_{S_p}\underline{\underline{U}}(\underline{x},\underline{x}_j)\cdot\underline{f}_T(\underline{x})\,dS_x - \int_{\Omega}\underline{\underline{U}}(\underline{y},\underline{x}_j)\cdot\underline{w}(\underline{y})\,dV_y \qquad (B3)$$

In the applications of interest in this work, we either know or have estimates of $\mathbf{w}$. Thus, it is possible to invert Eq. (B3) and obtain $\mathbf{f}_T$.

It is convenient to break up $\mathbf{v}_T$ into two parts,

$$\underline{v}_T(\underline{s}) \;=\; \underline{v}_0(\underline{s}) + \underline{v}(\underline{s}) \qquad (B4)$$

where $\mathbf{v}_0$ is the fluid velocity of the corresponding uncharged model particle in the same external flow field, $\mathbf{v}_\infty$, as the actual particle, and $\mathbf{v}$ represents the "disturbance flow" (around a stationary particle) due to $\mathbf{w}$. Consider, for the moment, the simpler flow field, $\mathbf{v}_0$. In the absence of external forces, Eq. (B3) reduces to

$$\underline{0} \;=\; \underline{v}_\infty(\underline{x}_j) - \int_{S_p}\underline{\underline{U}}(\underline{x},\underline{x}_j)\cdot\underline{f}_0(\underline{x})\,dS_x \qquad (B5)$$

Now $\mathbf{f}_0$ varies gradually over the particle surface. Consequently, S_p is approximated as a series of N interconnected flat plates and the assumption is made that $\mathbf{f}_0(\mathbf{x}) \cong \mathbf{f}_0(\mathbf{x_k}) = \mathbf{f}_{ok}$ for points, $\mathbf{x}$, on surface S_k, and $\mathbf{x}_k$ is the centroid of platelet k. Also define

$$\underline{\underline{U}}_{jk} \;=\; \int_{S_k}\underline{\underline{U}}(\underline{x},\underline{x}_j)\,dS_x \qquad (B6)$$

which is computed numerically for $j \neq k$. For $j = k$, the integral is given analytically by[148,149]

$$\underline{\underline{U}}_{jj} = -\frac{1}{8\eta}\sqrt{\frac{S_j}{\pi}}\left[3\underline{\underline{I}} - n_j n_j\right] \qquad (B7)$$

where S_j is the area of surface platelet k, $\mathbf{n}_j$ is the outward normal to the platelet, and $\mathbf{n}_j\,\mathbf{n}_j$ is the dyadic formed from the outward normal. With this discretization approximation, Eq. (B5) can be written

$$\underline{v}_{\infty j} = \sum_k \underline{\underline{U}}_{jk} \cdot \underline{f}_{0k} \qquad (B8)$$

where $\mathbf{v}_{\infty j} = \mathbf{v}_{\infty}(\mathbf{x}_j)$. It is convenient to introduce supervector/supermatrix notation at this time. Let $\mathbf{v}_{\infty}$ denote the 3N by 1 column vector formed by stacking the N 3x1 column vectors, $\mathbf{v}_{\infty j}$, on top of each other. The supervector $\mathbf{f}_0$ (and others introduced later in this appendix) have a similar meaning. Also, define the 3N by 3N supermatrix, $\mathbf{U}$, by

$$\underline{\underline{U}} = \begin{bmatrix} \underline{\underline{U}}_{11} & \underline{\underline{U}}_{12} & .. & .. & \underline{\underline{U}}_{1N} \\ \underline{\underline{U}}_{21} & \underline{\underline{U}}_{22} & .. & .. & \underline{\underline{U}}_{2N} \\ .. & .. & .. & .. & .. \\ .. & .. & .. & .. & .. \\ \underline{\underline{U}}_{N1} & \underline{\underline{U}}_{N2} & .. & .. & \underline{\underline{U}}_{NN} \end{bmatrix} \qquad (B9)$$

Then Eq. (B8) can be inverted to yield

$$\underline{f}_0 = \underline{\underline{U}}^{-1} \cdot \underline{v}_{\infty} \qquad (B10)$$

Once a particular model is defined, it is straightforward to compute the $\mathbf{U}$ – matrix and invert it to obtain $\mathbf{U}^{-1}$. Hydrodynamic boundary conditions determine $\mathbf{v}_{\infty}$ and Eq. (B10) is used to determine $\mathbf{f}_0$. Then Eq. (B1) can be used to solve for $\mathbf{v}_0(\mathbf{s})$ at points in the fluid. If $\mathbf{s}$ is near S_p, $\mathbf{v}_0(\mathbf{s})$ varies linearly moving outward from the particle surface. Let $\mathbf{s} = \mathbf{x}_j + x'\,\mathbf{n}_j$ where $\mathbf{x}_j$ is the centroid of surface platelet j, $\mathbf{n}_j$ is the outward unit normal, and x' is the normal distance of $\mathbf{s}$ from $\mathbf{x}_j$. To a good approximation, we can write

$$\underline{v}_0(\underline{s}) \quad = \quad \underline{v}_0(\underline{x}_j + x'\underline{n}_j) \quad = \quad \underline{d}_j x' \qquad (B11)$$

where $\mathbf{d}_j$ is a constant vector. Eq. (B11) is valid for x' << L, where L is the smallest linear dimension of the model particle. In the present work, we shall only be interested in points near the surface of "large" particles. The advantage of Eq. (B11) is the determination of $\mathbf{v}_0(\mathbf{s})$ at N points directly above the N surface platelets allows us to completely define $\mathbf{v}_0(\mathbf{s})$ at all points of interest in the fluid.

Two particular cases serve to illustrate the physical breakdown of $\mathbf{v}_T(\mathbf{s})$ defined by Eq. (B4). In Case One, a highly charged model particle translates with velocity $\mathbf{u}$ through a fluid that is at rest except for the disturbance produced by the particle itself. In a reference frame stationary with respect to the particle, the fluid at considerable distance from S_p appears to flow past with velocity $-\mathbf{u}$ and hence $\mathbf{v}_\infty(\mathbf{s}) = -\mathbf{u}$. Solution of Eqs. (B10-B11) gives $\mathbf{v}_0(\mathbf{s})$, but this is not the total fluid velocity. As the (highly charged) particle translates, there is a tendency of the ion atmosphere to lag behind the particle, and this distortion of the ion atmosphere generates external forces that result in additional drag, or "electrolyte friction".[20,92] Thus, $\mathbf{v} \neq \mathbf{0}$. In Case Two, a stationary, highly charged particle is placed in a stationary fluid, but it is subjected to a constant external electric field, $\mathbf{e}$. Under these conditions, $\mathbf{v}_0(\mathbf{s}) = \mathbf{0}$, but because of the interaction of $\mathbf{e}$ with local fluid charge densities that are large near S_p, substantial convective flows develop, and $\mathbf{v} \neq \mathbf{0}$. (The only instance where $\mathbf{v} = \mathbf{0}$ in Case Two is for a charged macroion in the absence of counterions or added salt. This unphysical special case can be ignored.) Attention shall now be turned to $\mathbf{v}(\mathbf{s})$.

Start with Eq. (B1) setting $\mathbf{v}_\infty(\mathbf{s}) = \mathbf{0}$ and discretizing the surface and volume elements around the model particle as discussed following Eq. (B5)

$$\underline{v}(\underline{s}) \quad = \quad -\sum_k \left[\left[\int_{S_k} \underline{\underline{U}}(\underline{x},\underline{s})dS_x \right] \cdot \underline{f}_k + \int_{V_k} \underline{\underline{U}}(\underline{y},\underline{s}) \cdot \underline{w}(\underline{y})dV_y \right] \qquad (B12)$$

where V_k is the fluid volume external to surface platelet k. Because $\mathbf{w}(\mathbf{y})$ varies as $n_{\alpha 0}(\mathbf{y}) - c_\alpha$

(see Eq. (6-12), it falls off rapidly with distance moving away from S_p. To a good approximation, V_k can be truncated, to a good approximation, at a distance of several κ^{-1} from S_p. Call this distance b. Furthermore, V_k can be viewed as a triangular disk of basal area S_k and thickness b. The volume element dV_y can be written $dS_x dx'$ where $\mathbf{y}$ is replaced with $\mathbf{x} + x'\mathbf{n}_k$. This approximation will be accurate provided b is much less than the local radius of curvature of the macroion, which will be valid for large particles in the thin double layer, TDL, limit. Also define $\mathbf{s} = \mathbf{x}_j + \Delta\mathbf{n}_j$ where Δ represents the distance of closest approach of the field point $\mathbf{s}$, from S_p. Previous investigators[116,122] have also shown that Φ_α varies slowly near S_p. (The subscript, α, indicates the mobile ion species present in solution.) Thus, we can approximate $\mathbf{w}(\mathbf{y})$ in Eq. (B12) with

$$\underline{w}(\underline{y}) \;=\; \sum_\alpha \sigma_{\alpha k}(x')\underline{\xi}_{\alpha k} \qquad (B13)$$

where

$$\sigma_{\alpha k}(x') \;=\; qz_\alpha\big[n_{\alpha 0}(\underline{x}_k + x'\underline{n}_k) - c_\alpha\big] \qquad (B14)$$

$$\underline{\xi}_{\alpha k} \;=\; \underline{\nabla}\,\Phi_\alpha(\underline{x}_k) + \underline{e} \qquad (B15)$$

Also define $\mathbf{v}_j(\Delta) = \mathbf{v}(\mathbf{x}_j + \Delta\mathbf{n}_j)$ and

$$\underline{\underline{H}}_{jk}(x',\Delta) \;=\; \int_{S_k} \underline{\underline{U}}(\underline{x} + x'\underline{n}_k, \underline{x}_j + \Delta\underline{n}_j)\,dS_x \qquad (B16)$$

Eq. (B12) can then be written

$$\underline{v}_j(\Delta) = -\sum_k \left[\underline{\underline{H}}_{jk}(0,\Delta)\cdot \underline{f}_k + \sum_\alpha \int_0^b dx'\,\sigma_{\alpha k}(x')\int_{S_k} dS_x\,\underline{\underline{U}}(\underline{x} + x'\underline{n}_k, \underline{x}_j + \Delta\underline{n}_j)\cdot\underline{\xi}_{\alpha k} \right] \qquad (B17)$$

Because the present work is restricted to the TDL approximation, this can be simplified further. Expanding $\mathbf{U}$ in Eq. (B16-17) to first order terms in x' and Δ,

$$\underline{\underline{H}}_{jk}(x',\Delta) \quad = \quad \delta_{jk}\left[\underline{\underline{U}}_{jj} + |\, x' - \Delta \,|\, \underline{\underline{T}}_{jj}\right] + (1 - \delta_{jk})\left[\underline{\underline{U}}_{jk} + x'\underline{\underline{T}}_{jk} - \Delta\underline{\underline{W}}_{jk}\right] \qquad (B18)$$

where the **U**'s have been defined previously, δ_{jk} is the Kroneker delta,

$$\underline{\underline{T}}_{jj} \quad = \quad \frac{1}{2\eta}\left[\underline{\underline{I}} - \underline{\underline{n_j n_j}}\right] \qquad (B19)$$

$$\underline{\underline{T}}_{jk} \quad = \quad -\frac{1}{8\pi\eta}\int_{S_k}\frac{dS_x}{r^3}\left[\underline{\underline{n_k r}} + \underline{\underline{rn_k}} - \underline{\underline{I}}(\underline{n}_k \cdot \underline{r})\right] \qquad (j \neq k) \quad (B20)$$

$$\underline{\underline{W}}_{jj} \quad = \quad -\underline{\underline{T}}_{jj} \qquad (B21)$$

$$\underline{\underline{W}}_{jk} \quad = \quad -\frac{1}{8\pi\eta}\int_{S_k}\frac{dS_x}{r^3}\left[\underline{\underline{n_j r}} + \underline{\underline{rn_j}} - \underline{\underline{I}}(\underline{n}_j \cdot \underline{r})\right] \qquad (j \neq k) \quad (B22)$$

and $\mathbf{r} = \mathbf{x} - \mathbf{x}_j$. Eqs. (B19-B22) along with the **U**'s defined previously are computed at the start of the calculation and saved for later use. In order for Eq. (B18) to be strictly valid, we should have $|x'\mathbf{n}_k - \Delta\mathbf{n}_j| \ll |\mathbf{x}_j - \mathbf{x}_k|$ or $b \leq |\mathbf{x}_j - \mathbf{x}_k|$. (The less restrictive latter condition comes from the fact that the most significant terms in the volume integrals occur when $|x'\mathbf{n}_k - \Delta\mathbf{n}_j|$ is substantially less than b). Although this condition is readily satisfied when platelets j and k are far apart, when applied to nearest neighbors, it places a restriction on how large N can be set. If S_{tot} represents the total surface area of S_p, it straightforward that the maximum N is given by

$$N_{max} \quad \approx \quad S_{tot}/b^2 \qquad (B23)$$

Provided b is chosen sufficiently large that equilibrium ion densities are negligible for $x' > b$, the upper limit on the dx' integrations in Eq. (B17) can be extended to infinity. With the additional definition

$$\underline{\Gamma}_{\alpha k}{}^{(m)} = \underline{\xi}_{\alpha k} \int_0^\infty dx' x'^m \sigma_{\alpha k}(x') \quad (B24)$$

Eq. (B17) can be written

$$\begin{aligned}
\underline{v}_j(\Delta) &= -\sum_k \left[\underline{\underline{U}}_{jk} - \Delta \underline{\underline{W}}_{jk} \right] \cdot \underline{f}_k - \sum_\alpha \underline{\underline{T}}_{jj} \cdot \underline{\xi}_{\alpha j} \int_0^\infty dx' \sigma_{\alpha j}(x') \, | \Delta - x'| \\
&\quad - \sum_{\alpha,k} \underline{\underline{U}}_{jk} \cdot \underline{\Gamma}_{\alpha k}{}^{(0)} - \sum_{\alpha,k \ne j} \left[\underline{\underline{T}}_{jk} \cdot \underline{\Gamma}_{\alpha k}{}^{(1)} - \Delta \underline{\underline{W}}_{jk} \cdot \underline{\Gamma}_{\alpha k}{}^{(0)} \right] \quad (B25)
\end{aligned}$$

Being particularly careful with regards to the self (j = k) terms, this can be rearranged to give

$$\begin{aligned}
\underline{v}_j(\Delta) &= 2\sum_\alpha g_{\alpha j}(\Delta) \underline{\underline{T}}_{jj} \cdot \underline{\xi}_{\alpha j} - \sum_k \left[\underline{\underline{U}}_{jk} - \Delta \underline{\underline{W}}_{jk} \right] \cdot \underline{f}_k \\
&\quad - \sum_{\alpha,k} \left[\underline{\underline{U}}_{jk} \cdot \underline{\Gamma}_{\alpha k}{}^{(0)} + \underline{\underline{T}}_{jk} \cdot \underline{\Gamma}_{\alpha k}{}^{(1)} - \Delta \underline{\underline{W}}_{jk} \cdot \underline{\Gamma}_{\alpha k}{}^{(0)} \right] \quad (B26)
\end{aligned}$$

where

$$g_{\alpha j}(\Delta) = \int_0^\Delta dx' \sigma_{\alpha j}(x') x' + \Delta \int_\Delta^\infty dx' \sigma_{\alpha j}(x') \quad (B27)$$

The first term on the rhs of Eq. (B25) represents the value in the limit of an infinite flat plane. For this reason, it is convenient to define

$$\underline{v}_j^{(fp)}(\Delta) = 2\sum_\alpha g_{\alpha j}(\Delta) \underline{\underline{T}}_{jj} \cdot \underline{\xi}_{\alpha j} \quad (B28)$$

Employing the same supervector-supermatrix notation employed with regard to $\mathbf{v}_0(\mathbf{s})$, Eq. (B26) can be written

$$\underline{v}(\Delta) = \underline{v}^{(fp)}(\Delta) - (\underline{\underline{U}} - \Delta \underline{\underline{W}}) \cdot \underline{f} - \sum_\alpha \left[\left[\underline{\underline{U}} - \Delta \underline{\underline{W}} \right] \cdot \underline{\Gamma}_\alpha{}^{(0)} + \underline{\underline{T}} \cdot \underline{\Gamma}_\alpha{}^{(1)} \right] \quad (B29)$$

On S_p, $\mathbf{v}(0) = 0$. Also, $\mathbf{v}^{(fp)}(0) = 0$ since $g_{\alpha j}(0) = 0$. Solving Eq. (B29) for $\mathbf{f}$

$$\underline{f} \quad = \quad -\sum_\alpha \left[\underline{\Gamma_\alpha}^{(0)} + \underline{\underline{U}}^{-1} \cdot \underline{\underline{T}} \cdot \underline{\Gamma_\alpha}^{(1)} \right] \qquad (B30)$$

Substituting this into Eq. (B29) yields a relatively simple expression for $\mathbf{v}(\Delta)$

$$\underline{v}(\Delta) \quad = \quad \underline{v}^{(fp)}(\Delta) - \Delta \underline{\underline{W}} \cdot \underline{\underline{U}}^{-1} \cdot \underline{\underline{T}} \cdot \left[\sum_\alpha \underline{\Gamma_\alpha}^{(1)} \right] \qquad (B31)$$

The second term on the rhs of Eq. (B32) represents a correction in the perturbed velocity field that accounts, to first order, for the finite dimensions of the model particle. Other investigators[116] employing entirely different means have obtained the first term ($\mathbf{v}^{(fp)}(\Delta)$) of Eq. (B32). It is straightforward, but tedious, to generalized Eq. (B32) to include second order terms in Δ and/or z', but the resulting fluid velocities are either indistinguishable from those using Eq. (B32) (for b << L) or yield unphysical fluid velocities as the TDL approximation breaks down. On physical grounds, one would expect a second order algorithm to extend the accuracy of the numerical method to smaller particles, but a whole array of other approximations evidently lead to significant error. These possibly include the manner the volume integrations are handled, the approximation that $\nabla\Phi_\alpha$ is constant in the double layer, discretization errors imposed by the limitation of Eq. (B23), and others. Since dealing with of all these approximations substantially complicates the algorithm and serves to defeat the objective of the TDL approximation in the first place, extending the algorithm beyond first order in Δ and x' was not pursued.

In summary, the total fluid velocity above platelet j can be written

$$\underline{v}_{Tj}(\Delta) \quad = \quad \underline{v}_j^{(fp)}(\Delta) + \Delta \underline{h}_j \qquad (B32)$$

where

$$h_j \;\;=\;\; \underline{d}_j - \left[\underline{\underline{W}} \cdot \underline{\underline{U}}^{-1} \cdot \underline{\underline{T}} \cdot \left[\sum_\alpha \underline{\Gamma}_\alpha{}^{(1)} \right] \right]_j \qquad (B33)$$

In Eq. (B32), $\mathbf{v}_j^{(fp)}(\Delta)$ exhibits a complex and nonlinear variation in Δ whereas the latter term varies linearly with Δ ($\mathbf{h}_j$ is a constant vector).

Appendix C: Treatment of Φ_α in the TDL Regime

The procedure of O'Brien and coworkers[116,117] shall be followed in which the boundary condition on Φ_α on S_p is replaced with revised boundary conditions on a new surface, S_{dl}, which lies outside the double layer of the model particle. In the present work, S_{dl} is defined to enclose S_p plus a layer of fluid of thickness b. For large particles of smallest linear dimension L, it is assumed b $\ll$ L. This procedure is possible since Φ_α varies gradually over distances of order b.[122] By moving the boundary outward, the volume integrations (Eq. (A24)) can be neglected and the BE calculation of Φ_α and $\nabla\Phi_\alpha$ simplifies to involve only surface integrations. However, considerable care must be exercised in defining revised boundary conditions on S_{dl}.

Consider a roughly disc shaped triangular volume element, V_j, of inner surface area S_j, outer surface area, S_j^{dl}, and thickness b as shown in Figure 2. The inner and outer surfaces lie on S_p and S_{dl}, respectively. (S_j represents the area of (inner) surface platelet j.) Some useful identities are: $\mathbf{n}_j$ and $\mathbf{n}_{jk}$ are the outward unit normals to platelet j and its k-th neighbor (k=1,2, or 3); $\mathbf{c}_{j1}(x')$ through $\mathbf{c}_{j3}(x')$ define the three side vectors of platelet j at normal distance x' from S_j; and $\mathbf{t}_{j1}$ through $\mathbf{t}_{j3}$ represent the outward unit normals to the three side faces of V_j. (The $\mathbf{t}_{jk}$ vectors are approximated as the cross product of ($\mathbf{n}_j + \mathbf{n}_{jk}$) and $\mathbf{c}_{jk}(0)$ followed by normalization.) For large model particles, ion current fluxes, $\mathbf{j}_\alpha$, for ion α defined by Eq. (6-

7), vary gradually tangent to S_p, but rapidly in the normal direction. Because the particle is impermeable to the passage of fluid and ions, $\mathbf{j}_\alpha \mathbf{A} \mathbf{n}$ vanishes across S_p, but not S_{dl} or the side faces of V_j. Let $\mathbf{j}_\alpha(\mathbf{x}_j, b)$ denote the current density of the α ion across S_{dl} at platelet j (assumed uniform), and $\mathbf{j}_\alpha(\mathbf{c}_{jk}, x')$ the current density across the k-th side of V_j at height x' (assumed uniform). Integrating Eq. (6-7) over V_j and applying the divergence theorem,

$$S_j^{dl} \underline{j}_\alpha(\underline{x}_j, b) \cdot \underline{n}_j \quad = \quad -\sum_{k=1}^{3} \underline{t}_{jk} \cdot \int_0^b \underline{j}_\alpha(\underline{c}_{jk}, x') c_{jk}(x') dx' \qquad (C1)$$

where $c_{jk}(x') = |\mathbf{c}_{jk}(x')|$. Since the fluid is incompressible, $\nabla \mathbf{A} \mathbf{v}_T$ is also zero. ($\mathbf{v}_T$ is total fluid velocity defined by Eq. (B4)). Analagous to Eq. (C1), we can write

$$S_j^{dl} \underline{v}_T(\underline{x}_j, b) \cdot \underline{n}_j \quad = \quad -\sum_{k=1}^{3} \underline{t}_{jk} \cdot \int_0^b \underline{v}_T(\underline{c}_{jk}, x') c_{jk}(x') dx' \qquad (C2)$$

It is useful at this time to define the "tangential divergence", $\nabla \mathbf{t} \mathbf{A}$, of an arbitrary vector field, $\boldsymbol{\omega}$,

$$\underline{\nabla t} \cdot \underline{\omega}_j \quad = \quad \frac{1}{S_j^{dl}} \sum_{k=1}^{3} \underline{t}_{jk} \cdot \int_0^b \underline{\omega}(\underline{c}_{jk}, x') c_{jk}(x') dx' \qquad (C3)$$

The vector field, $\boldsymbol{\omega}$, is assumed to vary slowly tangent to S_p, but may vary rapidly normal to S_p. Also, it shall be assumed we have values for $\boldsymbol{\omega}$ above the individual platelets, and approximate

$$\underline{\omega}(\underline{c}_{jk}, x') \quad = \quad \frac{1}{2}\left[\underline{\omega}(\underline{x}_j, x') + \underline{\omega}(\underline{x}_{jk}, x')\right] \qquad (C4)$$

where $\mathbf{x}_{jk}$ is the centroid of the k-th neighbor of platelet j. The quantity $\mathbf{c}_{jk}(x')$ varies only slightly with x'. Also, the most significant overall contributions for the vector fields of

interest in the present work are those near S_p.   Consequently, $c_{jk}(x')$ is approximated with $c_{jk}(0)$ in Eq. (C3). With this approximation and Eq. (C4), Eq. (C3) becomes

$$\underline{\nabla t}\cdot\underline{\omega}_j \quad = \quad \frac{1}{2S_j^{dl}}\sum_{k=1}^{3}c_{jk}(0)\underline{t}_{jk}\cdot\int_0^b\left[\underline{\omega}(\underline{x}_j,x')+\underline{\omega}(\underline{x}_{jk},x')\right]dx' \qquad (C5)$$

From Eq. (7) and the previous development, Eq. (C1) can be written

$$(\underline{\nabla\Phi}_\alpha)_j^{dl}\cdot\underline{n}_j \quad = \quad -\underline{e}\cdot\underline{n}_j - \underline{\nabla t}\cdot\left[\left[\frac{k_BT}{qz_\alpha D_\alpha}\left[\frac{n_{\alpha 0}(x')}{c_\alpha}-1\right]\underline{v}_{Tj}(x')\right]+\frac{n_{\alpha 0}(x')}{c_\alpha}\underline{\xi}_{\alpha j}\right] \qquad (C6)$$

where $(\underline{\nabla\Phi}_\alpha)_j^{dl}\cdot\mathbf{n}_j$ is the normal derivative of Φ_α for platelet j on S_{dl}, and $\underline{\xi}_{\alpha j}$ is defined by Eq. (B15). From Eqs. (B19), (B27), and (B32),

$$\underline{v}_{Tj}(x') \quad = \quad \frac{1}{\eta}\sum_\gamma g_{\gamma j}(x')\left[\underline{\underline{I}} - \underline{n}_j\underline{n}_j\right]\cdot\underline{\xi}_{\alpha j} + x'\underline{h}_j \qquad (C7)$$

where $g_{\gamma j}(x')$ is defined by Eq. (B26). Substituting these into Eq. (C6), we obtain a usable expression for expressing the boundary condition on S_{dl}.

$$(\underline{\nabla\Phi}_\alpha)_j^{dl}\cdot\underline{n}_j \quad = \quad -\underline{e}\cdot\underline{n}_j - \underline{\nabla t}\cdot\underline{\zeta}_{\alpha j} \qquad (C8)$$

where

$$\underline{\zeta}_{\alpha j} \quad = \quad \frac{(n_{\alpha 0}(x'))_j}{c_\alpha}\underline{\xi}_{\alpha j} + \frac{k_BT}{qz_\alpha D_\alpha}\left[\frac{(n_{\alpha 0}(x'))_j}{c_\alpha}-1\right]\left[\frac{1}{\eta}\sum_\gamma g_{\gamma j}(x')\left[\underline{\underline{I}} - \underline{n}_j\underline{n}_j\right]\cdot\underline{\xi}_{\alpha j} + x'\underline{h}_j\right] \qquad (C9)$$

The second term on the rhs of Eq. (C8) reflects the influence of nonequilibrium fluxes within the double layer on the boundary condition of $\Phi_{\alpha j}$. Making use of the definition of the "tangential divergence" given by Eq. (C5), it can be computed numerically prior to the calculation of revised estimates of the surface components, $\Phi_{\alpha j}$. From Eq. (A23), (employing the same supermatrix notation of Appendix A), the surface components are given by

$$\underline{\Phi}_\alpha \quad = \quad -\left[\frac{1}{2}\underline{\underline{I}} + \underline{\underline{A}}\right]^{-1}\cdot\underline{\underline{C}}\cdot\underline{p}_\alpha^e \qquad (C10)$$

where **A** and **C** involve surface integrals (Eq. (A11)) over surface platelets of S_{dl}, and the components of $\mathbf{p}_\alpha^e$ are given by Eq. (C8). Once these are determined, we need to know

$\nabla\Phi_\alpha(\mathbf{s})$ for field points, $\mathbf{s}$, within the double layer. Since Φ_α and $\nabla\Phi_\alpha$ vary slowly over length scales of magnitude b, $\nabla\Phi_\alpha(\mathbf{s})$ within the double layer can be determined by straightforward interpolation of $\nabla\Phi_\alpha(\mathbf{s})$ for field points, $\mathbf{s}$, just outside the double layer. They can be written (6-14)

$$\underline{\nabla\Phi_\alpha}(\underline{s}) \;=\; -\sum_k \underline{\underline{H_1}}(0,k,\underline{s})\Phi_{\alpha k} \;-\; \sum_k \underline{\underline{H_2}}(0,k,\underline{s})p_{\alpha k}^e \qquad (C11)$$

where

$$\underline{\underline{H_1}}(0,k,\underline{s}) \;=\; -\int_{S_k}\underline{\nabla_s}F'(0,\underline{x},\underline{s})\,dS_x \qquad (C12)$$

$$\underline{\underline{H_2}}(0,k,\underline{s}) \;=\; \int_{S_k}\underline{\nabla_s}F(0,\underline{x},\underline{s})\,dS_x \qquad (C13)$$

$\mathbf{\nabla}_s$ is the gradient operator that acts on "field" variable, $\mathbf{s}$, F and F' are defined by Eqs. (A7) and (A8). Since $\mathbf{s}$ lies close to S_{dl}, special "mirror image" methods need to be employed to compute $\nabla\Phi_\alpha(\mathbf{s})$ with accuracy. Since these are straightforward and have been discussed in detail in Appendix A of reference 14, they shall not be discussed further here.

Appendix D: Total force exerted by a TDL particle on the fluid

Consider a large model particle with surface of hydrodynamic shear, S_p. External to S_p lies surface S_{dl} that completely encloses S_p plus the ionic double layer that surrounds it. Since the total charge due to the particle, counterions, and coions within S_{dl} is zero to a good approximation, the total force exerted by the particle on the fluid can be written[31]

$$\underline{z_T} \;=\; -\int_{S_{dl}}\underline{\underline{\sigma_T}}\cdot\underline{n}\,dS \;=\; \int_{S_{dl}}\underline{f_T}\,dS \quad (D1)$$

where $\boldsymbol{\sigma}_T$ is the hydrodynamic stress tensor, $\mathbf{n}$ is the local outward unit normal to S_{dl}, and $\mathbf{f}_T = -\boldsymbol{\sigma}_T\cong \mathbf{n}$. The m, n component of $\boldsymbol{\sigma}_T$ can be written

$$(\underline{\underline{\sigma_T}})_{mn} \;=\; -p_T\,\delta_{mn} + \eta(\nabla_m v_{Tn} + \nabla_n v_{Tm}) \qquad (D2)$$

where p_T is the local pressure, δ_{mn} is the Kronecker delta, and $\mathbf{v}_T$ is the local fluid velocity.

The disadvantage of Eq. (D1) is we need to know the local pressure in addition to the fluid velocity on S_{dl}. Although this can be computed by a BE procedure similar to that employed in the determination of $\mathbf{v}_T$,[149] it can be avoided by following a slightly different procedure based on the work of Teubner.[150] Consider the differential form of the Lorentz Reciprocal Theorem[48,58] applied to the domain of an incompressible fluid where external fluid forces ($\mathbf{w}$ in Eq. (6-11)) can be ignored.

$$\underline{\nabla} \cdot (\underline{v}' \cdot \underline{\underline{\sigma}}_T) = \underline{\nabla} \cdot (\underline{v}_T \cdot \underline{\underline{\sigma}}') \qquad (D3)$$

where $\mathbf{v}_T$ and $\mathbf{\sigma}_T$ denote the actual fluid velocity and stress fields of our model particle, and $\mathbf{v}'$ and $\mathbf{\sigma}'$ denote some corresponding "trial" fields that also satisfy Eqs. (6-11) and (6-12) with $\mathbf{w} = \mathbf{0}$. Assume we are in a frame of reference where $\mathbf{v}_T$ and $\mathbf{v}'$ vanish far from the model particle. Integrate Eq. (D3) over the fluid volume exterior to S_{dl} and employ the divergence theorem.

$$\int_{S_{dl}} \underline{v}' \cdot \underline{f}_T \, dS = \int_{S_{dl}} \underline{v}_T \cdot \underline{f}' \, dS \qquad (D4)$$

For the trial field, choose an uncharged rigid model particle with a surface of hydrodynamic shear corresponding to S_{dl} and translating with speed u_0 in direction k. We have

$$\underline{v}'|_{S_{dl}} = u_0 \, \underline{e}_k \qquad (D5)$$

$$\underline{f}' = \underline{f}^{(0k)} \qquad (D6)$$

where $\mathbf{e}_k$ is the unit vector in direction k. Because of Eq. (D5), $\mathbf{v}'$ can be taken outside of the integral on the left hand side of Eq. (D4). From the definition of $\mathbf{z}_T$ given by Eq. (D1)

$$\underline{z}_T \cdot \underline{e}_k = \frac{1}{u_0} \int_{S_{dl}} \underline{v}_T \cdot \underline{f}^{(0k)} \, dS \qquad (D7)$$

In order to calculate the total force $\mathbf{z}_T$; $\mathbf{v}_T$ on S_{dl}, and also $\mathbf{f}^{(0k)}$ must be known. Procedures leading up to and including Eq. (B10) are used to compute the components of $\mathbf{f}^{(0k)}$ (k = 1, 2, 3) at the beginning of the calculation. To calculate $\mathbf{v}_T$ on S_{dl}, Eq. (B32) is used. In turn, this

requires $\boldsymbol{\nabla}\boldsymbol{\Phi}_\alpha$ and Λ_0.

Chapter 7

Summary

A bead model of a weakly charged peptide is developed to determine its electrophoretic mobility. Each amino acid is represented by two beads: the backbone bead radius is set to one half of the nearest neighbor C_α- C_α distance, and the radius of the side chain bead is chosen on the basis of the diffusion constant of the free amino acid. Expressions to calculate the mobility of a peptide are derived. The bead model works as well as semi empirical and boundary element models in explaining experimental mobilities.

For highly charged peptides, the ion relaxation effect that reduces the absolute mobility must be considered. The ion relaxation effect is accounted by correcting "unrelaxed" mobility on the basis of model size and its average electrostatic surface potential, or ς potential. Correction factors are estimated using those of spheres and are readily determined. In addition, a more accurate account is taken of the finite size of the beads making up the structure. This improvement makes the bead model applicable at higher salt concentrations and/or model macromolecules made up of larger subunits.

In addition to the development of a peptide bead model, a spherical gel-layer model of a "hairy" surface colloid particle is extended to include charge regulation and applied to polystyrene sulfonate. The actual charge state of the particle depends on the intrinsic pK_a of the acidic group on the surface, its nearby charged residues, the salt concentration, salt type, and pH. Free energy considerations coupled with Poisson-Boltzmann theory are used to estimate how the local electrostatic environment of a charged gel layer alters the local pK_a of the acidic groups. Based on this modulation of the charge state, the mobility and viscosity

modeling give a reasonable prediction of the structural and charge properties of the gel layer of polystyrene sulfonate.

Finally, a boundary element approach is applied to the electrophoresis of rigid macroions in the thin double layer limit. This BE-TDL method should be useful in modeling large particles of arbitrary shape. In the present work, a compact, high molecular weight DNA-spermidine complex is examined. To reconcile experimental and model mobilities, 95% of the spermidine is predicted to the "specifically bound" to DNA. Further consideration of the validity of PB equation in the presence of complex salt, such as trication spermidine, will make this approach more accurate.

References

1) P.H. Wiersema, Ph.D. thesis, Utrecht University, The Nertherlands, 1964.

2) D.V. Messana, L. Rossetti, F. Cassiano, B. Misiti, M.Giardina, J. Castagnola, Chromatogr. B. 699 (1997) 149

3) B.R. Sitaram, H.H. Keah, M.T.W. Hearn, J. Chromatogr. A. 857 (1999) 263

4) D.J. Winzor, S. Jones, S.E. Harding, Anal. Biochem. 333 (2004) 225

5) D.J. Winzor, J. Chromatogr. A. 1015 (2003) 199

6) S.A. Allison, J.D. Carbeck, C. Chen, F. Burkes, J. Phys. Chem. B. 108 (2004) 4516

7) G.M. Janini, C.J. Metral, H.J. Issaq, J. Chromatogr. A. 924 (2001) 291

8) R. Plasson, H. Cottet, Anal. Chem. 77 (2005) 6047

9) S. Ma, M. Nishikawa, H. Katsumi, F. Yamashita, M. Hashida, J. Control. Release 102 (2005) 583

10) J. Kim, R. Zand, D.M. Lubman, Electrophoresis 23 (2002) 782

11) A. Zuskova, K. Novotna, B. Vcelakova, J. Chromatogr. B 841 (2006) 129

12) G.M. Janini, C.J. Metral, H.J. Issaq, G.M. Muschik, J. Chromatogr. A 848 (1999) 417

13) M. Jalali-Heravi, Y. Shen, M. Hassanisadi, M.G. Khaledi, Electrophoresis 26 (2005) 874

14) M. Jalali-Heravi, Y. Shen, M. Hassanisadi, M.G. Khaledi, J. Chromatogr. A 1096 (2005) 58

15) C. Simo, A. Cifuentes, Electrophoresis 24 (2003) 834

16) M.V. Piaggio, M.B. Peirotti, J.A. Deiber, Electrophoresis 27 (2006) 4631

17) J.Y. Kim, S.H. Ahn, S.T. Kang, B.J. Yoon, J. Colloid Interface Sci. 299 (2006) 486

18) C. Ma, V.A. Bloomfield, Biopolymers 35 (1995) 211

19) G.J. Foulds, F.A. Etzkorn, Nucleic Acids Research 26 (1998) 4304

20)   S.A. Allison, C. Chen, D. Stigter, Biophys. J. 81 (2001) 2558

21)   S.A. Allison, J. Colloid Interface Sci. 277 (2004) 248

22)   M.J. Garcia-Salinas, F.J. de las Nieves, Langmuir 16 (2000) 715

23)   B. Neu, H.J. Meiselman, Langmuir 17 (2001) 7973

24)   J.P. Hsu, T.S. Hsieh, T.H. Young, S. Tserg, Electrophoresis 24 (2003) 1338

25)   J.P. CamP, A.T. Capitano, Biophys. Chem. 113 (2005) 115

26)   E. Huckel, Physik Zeitsch. 25 (1924) 204

27)   M. Smoluchowski, in "Handbuch der Electrizitat und des Magnetismus, Volume 2," L. Graetz, Ed., Barth, Leipzig, 1921.

28)   D.C. Henry, Proc. R. Soc. London Ser. A. 133 (1931) 106

29)   R.J. Hunter, "Introduction to Modern Colloid Science," Oxford University Press, Oxford, (2002), Chapter 7.

30)   P.H.Wiersema, A.L. Loeb, J.Th.G. Overbeek, J. Colloid Interface Sci. 22 (1966) 78

31)   R.W. O'Brien, L.R. White, J. Chem. Soc. Faraday Trans. 274 (1978) 1607

32)   B.J.Yoon, S. Kim, J. Colloid Interface Sci. 128 (1989) 275

33)   D. J. Stigter, Phys. Chem. 82 (1978) 1417

34)   S.A. Allison, Macromolecules 29 (1996) 7391

35)   S.A. Allison, M. Potter, J.A. McCammon, Biophys. J. 73 (1997) 133

36)   D. Zanchet, C.M. Micheel, W.J. Parak, D. Gerion, S.C. Williams, A.P. Alivisatos, J. Phys. Chem B 106 (2002) 11758

37)   T. Pons, H.T. Uyeda, I.L. Medintz, H. Mattoussi, J. Phys. Chem. B 110 (2006) 20308

38)   E. Stellwagen, Y. Lu, N.C. Stellwagen, Nucleic Acid Res. 33 (2005) 4425

39)   N.C. Stellwagen, Electrophoresis 27 (2006) 1163

40)   R. E. Offord, Nature (London) 211 (1966) 591

41)   S.A. Allison, Y. Xin, H. Pei, J. Colloid Interface Sci. 313 (2007)   328

42)   J. Th. G. Overbeek, Kolloid-Beih., 54 (1943) 287

43)   S.A. Allison, Y. Xin, H. Mitchell, Recent Res. Devel. Macromol. 8 (2005) 25

44)   F. Booth, Proc. R. Soc. London Ser. A. 203 (1950) 514

45)   J. D. Carbeck, R. S. Negin, J. Am. Chem. Soc. 123 (2001) 1252

46)   C.J.F. Bottcher, "Theory of Electric Polarization" Elsevier, New York, (1973).

47)   J. Happel, H. Brenner, "Low Reynolds Number Hydrodynamics" Martinus Nijhoff, The Hague, (1983).

48)   S. Kim, S.J. Karrila, "Microhydrodynamics," Butterworth-Heinemann, Boston (1991).

49)   S. Mazur, C. Chen, S.A. Allison, J. Phys. Chem. B 105 (2001) 1100

50)   S.A. Allison, D. Stigter, Biophys. J. 78 (2000) 121

51)   "Macromolecules: J.G. Kirkwood," Oppenheim, I., and Auer, P.L., Eds., Gordon and Breach, New York (1967).

52)   V.A. Bloomfield, W.O. Dalton, K.E. Van Holde, Biopolymers 5 (1967) 137

53)   Y. Ikeda, Kobayashi Rigaku Kenkyusho Hokuku 6 (1956) 44

54)   R. Zwanzig, J. Chem. Phys. 44 (1966) 1858

55)   H. Yamakawa, J. Yamaki, J. Chem. Phys. 58 (1973) 2049

56)   J. Garcia de la Torre, V.A. Bloomfield, 16 (1977) 1747

57)   J.Garcia de la Torre, M.C. Lopez Martinez, M.M Tirado, J.J. Freire, Macromolecules 17 (1984) 2715

58)   H.A. Lorentz, Versl. Kon. Akad. Wetensh. Amsterdam 5 (1896)168

59)   R.J.Lewis, S.A. Allison, D. Eden, R. Pecora, J. Chem. Phys 89 (1988) 2490

60)   R.F. Cross, J. Cao, J. Chromatogr. A. 786 (1997) 171

61)   P.D. Grossman, J.C. Colburn, H.H. Lauer, Anal. Biochem. 179 (1989) 28

62)   E.C. Rickard, M.M. Strohl, R.G. Nielsen, Anal. Biochem. 197 (1991) 197

63) C. Branden,J. Tooze, Introduction to protein structure, Garland Publishing, Inc. New York (1998) p. 8

http://www.chemistry.gsu.edu/faculty/Yang/Protein-lecture.htm

64) V. Sasisekharan, in "Collagen," Ramanathan, N., Ed., Interscience, New York (1962) p. 39

65) A. Polson, Biochem. J. 31 (1937) 1903

66) L.G.Longsworth, "Diffusion in Liquids and the Stokes Einstein Relation," in "Electrochemistry in Biology and Medicine," Shedlovsky, T., Ed., J. Wiley, New York, (1955) p. 225

67) M.A Cremasco, B.J. Hritzko, Y. Xie, N.H.L.Wang, Brazilian J. Chem. Eng. 18 (2001) 181

68) J.T. Edward, J. Chem Ed. 47 (1970) 261

69) G.E. Schultz, R.H. Schirmer, "Principles of Protein Structure," Springer-Verlag, New York (1979)

70) P.J. Flory, "Statistical Mechanics of Chain Molecules," J. Wiley, New York (1969) Chapter 7

71) G.N. Ramachandran, C. Ramakrishnan, V. Sasisekharan, J. Mol. Biol. 7 (1963) 95

72) P.J. Hagerman, B.H. Zimm, Biopolymers 20 (1981) 1481

73) S. Fraga, J.M.R. Parker, J.M. Pocock, "Computer Simulations of Protein Structures and Interactions," Springer-Verlag, New York (1995)

74) K.C. Linderstrom-Lang, Trav. Lab. Carlsberg 15 (1924) 1

75) M.W. Germann, T. Turner, and S.A. Allison, J. Phys. Chem. A, 111 (2007) 1452

76) J.D. Carbeck, I.J. Colton, J.R. Anderson, J.M. Deutch, G.M. Whitesides, J. Am. Chem. Soc. 121 (1999) 10671

77) A.-S. Yang, M.R.Gunner, R. Sampogna, K. Sharp, B. Honig, Proteins 15 (1993) 252

78)   T. Grycuk, J. Phys. Chem. B 106 (2002) 1434

79)   D. Bashford, M. Karplus, Biochemistry 29 (1990) 10219

80)   J. Antosiewicz, J.M. Briggs, A.H. Elcock, M.K.Gilson, J.A. McCammon, J. Comput.

       Chem. 17 (1996) 1633

81)   H.-X. Zhou, M.Vijayakumar, J. Mol. Biol. 267 (1997) 1002

82)   L.K. Lee, C.A. Fitch, B.E. Garcia-Moreno, Protein Sci. 11 (2002) 1004

83)   U. Sharma, R.S. Negin, J.D. Carbeck, J. Phys. Chem. B 107 (2003) 4653

84)   Y. Nozaki, C.Tanford, J. Am. Chem. Soc. 89 (1967) 742.

85)   S. Aragon, J. Comp. Chem. 25 (2004) 1191

86)   M.J. Conolly, J. Mol. Graphics 11 (1993) 139

87)   J. Garcia de la Torre, S. Navarro, M.C. Lopez Martinez, F.G. Diaz, J.J. Lopez Casales,

       Biophys. J. 67 (1994) 530

88)   Y. Xin, H. Mitchell, H.Cameron, S.A. Allison, J. Phys. Chem. B 110 (2006) 1038

89)   J. Garcia de la Torre, V.A. Bloomfield, Quart. Rev. Biophys. 14 (1981) 81

90)   S.A. Allison, J. Colloid Interface Sci. 282 (2005) 231

91)   S.A. Allison, Biophys. Chem. 93 (2001) 197

92)   P.J. Hagerman, B.H. Zimm, Biopolymers 20 (1981) 1481

93)   H.C. Brinkman, Appl. Sci. Res. A 1 (1947) 27

94)   P. Debye, A.M. Bueche, J. Chem. Phys. 16 (1948) 573

95)   M.J. Garcia-Salinas, J.J. de las Nieves, Colloids and Surfaces A 222 (2003) 65

96)   B.-R. Paulke, P.-M. Moglich, E. Knippel, A. Budde, R. Nitzsche, R.H. Muller,

       Langmuir 11 (1995) 70

97)   M. Rasmusson, S. Wall, J. Colloid and Interface Sci. 209 (1999) 312

98)   H. Ohshima, T. Kondo, J. Colloid Interface Sci. 116 (1987) 305

99)   H. Ohshima, J. Colloid Interface Sci. 163 (1994) 474

100) H. Ohshima, J. Colloids and Surfaces A 103 (1995) 249

101) H. Ohshima, J. Colloid Interface Sci. 228 (2000) 190

102) R.J. Hill, D.A. Saville, W.B. Russel, J. Colloid Interface Sci. 258 (2003) 56

103) I.G. Watterson, L.R. White, J. Chem. Soc. Faraday Trans. 2, 77 (1981) 1115

104) B.U. Felderhof, J.M. Deutch, J. Chem. Phys. 62 (1975) 2391

105) S.A. Allison, S. Wall, M. Rasmusson, J. Colloid Interface Sci. 263 (2003) 84

106) P. Borget, F. Lafuma, C. Bonnet-Gonnet, J. Colloid Interface Sci. 285 (2005) 136

107) J. Laven, H.N. Stein, J. Colloid Interface Sci. 238 (2001) 8

108) K.A. Sharp, B. Honig, J. Phys. Chem. 94 (1990) 7684

109) E. Kreysig, Advanced Engineering Mathematics, Eighth Ed., Wiley, New York, 1999, p. 958

110) M.J. Garcia-Salinas, F.J. de las Nieves, Langmuir, 16 (2000) 7150

111) D.R. Lide (Ed.), CRC Handbook of Chemistry and Physics, 82th Ed., CRC Press, Boca Raton, FL (2001)

112) J.D. Sherwood, J. Fluid Mech. 101 (1980) 609

113) J.M Roberts, P. Linse, J.G. Osteryoung, Langmuir 14 (1998) 204

114) S.A. Allison, Y. Xin, J. Colloid Interface Sci. 288 (2005) 616

115) S. Dukhin, in "Research in Surface Forces," Vol. 2, Deryaguin, B.V., Ed., Consultants Bureau, New York (1966) p. 54

116) R.W. O'Brien, J. Colloid Interface Sci. 92 (1983) 204

117) R.W. O'Brien, D.N. Ward, J. Colloid Interface Sci. 121 (1988) 402

118) M.C. Fair, J.L. Anderson, Langmuir 8 (1992) 2850

119) Y.E. Solomentsev, Y. Pawar, J.L. Anderson, J. Colloid. Interface Sci. 158 (1993) 1

120) S.A. Allison, Macromolecules 31 (1998) 4464

121) D.M. McQuarrie, "Statistical Mechanics," Harper & Row, New York (1976) Chapter 15

122) R.W. O'Brien, R.J. Hunter, Canadian J. Chem. 59 (1981) 1878

123) E. Kreysig, "Advanced Engineering Mathematics," 8th Edition, John Wiley, New York (1999) Chapter 19

124) S.S. Dukhin, V.N. Shilov, Adv. Colloid Interface Sci. 13 (1980) 153

125) P.M. Morse, H. Feshbach, "Methods of Theoretical Physics," Part II, McGraw-Hill, New York (1953) Chapter 10

126) L.G. Gosule, J.A. Schellman, Nature 259 (1976) 333

127) V.A. Bloomfield, Biopolymers 44 (1998) 269

128) T.H. Eickbush, E.N. Moudrianakis, Cell 13 (1976) 295

129) S.A. Allison, J. Herr, J.M. Schurr, Biopolymers 20 (1981) 469

130) K.A. Marx, G.C. Ruben, Biophysical J. 49 (1986) 53

131) J.A. Schellman, N. Parthasarathy, J. Mol. Biol. 175 (1984) 313

132) Y. Yamasaki, Y. Teramoto, K.Yoshikawa, Biophysical J. 80 (2001) 2823

133) S.A. Allison, R.A.Easterly, D.C. Teller, Biopolymers, 19 (1980) 1475

134) S.L. Goren, M.E. O'Neill, J. Fluid Mech. 101 (1980) 97

135) C.F. Anderson, M.T. Record, Annu. Rev. Phys. Chem. 46 (1995) 657

136) M.C. Olmstead, C.F. Anderson, M.T. Record, Proc. Natl. Acad. Sci. USA 86 (1989) 7766

137) M.T. Record, T.M. Lohman, Biopolymers 17 (1978) 159

138) I.A. Shkel, O.V. Tsodikov, M.T. Record, J. Phys. Chem. B 104 (2000) 5161

139) G.S. Manning, Annu. Rev. Phys. Chem. 23 (1972) 117

140) M. LeBret, B.H. Zimm, Biopolymers 23 (1984) 270

141) J. Ulander, H. Greberg, R. Kjellander, J. Chem. Phys. 115 (2001) 117

142) P. Leroy, A. Revil, J. Colloid Interface Sci. 270 (2004) 371

143) M. Fixman, J. Chem. Phys. 70 (1979) 4995

144) B.J. Yoon, A.M. Lenhoff, J. Comput. Chem. 11 (1990) 1080

145) A.H. Juffer, E.F.F. Botta, B.A.M. Van Keulen, A.Van Der Ploeg, H.J.C. Berendsen, J. Comput. Chem. 97 (1991) 144

146) H.-X. Zhou, Biophys. J. 65 (1993) 955

147) H.-X. Zhou, J. Chem. Phys. 100 (1994) 3152

148) G.K. Youngren, A. Acrivos, J. Fluid Mech. 69 (1975) 377

149) S.A. Allison, P. Nambi, Macromolecules 25 (1992) 3971

150) M. Teubner, J. Chem. Phys. 76 (1982) 5564